TRIBOLOGICAL PROPERTIES OF MOS_2 ON SEMICONDUCTING AND METALLIC SURFACES

A Dissertation

by

ZHUOTONG LIU

Submitted to the Office of Graduate and Professional Studies of
Texas A&M University
in partial fulfillment of the requirements for the degree of

DOCTOR OF PHILOSOPHY

Chair of Committee,	James Batteas
Committee Members,	Jaime Grunlan
	Matthew Sheldon
	Jonathan Felts
Head of Department,	Simon North

May 2020

Major Subject: Chemistry

ABSTRACT

It is of great interest to seek lubrications for friction minimization in order to save energy and thus reduce cost. Two dimensional MoS_2 exhibits promising friction reduction and anti-wear properties. Moreover, the use of single layer MoS_2 (SLM) in nano-devices receives significant research interest because it has remarkable electronic and optical properties compared to bulk MoS_2. Therefore, it is important to investigate the tribological behavior of SLM under various conditions.

My study is divided into three projects. The first project investigated the mechanical and tribological behavior of MoS_2 nanoflakes on nanoscopically rough substrates. Single- and multi- layer MoS_2 nanoflakes were prepared on SiO_2 nanoparticle films, followed by Atomic Force Microscopy (AFM) characterization to reveal their conformity on nanoparticle films and tribological properties. The second project aimed at studying the adhesion and friction between MoS_2 and selected molecules. In this study, silicon tips were modified with two kinds of silane molecules terminated with -NH_2 and -SH groups. Modified AFM probes were utilized to obtain the friction and adhesion on single layer and bulk MoS_2. In the third project, tribological properties of MoS_2 are tuned by modifying its surface. Radical reactions between 4-nitrobenzenediazonium tetrafluoroborate (4-NBD) and MoS_2 in aqueous solution have been previously investigated as a means for facile modification, but a detailed study has yet to be carried out to reveal the nature of its chemical reactivity with MoS_2 on Au(111) substrates in terms of layer thicknesses. Here, the chemical and wear properties of single

and multilayer (bulk) MoS_2 on Au(111) substrates were investigated with AFM before and after being functionalized with 4-NBD in aqueous solution.

The study of the mechanical and tribological properties of MoS_2 on different substrates provides insightful perspective of using 2D material boundary lubricants under different conditions. In addition, tribological, chemical and optical properties of MoS_2 can be further tuned by manipulating its surface via chemical surface modification.

ACKNOWLEDGEMENTS

I would like to express my appreciation and thanks to my advisor Dr. Batteas for his support and mentoring during these past five years. I would also like to thank everyone in Batteas' Group, for their support and friendship. I would especially like to thank my mentor Meagan, for her patient guidance.

Most importantly, I would like to thank my family and friends for their support and encouragement.

CONTRIBUTORS AND FUNDING SOURCES

Contributors

This work was supervised by a dissertation committee consisting of Professor James Batteas and Matthew Sheldon of the Department of Chemistry, Professor Jamie Grunlan, jointly appointed in the Department of Chemistry and Department of Mechanical Engineering, and Professor Jonathan Felts of the Department of Mechanical Engineering.

The STM and XPS data in Chapter IV was provided by Fanglue Wu of the Department of Material Science.

All other work conducted for the dissertation was completed by the student independently.

Funding Sources

This work was made possible by the National Science Foundation under Grant CMMI-1436192 and NTESS, LLC - National Technology & Engineering Solutions of Sandia, under contracts #1919201 and #2021982.

TABLE OF CONTENTS

Page

LIST OF FIGURES

Page

LIST OF TABLES

Page

CHAPTER I

INTRODUCTION AND LITERATURE REVIEW: INTERFACIAL INTERACTIONS OF 2D MATERIALS

1.1 Overview

Minimizing friction and wear has been a critical problem in the field of mechanical and material engineering. It has been reported that 1.0% to 1.4% of the country's GDP is lost from tribological effects such. For example, the costs due to wear-and-t0ar of automobiles in the US alone exceeds 10 billion dollars per year.[1-2] The widely known bad effects of the energy loss and abrasion during sliding motivate the studies into lubricious liquids and coatings. Liquid lubrication is widely used in machines such as devices in cars, in which the liquids can separate the surfaces from rubbing each other, reducing the energy loss and friction. However, because of its high viscosity and sensitivity to temperature, it does not satisfy the requirement in specific circumstances such as in high temperature, low pressure or micro devices. To overcome these limitations, solid boundary lubricants are used as an alternative method for reducing friction and wear at sliding interfaces. Layered materials such as graphene, transition metal dichalcogenides (TMD) and hexagonal boron nitride (h-BN) have been studied and elucidated to be useful as surface lubricants.[3-6] The lattice structures of some types of layered materials are shown in Figure 1.1. They can not only be used as boundary lubricants on macro machines, but also can be used in micro devices and components working in vacuum or high temperature.

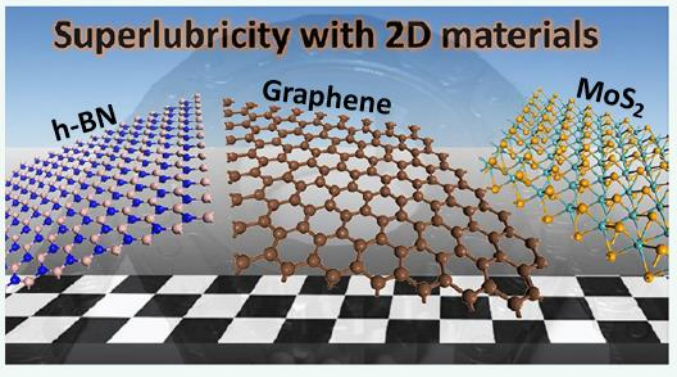

Figure 1.1 Atomic structures of single layer h-BN, graphene, and MoS_2. Reprinted with permission from Berman *et al.*[4] Copyright 2018 by ACS Publications.

The optical, electronic, mechanical and tribological properties of 2D films were explored due to the unique properties of these materials. Single layer graphene drew plenty of attention when it was first reported in 2004.[7] Graphene is a semimetal 2D crystal formed with carbon atoms arranged in a hexagonal structure. Graphene is widely studied because of its excellent electronic and tribological properties. The high thermal conductivity of graphene makes it a widely studied material in electronic applications.[8-9] Although graphene has excellent properties showed above, it does not have free carriers because it doesn't have band gaps.[8, 10] Electron and hole carriers can be produced in graphene by chemical doping and electrostatic gating. Due to lack of band gaps, graphene cannot meet the demand of several technological applications. In devices such as transistors, digital electronics and optoelectronics at visible frequencies, instead of graphene, semiconducting 2D materials such as transition metal dichalcogenides (TMD)

are more suitable.[11-15] Thus, it is critical for investigating the chemical, mechanical, and tribological properties of TMDs.

There are different methods for preparation of 2D materials on substrates. Depending on the conditions 2D lubrication need to be used in, one needs to take into consideration the purity and scale of the coating area. Exfoliating and chemically/physically forming 2D materials on substrates are the most common ways of preparing these layered materials on a substrate surface. Chemical vapor deposition (CVD) method is used for synthesizing large area 2D materials on substrates. [16-20] The size and layer thickness of 2D crystals can be controlled. In CVD method, precursor MoO_3 and sulfur (or H_2S) in the vacuum pump and let them react to form MoS_2 nanosheets (Figure 1.2). One of the most important advantages of this method is that it can be used to prepare thin layer (down to single layer) on various substrates and the substrates can even be fully covered with thin layer 2D materials if the correct temperature, reaction time, sample distances and gas flow rate are used.

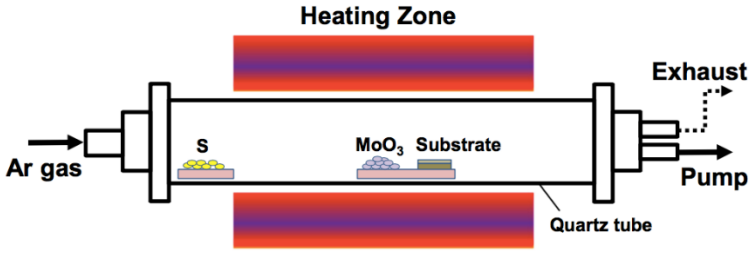

Figure 1.2 Schematic diagram of the CVD system for MoS_2 atomic layer growth. Reprinted with permission from Nguyen *et al.*[16] Copyright 2015 by Elsevier ScienceDirect.

Exfoliation method is widely used in studies due to the pristine layers produced and easy procedures for making samples.[21-23] In exfoliation method, a piece of tape is used to peel off a thin layer of 2D material and the material was transferred on the substrate. After manually pressed the tape/sample/substrate sandwich to let the 2D material attached stronger on substrates, adhesive tape is removed and leave single- and multi- layer flakes on the substrates. Figure 1.3 shows optical images of atomically thin graphene, MoS_2, $NbSe_2$ and h-BN flakes nanaoflakes on SiO_2/Si substrate prepared with exfoliation method. Areas in the red box has monolayer flakes of 2D materials.

Figure 1.3 Optical images of exfoliated thin films of 2D materials including graphene, MoS_2, $NbSe_2$ and h-BN. Scale bar, 10 µm. Adapted with permission from Lee *et al.*[24] Copyright 2010 by AAAS.

In recent years, the exfoliation method was improved by scientists. Huang and coworkers investigated that heating before peeling off the adhesive tape can produce more graphene flakes on silica substrates. The interactions between graphene surface and the substrate during exfoliation are van der Waals forces. The exfoliation process is a competition between the interlayer interactions and interfacial forces. As shown in Figure 1.4a, the heating step builds up pressure between graphene flakes and the

substrate. Gas that is between graphene flakes and the silica substrate is then released at the edges. This step makes graphene contact more tightly with the substrate and the increased van der Waals interaction stops gas from re-entering during the cooling down process (Figure 1.4b).[25]

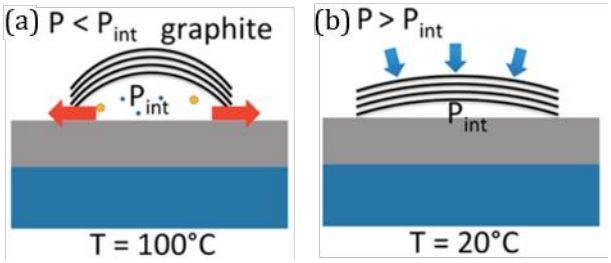

Figure 1.4 Schematics of (a) heating the substrate with graphite on adhesive tape and (b) Cooling to room temperature after annealing. Adapted with permission from Huang *et al.* [25] Copyright 2015 by ACS Publications.

In a study carried out by Magda and cowokers,[26] heat released tape was used to transfer MoS_2 on Au. As shown in Figure 1.5, after peeled off a thin layer of MoS_2 with thermal-released tape and put on Au, the sample was also annealed to release the tape, following by sonicating for a few seconds to peel off big MoS_2 flakes from the sample. This method induces large area (hundreds of microns) flakes on gold. These modified methods are promising for making large and pristine 2D flakes on substrates that have large adhesion with them.

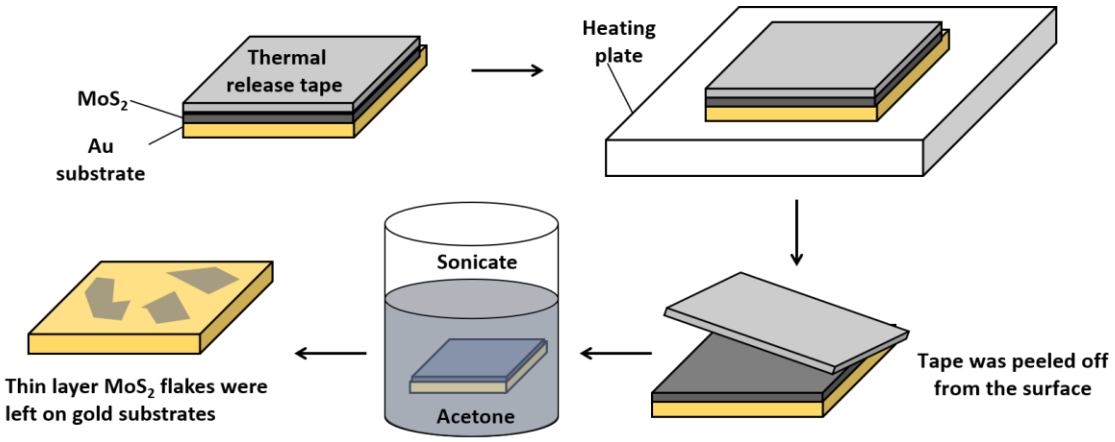

Figure 1.5 Diagram of thermal-released tape assisted exfoliation method to transfer atomically thin MoS_2 crystal on top of freshly cleaved gold substrates.

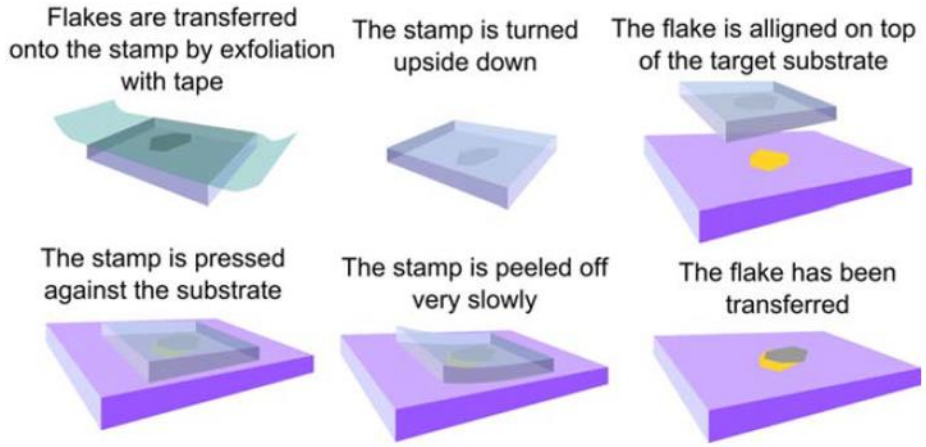

Figure 1.6 Schematic of the procedures for the use of viscoelastic stamp to transfer an atomically thin 2D material flake onto a targeted location. Adapted with permission from Castellanos-Gomez *et al.* [27] Copyright 2014 by IOP Publishing Ltd.

All-dry viscoelastic stamping is also used in transferring 2D materials on substrates.[27] As shown in Figure 1.6, in this method, flakes are transferred by a piece of tape on a stamp first. After that, the stamp is pressed against the substrate and then peeled off slowly, leaving material sheets on the substrate. This method is very useful

when preparing large area heterostructures, such as transferring MoS_2 on h-BN. The heterostructures prepared were proved to be without bubbles and wrinkles.

After the isolation of atomically thin 2D layers, especially monolayer 2D material sheets, their unique electronic, optical and lubricious properties can be investigated. Here, the sliding interfaces and tribological properties of 2D materials are explored and discussed. Understanding the interactions at the sliding interfaces is important for modulating the friction and guiding the use of 2D materials in real applications. Methods for tailoring surface friction include controlling the surface roughness, modifying the surface chemistry, and functionalizing the 2D materials. This review is focused on exploring the tribological properties of MoS_2, a semiconducting transition metal dichalcogenides.

1.2 Interactions at sliding interfaces

It is crucial to study the interfacial interactions as to tune the friction as well as reaction at sliding interfaces. Studies on the interactions at sliding interfaces has been carried out both computationally and experimentally. The mechanical properties at the sliding interface have been explained with stick-slip motion and commensurate/incommensurate sliding. In this part, the stick-slip motion, commensurate/incommensurate sliding as well as the sliding mechanism at the interfaces of 2D materials will be demonstrated. Understanding the mechanism during sliding is crucial for getting a way to modulate tribological properties at sliding interfaces.

One important mechanism to consider about when dealing with the sliding of two objects is stick-slip motion. Stick-slip motion occurs because of the static force is larger than the kinetic friction force and roughness at interfaces is a significant contributes to stick-slip phenomenon during sliding. As shown in Figure 1.7,[28] a resisting force is encountered as the slider climbs an asperity. And when the slider gets on top of the asperity, it slides down to the valley. The stick-slip phenomenon causes oscillation of friction. The oscillation of friction makes resistant force can be much higher than the averaged sliding friction and causes irreversible transformations of surfaces.[29-30] Hereby, it is important to reduce stick-slip motion to reduce friction and wear during sliding.

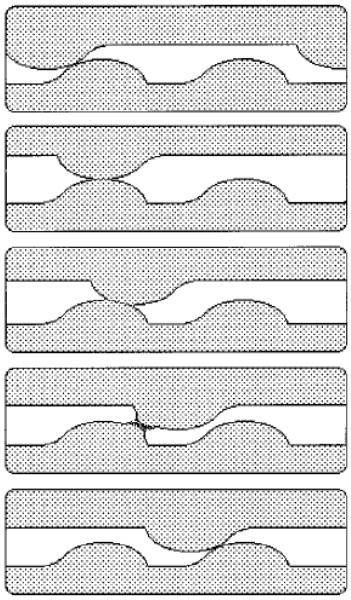

Figure 1.7 Schematic of the sliding interface showing a slide moving on a rough surface to break adhesive junctions. Adapted with permission from Berman *et al.* [28] Copyright 1996 by ACS Publications.

When go down to nanoscale studies, stick-slip motion allows AFM to obtain atomic scale images. Due to higher energy barrier, AFM tips was trapped when climbing

over potential barriers and slid afterwards. The "stick" motion of AFM tips induces in larger friction when climbing on energy barriers and "slip" motion makes the friction lower, allowing us to see periodicity of atoms in nanoscale images. Figure 1.8 illustrates the AFM atomic resolution images of graphene and MoS_2. The periodic variation of friction can be seen on the original friction images, and the Fourier transferred images show clear lattice of atomic periodicity. The measured lattices of graphene surface indicate single layer graphene is stretched during scanning.

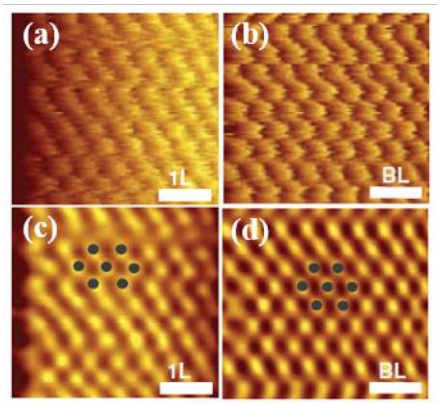

Figure 1.8 (a) and (b) are the friction images for monolayer and thick graphene samples, respectively. (c) and (d) are the corresponding filtered images. Black dots on (c) and (d) represent the periodic sites of the friction force signal. It can be clearly seen that the lattice of graphene is stretched during friction measurement. Scale bar 0.5 nm. Adapted with permission from Lee *et al.*[24] Copyright 2010 by AAAS.

Commensurate and incommensurate sliding is another important mechanism to pay attention to when study interfacial sliding mechanisms, especially when both of the sliding objects are 2D materials due to periodic lattice of atoms on the surface of 2D materials.[6] At the interface between atomically flat surfaces, commensurate sliding occurs for two matching lattices and the atoms of the lattice on one side perfectly fit the

atoms of the periodic potential landscape on the other side of the interface.[31-32] Commensurate and incommensurate sliding affects the frictional properties at the interface of 2D materials. As an example, it has been reported that on the surface of graphene, when scanning at various angles, commensurate sliding results in a large friction peak every 60°.[33-35] Achieving an incommensurate contact state is good for obtain superlubricity because of overcoming relatively small energetic barriers.[36]

1.3 Use of MoS_2 for reducing friction and wear

1.3.1 MoS_2 additives in oil lubricants

With excellent lubricious and structure properties, MoS_2 has been used as additives in lubricating oil. The reported advantages of nanoparticle lubricant additives include insolubility in oil lubricants, low reactivity, formation of films, good performance in durability and suitable in high temperature environments.[37] The layered close-packed hexagonal structure of MoS_2 makes it suitable for reducing friction and minimize wear. Studies of 2D materials nanoparticle additives in base oil have shown greater reduction of friction compared to base oil without additives.[38-42] Figure 1.9a shows the TEM image of inorganic fullerene-like (IF) MoS_2 nanoparticles. According to Figure 1.9d, IF MoS_2 has better anti-wear properties than layered MoS_2 (2H-MoS_2) additives in base oil and base oil without additives. Frictional studies also illustrate that IF MoS_2 has the lowest friction coefficient (Figure 1.9d).[43] Mechanism of the lubricating process of MoS_2 nanoparticles can be the rolling of nanoparticles at two

antagonist surfaces, and the deformation of nanoparticles with high contact pressure. An SEM image in Figure 1.9b shows that MoS_2 nanoparticles deforms after friction test.

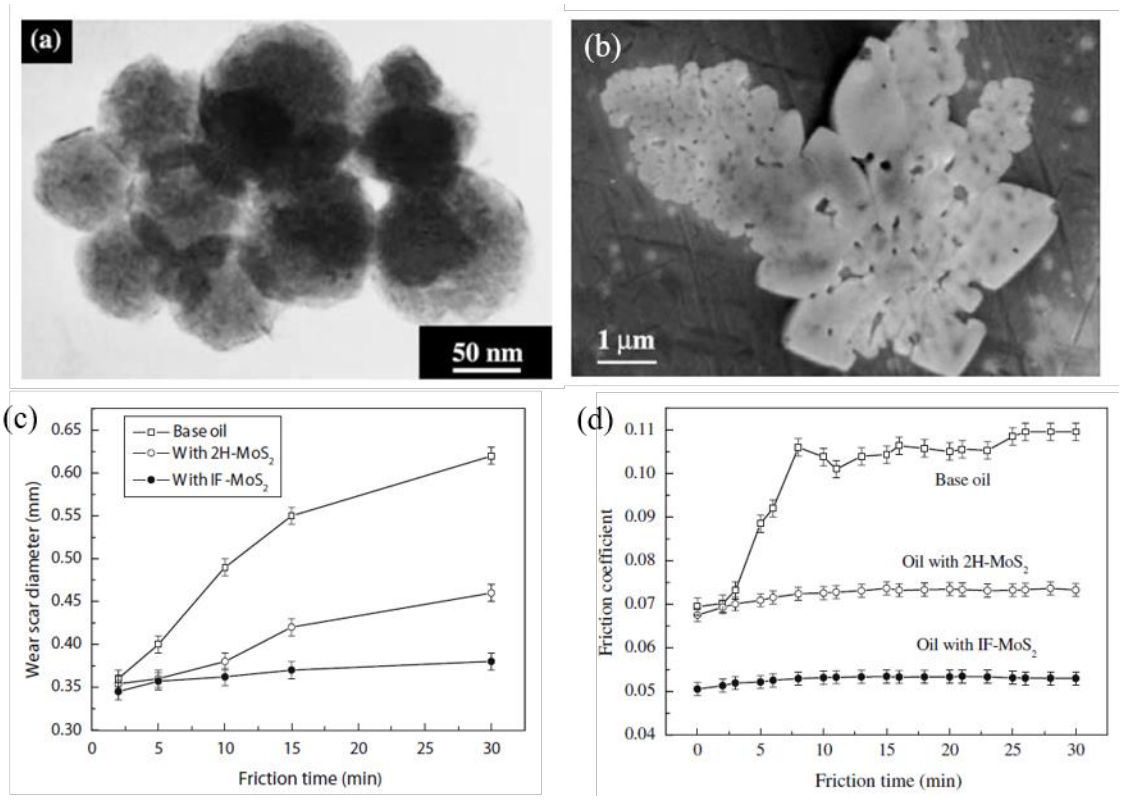

Figure 1.9 (a) TEM image of IF MoS_2 nanoparticles. (b) SEM image of IF-MoS_2 on the rubbing surface after friction test. (c)Wear scare diameter as a function of friction time for base oil, base oil with 2H-MoS_2 and with IF-MoS_2. (d) Measured friction coefficient as a function of friction time for three lubricants. Adapted with permission from Huang *et al.*[43] Copyright 2010 by Springer Science and Business Media, Inc.

Previous studies have demonstrated that different structures of MoS_2 additives appear to affect the friction and wear properties of oil lubricants. MoS_2 nanotubes as oil additives has been reported to reduce the friction in base oil. Figure 1.10(a) shows the TEM image of MoS_2 multiwall nanotube structure. As shown in Figure 1.10(b-c), nanotube-assisted oil lubricant (PAO+NT) has lower friction coefficient and superior

anti-wear properties than pure base oil (PAO).[44] Changsheng Li and coworkers have studied the synthesis and tribological properties of flower-like MoS_2 microspheres, indicating flower-like MoS_2 possessed better properties in reduce friction and wear than commercial MoS_2 plates.[45] The magnificent lubricating behavior of MoS_2 additives in base oil is raised from its layered structure and deformation into thin films during sliding.

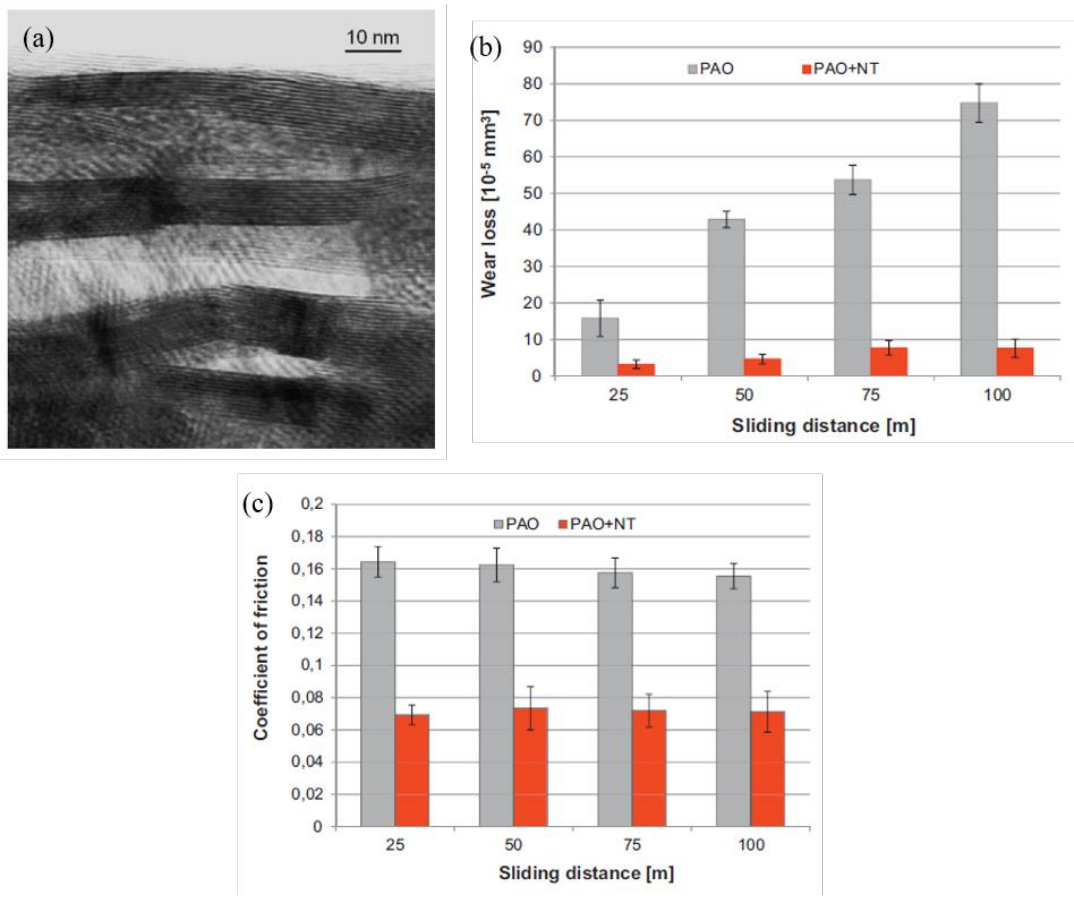

Figure 1.10 (a) TEM image of MoS_2 nanotubes. (b) Wear loss for base oil and base oil with MoS_2 nanotubes. (c) Friction coefficent for base oil and base oil with MoS_2 nanotubes. Adapted with permission from Kalin *et al.* [44] Copyright 2012 by Elsevier.

1.3.2 Use of atomically thin MoS_2 as boundary lubricants in nanoscale

Exploring the tribological properties of MoS_2 in nanoscale drew tremendous attention due to the development of micro-devices and its potential application in nano electronic devices.[44, 46-48] Additionally, monolayer MoS_2 has outstanding mechanical properties with high stiffness (180 ± 60 Nm^{-1}) and breaking strength (15 ± 3 Nm^{-1} or 23 GPa).[49] It has been reported in tribological studies that even a single layer of MoS_2 can reduce the surface friction a lot, due to its low frictional coefficient. The frictional response of MoS_2 sheets in nanoscale is influenced by multiple factors. Examples are layer thickness and roughness of substrates. Using exfoliation method for the preparation of atomically thin MoS_2 flakes on a SiO_2 substrate makes them loosely adhere to the surface. As shown in Figure 1.11(b), it was observed that the friction of MoS_2 nanosheets increases with decreasing layer thickness.[24] In the case of MoS_2 on SiO_2, because of the low interfacial adhesion and the out of plane flexibility of these nanoflakes, it will cause "puckering effect" while the AFM probe sliding on the materials (Figure 1.11(a)). And the friction enhancement is higher for thinner layer area, where the sliding probe induces larger out-of-plane deformation, leading to a larger contact area and thereby a larger friction.[24] A study using simulations has illustrated the true contact area between the tip and graphene surface that governs the frictional response on the grapheme sheet. The simulations showed that a larger contact area was related to larger friction, and was correlated with puckering effect. However, the change in contact area is smaller than the increase of friction (Figure 1.12). Therefore, the increase in friction cannot only be attributed to the changes of contact area caused by

puckering of the graphene surface. It was revealed in their study that the interface between tip and graphene became slightly more commensurate and the local pinning was enhanced with each slip of the AFM probe, and finally reached a stable value. This variation of overall commensurability and interfacial pinning considerably account for the layer dependence of friction.[50] From all the studies above, it can be concluded that the interfacial adhesion impacts the commensurability and hereby influences the stick-slip motion.

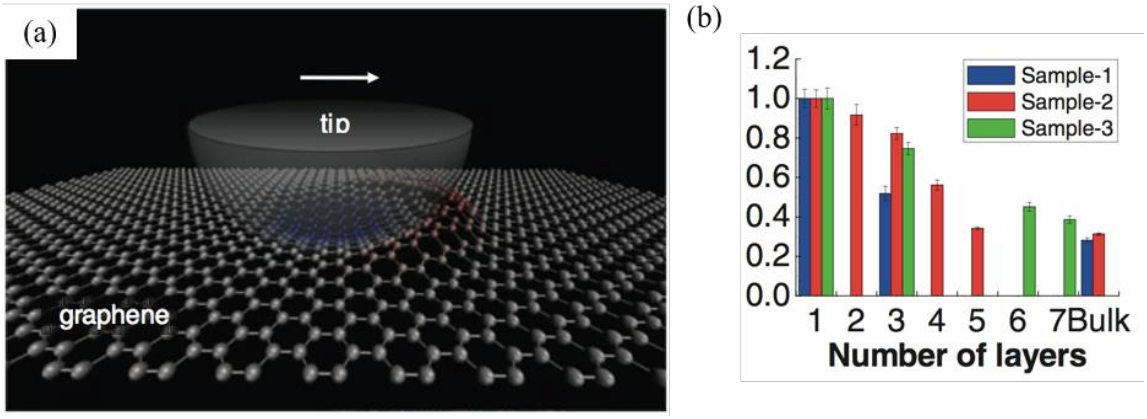

Figure 1.11 (a) Schematic showing the "puckering" effect. While AFM tip is canning on the graphene surface, graphene sheet formed ripples in front of the tip. (b) Friction on MoS_2 nanoflakes with different layer thickness. The friction signal is normalized to the value obtained for the thinnest layer. Adapted with permission from Lee *et al*.[24] Copyright 2010 by AAAS.

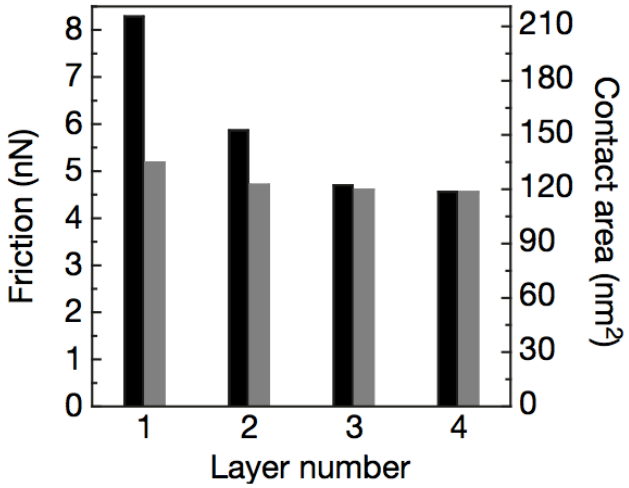

Figure 1.12 Variations of averaged friction (black) and contact area (grey) as a function of graphene layers. Adapted with permission from Li *et al.* [50] Copyright 2016 by Macmillan Publishers Limited, part of Springer Nature.

A further tribological study of MoS_2 deposited on atomically flat substrates (mica and h-BN) shows different sliding friction compared to MoS_2 nanosheets on silica surfaces. J. Quereda, et al. used mechanical exfoliation method to deposit MoS_2 on h-BN and mica substrates, AFM was subsequently used to measure the surface roughness and the friction on MoS_2 layers. It was revealed that MoS_2 monolayers transferred on mica and h-BN had a roughness about 50% lower than MoS_2 deposited on SiO_2. The friction of single layer MoS_2 on mica and h-BN is lower than that on SiO_2. However, the value of friction is not simply based on the surface roughness (Figure 1.13a). As shown in Figure 1.13b, even if the roughness of MoS_2 on h-BN is very similar to that of bulk MoS_2, the friction force is five times larger. Their work indicated that the friction of MoS_2 layers on substrates could be strongly tuned by the MoS_2-substrate interaction.[51]

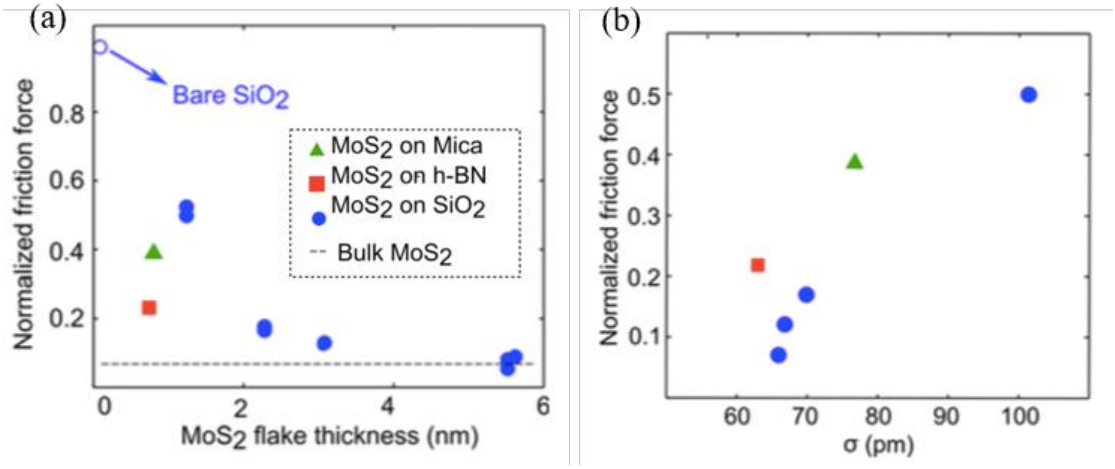

Figure 1.13 (a) Normalized friction force measured by AFM with various flake thickness for bulk MoS_2 and MoS_2 flakes on Mica (green), h-BN (red) and SiO_2 (blue). (b) Friction force of MoS_2 single layers as a function of the surface roughness. Adapted with permission from Quereda *et al.*[51] Copyright 2014 by AIP Publishing LLC.

Studies have also shown that similar to graphene, frictional properties on MoS_2 is also angle dependent due to changes of energy barrier throughout MoS_2 surface.[52-53] Simulation studies have elucidated that the potential energy on the topmost layer of MoS_2 is not uniform.[53-54] It has been reported by Tasuku Onodera and coworkers the friction at MoS_2/MoS_2 interface is anisotropic.[53] The misfit angle dependency of friction was investigated and it was found that the friction at the zigzag sliding motion is 100 times larger than the friction at smooth sliding motion. In another study executed by Levita and coworkers on the study of energy barriers on MoS_2. As shown in Figure 1.13(a), two layers of MoS_2 stack together with slightly shifts along y-axis to show the bottom layer. "2L-R180" was obtained by rotating top MoS_2 layer in "2L-R0" with 180° around z-axis. Figure 1.13(b) shows the 2D potential energy surfaces, illustrating that at R0 sliding mode, there is very little difference between load 0 and 10 GPa. However, at

R180 sliding mode, the potential energy surface is load-dependent: Highest potential energy region at zero load appears to be volcano-like shape at 10 GPa applied load. That is because of a lower energy enhancement of the Max structure compared to its shoulder. This phenomenon is also proven in Figure 1.14(c). [55] From all the studies before, it can be concluded that potential energy drops from on the top of S atoms to in between the S atoms, which means that going over S atoms on the surface will be more difficult and requires more energy than sliding between sulfur atoms. At different scanning directions with an AFM probe on MoS_2 crystal surface, it can be figured that the energy barriers the probe need to go over can also vary. At the MoS_2/MoS_2 interface, because the atom periodicities are the same, the incommensurate and commensurate scanning will have a very different magnitude of the friction at MoS_2/MoS_2 interfaces.

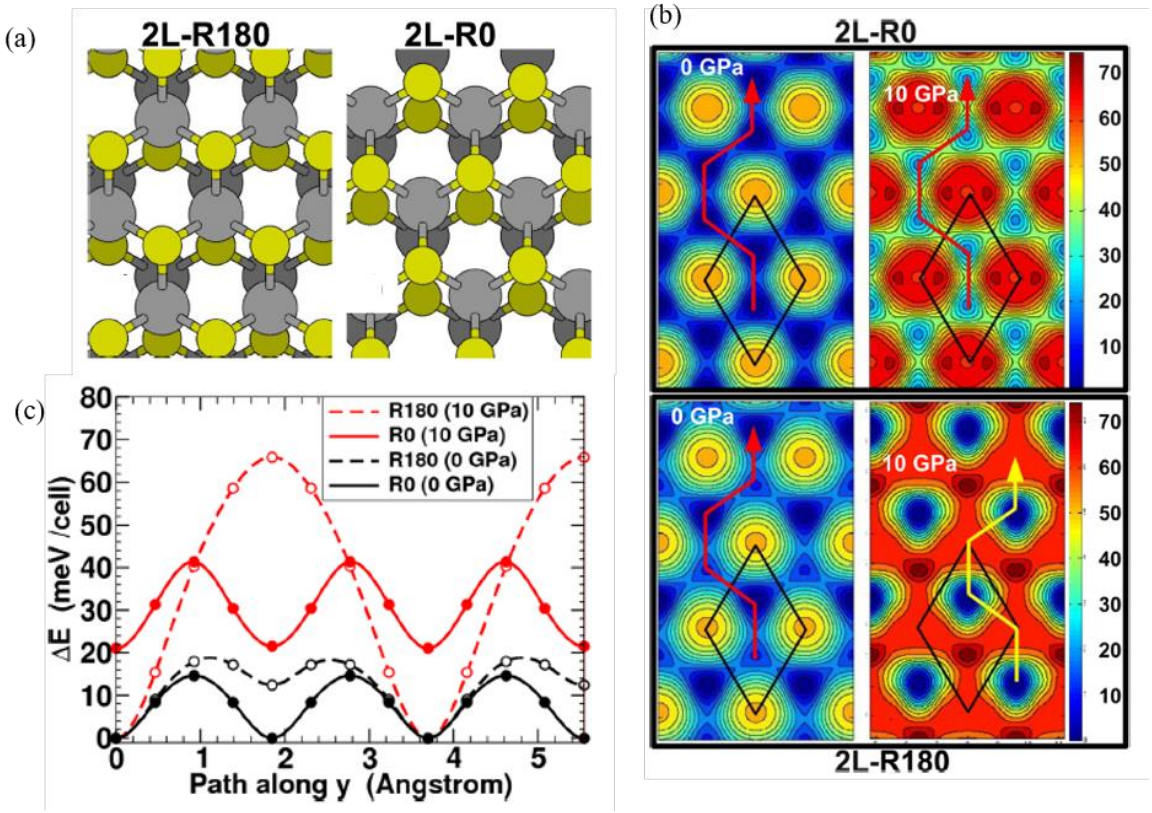

Figure 1.14 (a) Schematic of two MoS_2 layers put together either in R180 or in R0 configuration. Dark color is used for representing lower S-Mo-S layer. (b) Heat map showing the potential energy at MoS_2/MoS_2 interface for sliding motion in R0 (upper two images) and R180 (lower two images). Both loads at zero load and 10 GPa load were studied. Unit cells are demonstrated with black lines and red/yellow lines illustrate minimum energy paths. (c) Energy profiles show the minimum energy paths that refer to the paths shown in (b). The energy profiles compare the minimum energy paths for MoS_2/MoS_2 sliding motion R0 (solid lines) and R180 (dashed lines) at applied load 0 and 10 GPa. Adapted with permission from Levita *et al.*[55] Copyright 2014 by ACS Publications.

Above we talked about layer thickness, roughness of substrate, and scanning direction can be used to tune tribological properties of atomically thin MoS_2 nanosheets. Other studies have also shown that more factors also effect its frictional properties. Water plays a significant role in the sliding behavior on MoS_2 film.[56-58] Xueying Zhao

and coworker have shown that humidity influences the friction coefficient of MoS_2 film.[56] As shown in Figure 1.15, friction coefficient gets larger with increasing humidity at Si_3N_4 – MoS_2 interfaces. Other factors such as strain[59-60] and scan speed[61] have been reported to have influence on the friction of MoS_2 surface.

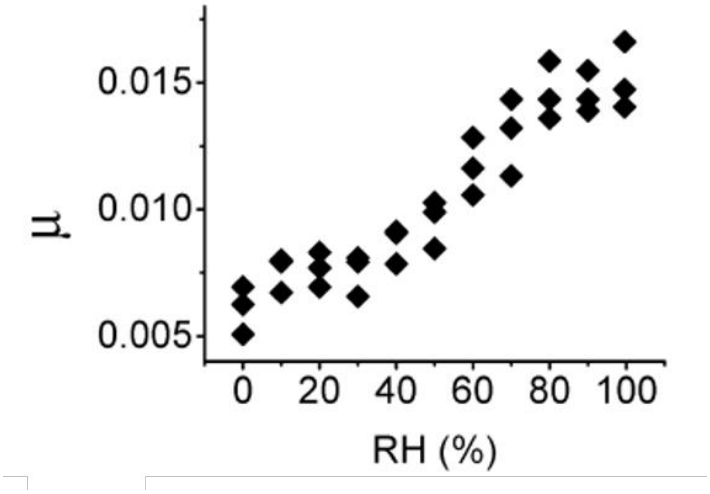

Figure 1.15 Friction coefficient (μ) as a function of relative humidity (RH) on MoS_2 surface with a Si_3N_4 tip. Adapted with permission from Zhao *et al.*[56] Copyright 2010 by ACS Publications.

1.4 Instrument: Atomic force microscopy (AFM)

As one of the instruments in scanning probe microscopy family, AFM is invented by Binning and others in 1986.[62] AFM is usually used to get high resolution (even atomic resolution) images from the sample surface. There are other instruments that can be used to get high resolution images of samples. Examples are scanning electron microscopy (SEM), transmission electron microscopy (TEM) and scanning tunneling microscopy (STM). Scanning electron microscopy requires conductive samples.

Transmission electron microscopy requires samples to be extremely thin (usually less than 100 nm), making sample difficult to prepare. Scanning tunneling microscopy (STM) was invented before AFM. STM is also a kind of scanning probe microscopy that can be used to obtain topography and density of states from the surface of materials. As shown in Figure 1.16,[63] in STM, a sharp conductive probe is used to scan the surface line by line. A bias is applied between tip and sample and in constant current mode, the feedback loop maintains constant tunneling current between tip and sample. Topography, electronic properties, and atomic resolution images can be extracted from the sample surface. Although STM can get high resolution images from the surface, it can only be used for conductive samples and when measuring polymer samples, polymers typically need to be nicely coated on a substrate to get high resolution images.

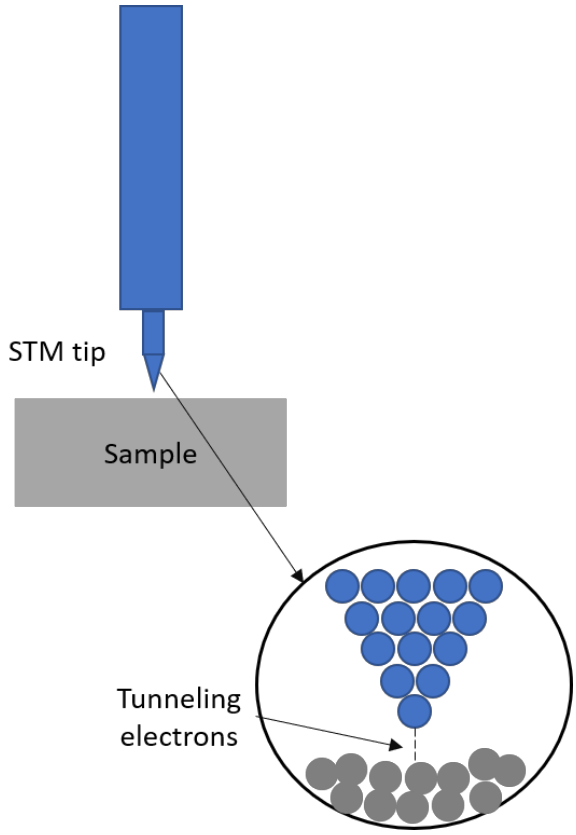

Figure 1.16 Diagram of scanning tunneling microscope. A sharp probe is used to scan the surface line by line. Tunneling electrons transfer between tip and sample surface.

AFM overcomes all the limitations listed above. It is suitable for the measurement of both conductive and insulating samples. In addition, it does not need ultrathin samples. AFM is widely used in engineer disciplines as well as science fields. The setup of AFM is shown in Figure 1.17, similar to STM, a sharp probe is mounted at the edge of a cantilever and is employed to scan the sample surface. However, the tip can be either conductive or nonconductive. A laser is reflected at the end of the cantilever onto a photodetector and topography images can be obtained with AFM. When AFM tip slides on the surface and encounters a protrusion, Figure 1.18 indicates

that at that time, laser spots on the photodetector moves up. As a result, feedback loop moves the tip up, keeping the laser spot in the middle to maintain a constant force.

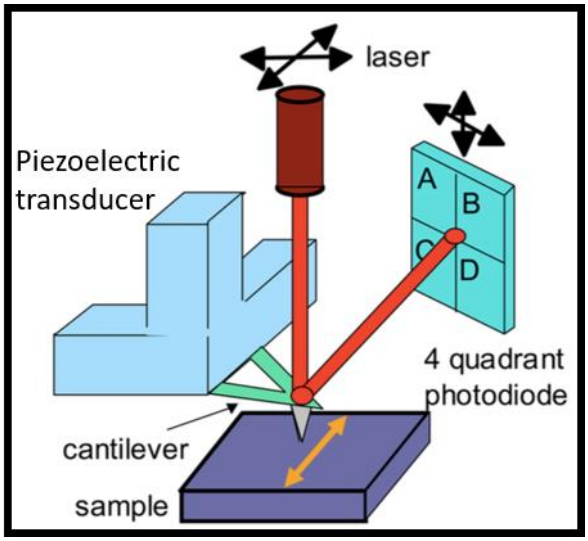

Figure 1.17 Diagram of atomic force microscope. A sharp probe is mounted on the cantilever. Laser is reflected at the back of the cantilever onto a photodetector. Adapted with permission from Park, *et al*.[64] Copyright 2013 by ACS Publications.

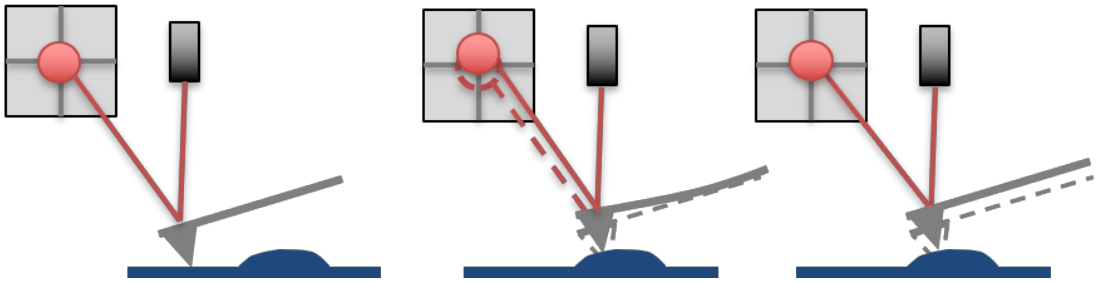

Figure 1.18 Schematics showing the up movement of laser spot on photodetector when an AFM tip encounters a protrusion on the surface. Feedback loop bring the tip up to maintain a constant force between tip and sample surface.

Frictional information of surface can also be measured with AFM. As shown in Figure 1.19, while the tip scans on the surface in contact mode, because of the static and kinetic friction between sample and tip, there is a torsional deformation of the cantilever, making the laser spot on photodetector moves left or right. The magnitude of the movement distance indicates the friction signal. Friction image is usually sensitive to the chemical composition of the surface due to variations of friction for different materials.

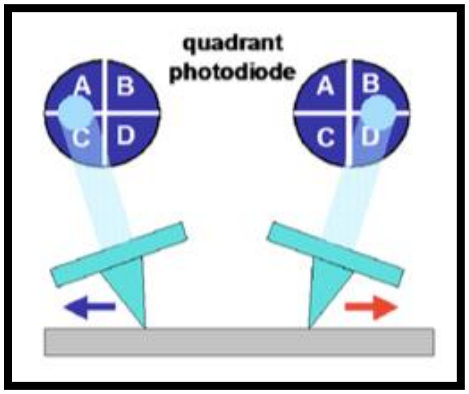

Figure 1.19 Image showing the torsional twisting of the cantilever when AFM scans in contact mode. As a result, the laser spot on photodetector moves left and right. Adapted with permission from Park, *et al*. [64] Copyright 2013 by ACS Publications.

The raw friction signal obtained from experiment is in volt. To convert that signal to force unit (newton), different lateral force calibration methods have been explored. One of the most commonly utilized methods is called "wedge method", in which a substrate with two well-defined slopes is employed.[65-67] To use this method, friction loops were measured by sliding the tip across the slopes. The tilt angle of the facet and width of the friction loop were used to calibrate the lateral force of AFM. Another simple lateral calibration method is direct force balance method (DFBM). In

this method, similar to wedge method, two well-defined slopes are also employed. However, instead of getting friction loops, force distance (FD) curves are obtained and the slopes in the friction force vs. distance curves are compared to determine the lateral detector sensitivity (Figure 1.20).[68-69] This method is useful for protecting AFM tips since it does not require friction loops that are obtained from scanning the surfaces.

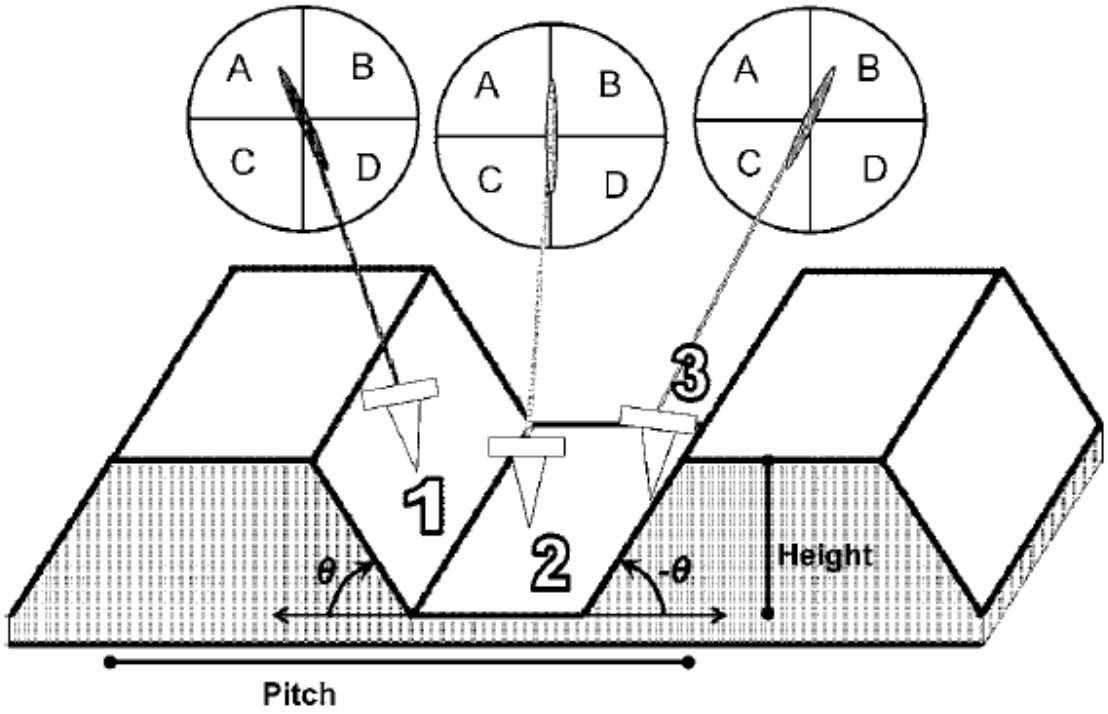

Figure 1.20 Substrates with known slopes are used in the lateral calibration of AFM. The trace on the photodetector showing the beam path of the laser during FD curve measurements on three different facets are illustrated. Adapted with permission from Asay, *et al.* [68] Copyright 2006 by American Institute of Physics.

1.5 Outlook

Reducing friction and wear with lubrication is critical for energy saving and extending lifetime of devices. Exploring new additives and boundary lubricants that can

be used under different conditions is a study people can perform. Simulation is also a good method for predicting the behavior of materials and explaining the mechanism for certain behavior of materials. Tailoring the friction with modulating the surface interactions and changing the chemistry of materials is promising for using these materials in real applications. In addition, heterostructures made from more than one 2D materials is also a way for tuning friction, making it different from the original 2D materials. Combining 2D materials with organic compounds might also be a way for expanding the use of these lubricants in different environments. Common 2D materials including graphene, TMDs and h-BN have been investigated on their tribological properties in recent years. Newly grown 2D materials such as MXene have been discovered and investigation of their tribological properties might open access to broader applications.

CHAPTER II

TUNING THE MECHANIAL AND FRICTIONAL PROPERTIES OF MOS_2 WITH NANOSCOPIC ROUGHNESS AND SURFACE CHEMISTRY*

2.1 Introduction

MoS_2 is a layered material that can be used as boundary lubricant for minimizing friction and alleviate wear.[70-73] Monolayer graphene was reported in 2004[74] and stimulated tremendous interests in researches of thin layer and even single layer MoS_2 recently. As a two-dimensional material, MoS_2 can be exfoliated down to a monolayer. Changes in optical properties influence Raman and photoluminescence spectra of MoS_2 with different layers. Previous studies indicated that atomic displacements of E_{2g}^1 (~383 cm^{-1})and A_{1g} (~408 cm^{-1})modes in MoS_2 were observed in Raman spectra near 400 cm^{-1}.[75-76] Raman spectra can be used to indicates layer thickness of MoS_2 with the distance of E^1_{2g} peak and A_{1g} peak. With thicker MoS_2 layers, the distance between two Raman peaks increases.[55, 77-78] Figure 2.1(a) indicates the shifts of Raman peaks with MoS_2 layer thickness. With increasing layer numbers, E^1_{2g} peak was detected to have a red shift and A_{1g} peak was observed to have a blue shift. The shifts A_{1g} of peak to higher frequency is because that the Van der Waals force between MoS_2 layers suppresses atom vibration with greater layer thickness. Meanwhile, the structure change induced by stacking in

---

* Part of this chapter is adapted from Elinski, M. B.; Liu, Z.; Spear, J. C.; Batteas, J. D., 2D or not 2D? The Impact of Nanoscopic Roughness and Substrate Interactions on the Tribological Properties of Graphene and MoS_2, *J. Phys. D: Appl. Phys.,* **2017** (50), 103003

multilayer MoS_2 play an important role in the variation of atomic vibration, inducing red-shift in E^1_{2g} peak. [79] Layer thickness of MoS_2 also influences photoluminescence spectra. Figure 2.1(b) elucidates that monolayer MoS_2 shows the strongest PL intensity. Meanwhile, bulk MoS_2 has a negligible PL signal. In PL spectra, there are two peaks A1 (~670 nm) and B1 (~630 nm) that are corresponding to direct excitonic transitions. The strongest PL intensity for single layer MoS_2 is featured with slower electronic relaxation. With outstanding optical properties, monolayer MoS_2 is a promising material that can be used in devices.

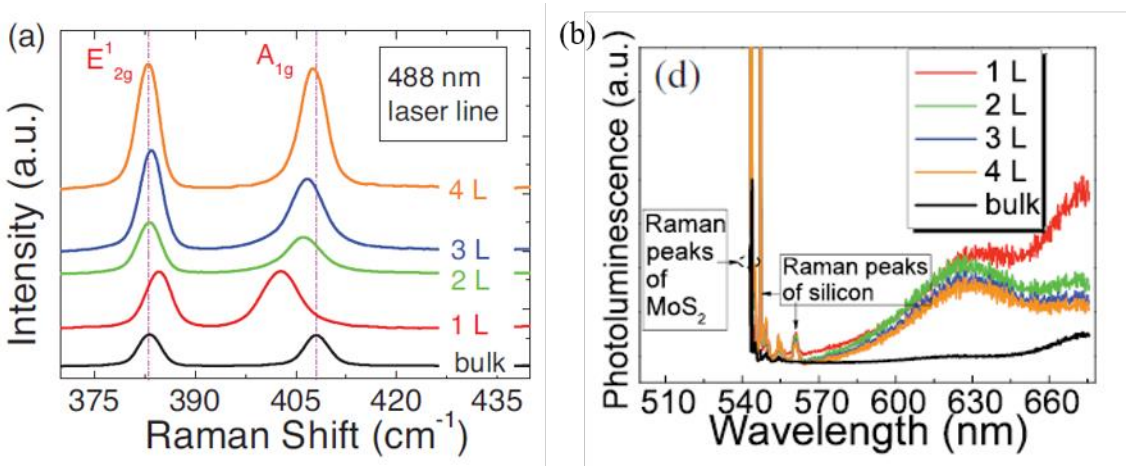

Figure 2.1 (a) Raman spectra of 1 layer (1L), 2 layers (2L), 3 layers (3L), 4 layers (4L) and bulk MoS_2 obtained with a 488 nm laser. (b) Photoluminescence and Raman spectra of MoS_2 layers with different thicknesses. The laser used was 532 nm. Adapted with permission from Li *et al.*[79] Copyright 2012 by WILEY-VCH Verlag GmbH & Co. KGaA, Weinheim.

As it is shown above, the layer thickness of MoS_2 modifies Raman and photoluminescence spectra of MoS_2. Additionally, the strained MoS_2 showed a significant redshift for both E_{2g}^1 and A_{1g} peaks, as shown in Figure 2.2(a). Raman

spectroscopy is sensitive to the strain of MoS_2 because of the phonon softening with increased strain.[76] Moreover, photoluminescence (PL) spectra of MoS_2 are influenced by the degree of strain.[80-82] The intensity of PL decreases with higher strain in monolayer MoS_2. This is because the level of strain affects the band structure and makes a K to K direct transition to a Γ to K indirect transition,[83] as shown in the inserted schematic of Figure 2.2(b).[76] Since the surface roughness affects the strain properties of MoS_2, it is expected to see the changes in PL intensity and shifts of Raman peaks after putting MoS_2 on NPs. Here, we modulate the surface roughness with SiO_2 nanoparticles and the optical properties of MoS_2 flakes on different substrates were studied.

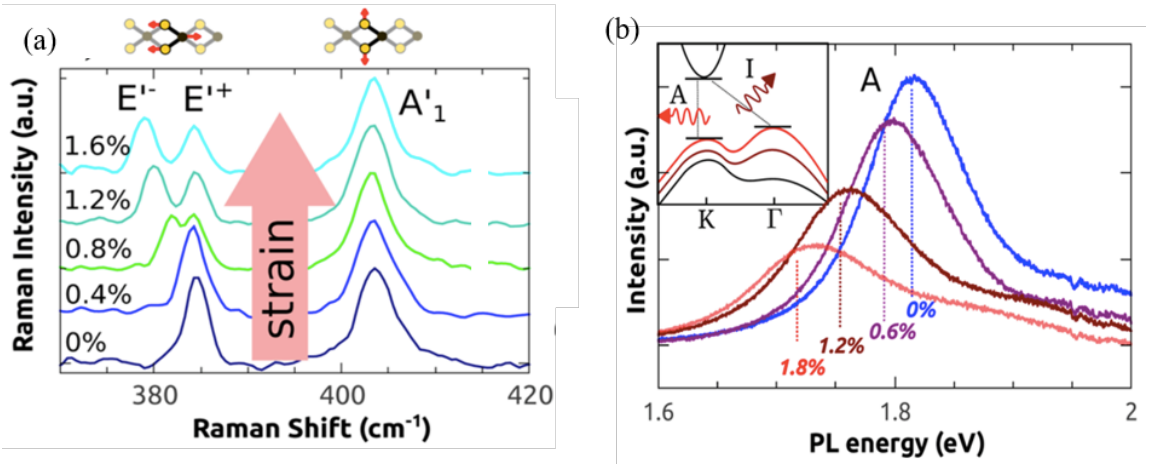

Figure 2.2 (a) Raman spectra of strained MoS_2 from 0 to 1.6%. (b) PL spectra of a monolayer MoS_2 as it is strained from 0 to 1.8%. Inserted schematic represents the band structure for monolayer MoS_2 devices that are progressively strained from 0% (black) to ~5% (maroon) and ~8% (red). Adapted with permission from Conley *et al.* [76] Copyright 2013 by ACS Publications.

Layer thickness of MoS_2 also has influence on the electronic properties of MoS_2. Studies indicates that bulk MoS_2 is a semiconductor with indirect band gap (1.2eV).[84-85]

And single layer MoS_2 has a direct band gap (1.8eV).[83, 86] The transition from indirect band gap to direct band gap makes monolayer MoS_2 a promising material in electronic devices.[87] Therefore it is important to studying the mechanical and tribological properties of monolayer MoS_2.

Changgu Lee and coworkers have done research on the frictional measurements of MoS_2 on SiO_2/Si substrates and found out that the friction is dependent on layer thickness of MoS_2. With thicker MoS_2 layers, friction decreases due to "puckering effect". The adhesive force between MoS_2 and substrate is van der Waals force (relatively small). In addition, MoS_2 is a lamella material with high out of flexibility. These factors induce the deformation of MoS_2 flakes by AFM tip during the scan ("puckering effect").[24] For 2D materials on mica or h-BN with atomically flat surface, friction becomes layer independent because of strong interfacial interaction.[24, 88] Hereby, interfacial interactions play an important role in the modification of the tribological properties of MoS_2 nanosheets.

In real applications, the surface has nanoscopic roughness, which impacts the frictional and electronic properties of atomically thin MoS_2 layers. It has been reported that the morphology of the surface impacts the tribological properties of 2D materials. Grephene on nanoscopically flat silica substrates displays layer-dependence of friction while the friction of graphene on atomically flat mica surface didn't show differences in friction between layers. [88-89] Jessica Spear and coworkers have shown that nanoscopic roughness influences the frictional response of graphene: the layer dependence of friction disappeared for graphene on a 20 nm silica NP film.[89] Although graphene and

MoS_2 are both 2D materials, they have different mechanical properties. The influences of nanoscopic roughness on the mechanical and tribological properties of MoS_2 are not as well studied.

Other than substrate morphology, another factor that impacts the interactions at interfaces is the surface chemistry. Self-assembled monolayers (SAMs) can be used to alter the MoS_2-substrate dipole-dipole interactions, causing changes of the interfacial adhesion. It has been reported that functionalizing the silica substrates with SAMs can reduce the surface energy and maximize the routes of energy dissipation, resulting in the minimization of friction and wear.[90-94] However, rubbing on SAMs induces irreversible damage of the monolayer.[91] Depositing MoS_2 on the top of SAMs prevents molecules from being shaved away while the molecules underneath tune the MoS_2-substrate adhesive force. Bulk MoS_2 is a slightly hydrophilic material with a water contact angle of ~90°, but single layer MoS_2 is more hydrophilic. It has been reported by Philippe Chow and coworkers that monolayer MoS_2 on SiO_2/Si substrates displays an advancing water contact angle of ~ 83°.[95] Therefore molecules with hydrophilic functional group are expected to have larger adhesive force with ultrathin MoS_2 flakes. Xueying Zhao and coworkers illustrate that the friction on MoS_2 surface increases with elevating relative humidity using both Si_3N_4 tip and MoS_2-coated tip. The hydrophilicity of the AFM probe and MoS_2 contributes to larger adhesive forces with higher relative humidity and results in higher friction.[96] Meagan Elinski and coworkers functionalized AFM probes with SAMs terminated with -NH_2, -CH_3, and -phenyl to compare the tip-graphene adhesive force. It was found that -phenyl terminated tip has the largest work of adhesion

with monolayer graphene while -OH terminated tip has the smallest work of adhesion.[97] Thus, using molecules with various functional groups offers a way to control the adhesive force at interfaces, giving rise to the changes of the frictional response of MoS_2 nanosheets on the top of SAMs. As shown in Figure 2.3(a), in this study, MoS_2 was exfoliated onto nanoscopically rough substrates, in addition to non-functionalized and functionalized flat substrates. AFM will be used to investigate the morphology and lubricating properties of MoS_2 on both flat and rough silica substrates and flat substrates with SAMs (Figure 2.3(b)). In addition, Raman spectroscopy was used to determine the number of layers and the strain resulting from the bending of the MoS_2 flakes by analyzing the shifts of the Stokes peaks versus flat MoS_2.

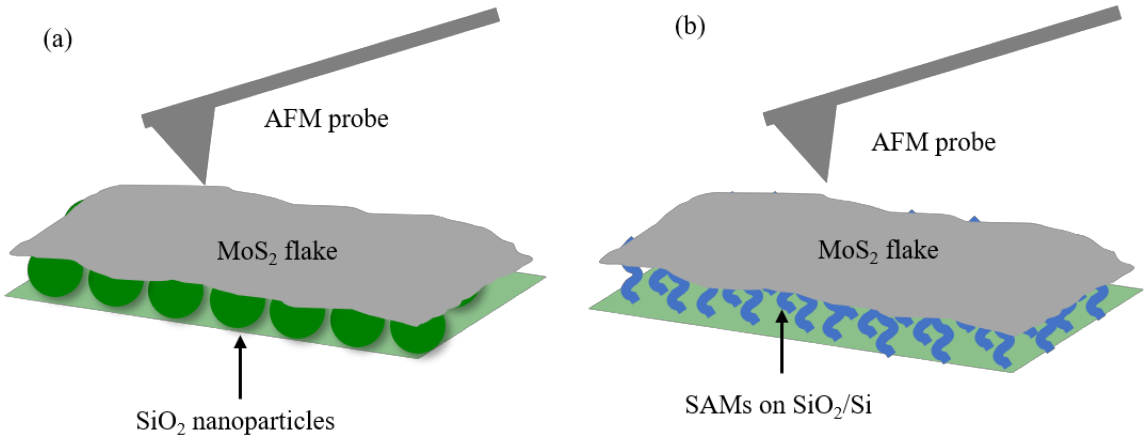

Figure 2.3 (a) Schematic of MoS_2 nanoflake on SiO_2 nanoparticles. (b)Schematic of MoS_2 flakes on SAM modified SiO_2/Si substrates.

2.2 Materials and Methods

2.2.1 Sample preparation

To prepare flat SiO_2/Si(100) substrates, score-cut Si wafers (Virginia Semiconductor) were first cleaned in a base piranha solution of high-purity H_2O (18.2 MΩ cm, Barnstead), H_2O_2 (30%) and concentrated NH_4OH with a ratio 4:1:1 at 85 ^oC for 20 min. Then the wafers were rinsed with high-purity water and ethanol, and dried with streaming N_2. The cleaned wafers were then thermally oxidized in a kiln at 1050 ^oC for 90 min to form 90 nm thick SiO_2 on the surface. Substrates with controlled roughness were prepared by spin coating 20 nm and 50 nm silica nanoparticle solutions on the cleaned silicon substrates. The silica NP solution (Ludox) was diluted from 40 wt% to 6 wt% using high-purity water. The diluted solution was sonicated for 1 hr, and spin coated (400 μL, 2000 rpm for 2 mins) to form a uniform NP film about 90 nm thick.. The rough substrates were then annealed at 500 ^oC for 5 hr. Both the flat SiO_2/Si substrates, and nanoparticle films were cleaned in base piranha again before MoS_2 was transferred onto them. Adhesive tape (Scotch) was used to mechanically exfoliate MoS_2 nanosheets. The tape-MoS_2-substrate samples were annealed at 80 ^oC for 2 min and cooled down to room temperature before peeling the tape off. Heating before removing the tape will release the gas at the MoS_2-substrate interface, increasing the efficiency of transferred material.[98]

To change the polarity of substrates, flat silica substrates were functionalized with either octadecyltrichlorosilane (OTS, Gelest, 95%), or (3-aminopropyl)triethoxysilane (APTES, Aldrich, 99%). The substrates were first cleaned

with base piranha and then rinsed with high-purity water, ethanol and dried with sreaming N_2. The cleaned substrates were put in a molecular solution (0.1 mM) for 7 hr to form a self-assembled monolayer. MoS_2 was transferred onto the functionalized substrates using the same exfoliation method described above.

2.2.2 Fourier transform infrared (FTIR) spectroscopy

A Thermo Nicolet 6700 FTIR with a liquid-nitrogen-cooled MCT (HgCdTe) detector was used to collect IR spectra from the functionalized substrates. A Harrick Scientific horizontal reflection Ge-attenuated total reflection accessory (VariGATR) using a semispherical Ge crystal as the optical element was used in the measurement. Spectra were collected with 1000 scans at a resolution of 1 cm^{-1}.

2.2.3 Raman microspectroscopy measurements of MoS_2 samples

A Raman microscope (Jobin-Yvon HORIBA LabRAM HR800) coupled to an Olympus BX41 microscope equipped with a 514.5 nm Ar ion laser was used to collect both Raman spectra. The measurements were taken in ambient environment and the grating was set to be 1800 gr/mm. The average power of the laser was kept below 10 mW to avoid the burning of SLM.

2.2.4 Photoluminescence of MoS_2 on flat and 20 nm NPs

Photoluminescence maps were collected with a confocal fluorescence (WITec Alpha 300R, Germany) equipped with an Ar ion laser (488 nm) and an Andor Peltier

cooled (−65 °C) CCD detector under room temperature. An objective (Nikon 100×) was used for imaging and spectral acquisition.

2.2.5 Atomic force microscopy measurements of MoS_2 samples

MoS_2 Samples were imaged using AFM (Agilent 5500) with contact silicon tips (Mikromasch CSC37) in nitrogen environment (0.1% RH and 20-25 ^oC). The spring constant of the cantilever was calculated with the Sader method.[99-100] Tip radii were measured by imaging on a Nioprobe sample (Aurora NanoDevices Inc.) three times and the averaged value was used. All the images, tip radii and force distance curves were processed with Scanning Probe Image Processing (SPIP) software (Image Metrology, Denmark). The applied load for the friction measurements was 5 nN unless otherwise stated. The friction data was obtained by averaging the friction signal of 3 scans of the same area measured by the same AFM probe.

2.3 Results and Discussion

It has been reported that the frictional properties of MoS_2 are influenced by the interfacial interactions.[24, 50, 88] Controlling the size of silica NPs and using molecules terminated with various functional groups allow for the tuning of forces at interfaces. To prepare MoS_2 samples on rough and functionalized substrates, an improved exfoliation method was used to make MoS_2 nanosheets more efficiently.[25] The tape-MoS_2-substrate samples were heated before peeling the tape off to increase the transfer yield by releasing the gas at interfaces. MoS_2 nanoflakes were located with Raman microscopy.

Figure 2.4(a) and (c) are the optical images of MoS_2 flakes on a flat silica surface and a 20 nm silica NP film, respectively, which indicates that the samples have clean MoS_2 flakes and even single layer MoS_2 (SLM) have good contrast from the surfaces. Raman microspectroscopy and AFM were further used to study the samples.

2.3.1 Raman spectra and photoluminescence (PL) map of MoS_2 nanosheets on flat and rough substrates

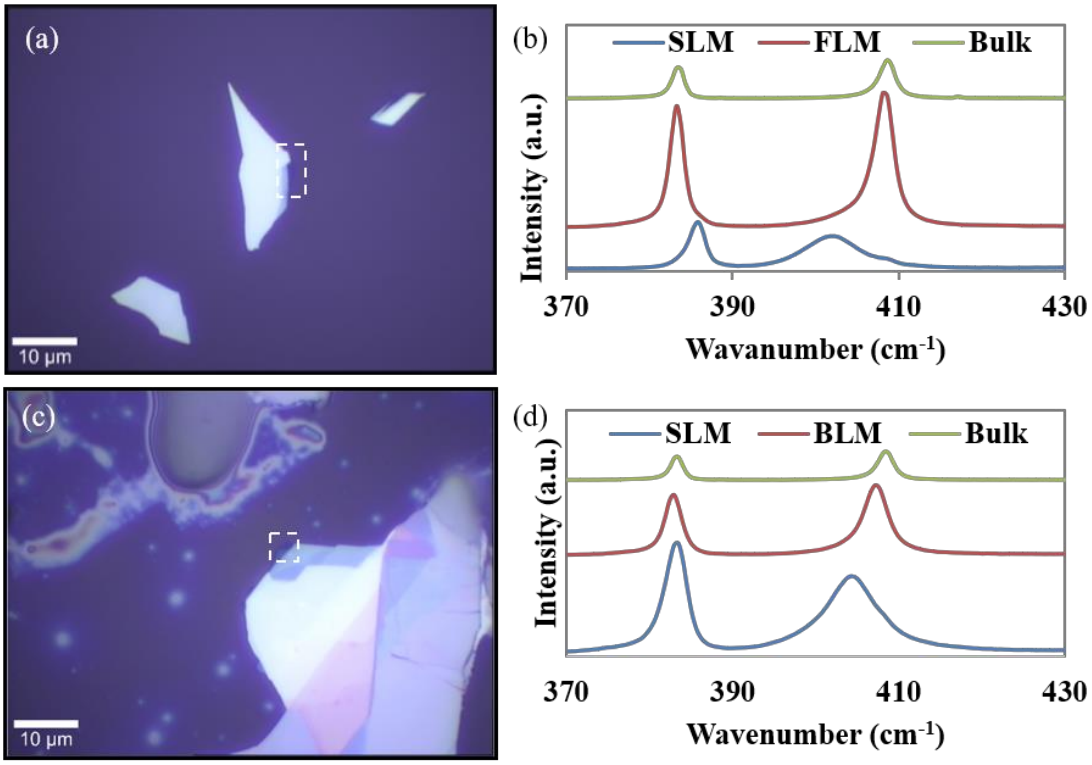

Figure 2.4 (a) and (c) are optical images of MoS_2 flakes on a flat substrate and on a 20 nm NP film, respectively. (b) Raman spectra of SLM, BLM and bulk MoS_2 on flat SiO_2 substrate, indicating a red shift of E^1_{2g} peak and blue shift of A_{1g} peak when the layer thickness becomes greater. (d) Raman spectra of SLM, BLM, Bulk MoS_2 on 20 nm NP film. E_{2g}^1 and A_{1g} peaks correspond to the vibrational modes of the MoS_2 crystal.

To examine the number of layers and the strain of MoS_2, Raman spectroscopy was used to characterize single- and multi- layer MoS_2 flakes. The displacements and distances of E^1_{2g} and A_{1g} peaks indicate the thickness of MoS_2 nanoflakes.[101-103] Raman spectra of SLM, few layer MoS_2 (FLM) and bulk MoS_2 on flat silica substrates were shown in Figure 2.4(b). The distances between the E_{2g}^1 and A_{1g} peaks for SLM, FLM and bulk MoS_2 are 16.38 cm^{-1}, 24.84 cm^{-1} and 25.37 cm^{-1}, respectively. The result agrees with the previous studies that have shown a red shift of E_{2g}^1 peak (around 384 cm^{-1}) and a blue shift of A_{1g} (around 405 cm^{-1}) with the increase of layer thickness[79, 102-103]. Figure 2.4(d) shows the Raman spectra of SLM, BLM and bulk MoS2 on 20 nm NPs, showing the peak to peak distances are 20.98 cm^{-1}, 24.21 cm^{-1} and 24.75 cm^{-1}, respectively. Compared to SLM on a flat surface, SLM on 20 nm NPs experiences a blue shift of theA_{1g} peak to a larger wavenumber by 2.2 cm^{-1} and a red shift of the E_{2g}^1 peak to a smaller wavenumber by 2.39 cm^{-1}. However, according to previous study, the strain of SLM caused the shift of the E_{2g}^1 peak, while the position of A_{1g} peak remains the same within the changes of strain.[76, 104] The shift of the A_{1g} peak in the SLM on 20 nm NPs might be due to the small area of SLM (~1 μm^2) compared to the resolution of Raman spectroscopy (hundreds of nanometers), thus the multilayer MoS_2 around it may impact the peak position of SLM in the Raman spectra. The strain of SLM on 20 nm NPs was estimated to be 0.6% based on the shifts of the E_{2g}^1 peak.[104]

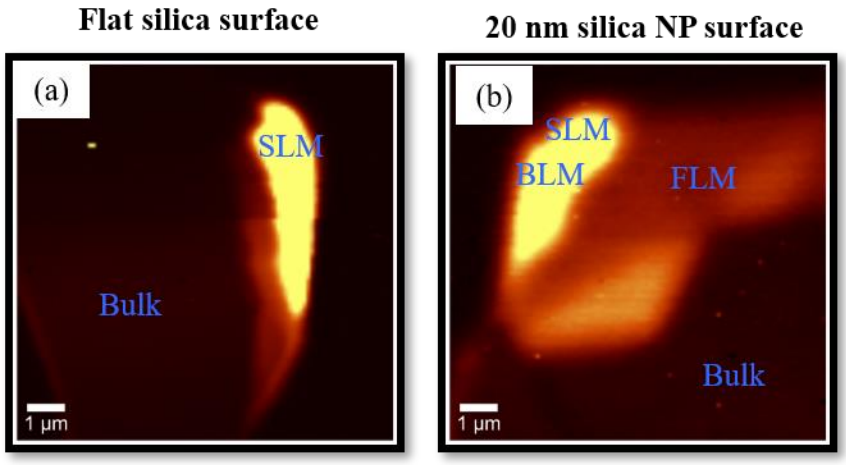

Figure 2.5 (a) and (b) are the PL mapping images of the area in white boxes indicating in the optical images in Figure 2.4 (a) and (c). It can be seen that with thinner MoS_2 layers, the PL intensity becomes higher.

Photoluminescence intensity was explored for MoS_2 flakes on flat SiO_2/Si and 20 nm SiO_2 NP substrates. Figure 2.5(a) demonstrates that on flat surface, with thinner MoS_2 layers, the PL signal becomes larger, which is consistent with the previous studies. For MoS_2 flakes exfoliated on 20 nm NPs (Figure 2.5(b)), both monolayer and bilayer MoS_2 have significantly higher PL intensity than MoS_2 over 2 layers. The reason is that the strain in monolayer MoS_2 induces transition from direct band gap to indirect band gap. Meanwhile, strain results in transition from indirect band gap to direct band gap for bilayer MoS_2.[83] This makes the PL intensity for SLM decreased and for BLM increased. Thus, the PL intensity for SLM and BLM on 20 nm NPs are very close, although the PL signal for SLM on flat surface should be much higher according to previous studies. [76]

2.3.2 The impacts of layer thickness and applied loads on the conformity and roughness of MoS_2

To investigate the changes of interaction forces and frictional properties of MoS_2 with substrates of varyings surface roughness, MoS_2 nanoflakes were made on 20 nm and 50 nm NP films. Topography images (Figure 2.6(a-b)) were obtained using AFM and show that thin layer MoS_2 membrane is partially conformed to the NPs. The line profiles (Figure 2.6(e-f)) from the black lines in the topography images illustrate that the degree of conformity decreases with increase in layer thickness, which is due to the higher stiffness for thicker MoS_2 layers. In addition, the inserted topography image of Figure 2.6(b) illustrates that SLM on 50 nm NPs forms wrinkles on the surface, which were not seen for SLM on 20 nm NPs. The possible reason might be that the space was larger between 50 nm NPs, which makes the AFM probe can press deeper. Another possible reason is that the interaction forces are stronger between SLM and the substrate underneath, causing MoS_2 to conform more on larger NPs.

Different applied loads were used to scan a SLM MoS_2 flake on 20 nm NPs. The morphology images with 5 nN and 125 nN applied loads of the same area are shown in Figure 2.6(c-d). Figure 2.6(g) shows the corresponding line profiles where the red line is for the 5 nN image and blue line is for the 125 nN image. It can be seen from the topography images that the image is sharper for higher applied load. In addition, the line profiles indicate a larger degree of conformity under higher applied load. The MoS_2 membrane was pushed 1-2 nm deeper at 125 nN force, which is close to the deformation of graphene on 20 nm NP film[89], regardless of the different elastic modulus of single

layer MoS_2 (270±100 GPa)[105] and graphene (~1TPa).[106-107] Using the deformation of the MoS_2 membrane at various pushing forces, and a simplistic Hertz model,[108-110] the Young's modulus for SLM was calculated to be ~1 GPa. This value is relatively small compared to the reported Young's modulus for SLM from other sources.[105] However, this value is very close to the calculated Young's modulus of single layer graphene on 20 nm NP film from the work of Spear et al.[89] The possible reason is that when tip pressed on the suspended MoS_2 between NPs, it touched the nanoparticles on the side, which impact the deformation of the MoS_2 nanoflake and the measurements of elastic modulus. From the line profiles, the length of MoS_2 membrane without conformation on the NPs was calculated to be 388.0 nm. At 5 nN, the length of MoS_2 membrane at the measured area was calculated to be 389.0 nm and the length was elongated to be 395.3 nm at 125 nN. The percentage that MoS_2 stretches is 0.2% when using 5 nN applied load to scan on the MoS_2 nanoflake and 1.8% when the applied load elevated from 5 nN to 125 nN. As shown in the supporting information, the stretching of SLM on 50 nm NPs was also studied and the strain of MoS_2 nanosheet was 1.0% and 2.3% when using 5 nN and 125 nN applied load, respectively. The Young's modulus was calculated to be ~1.5 GPa for MoS_2 on 50 nm NPs. The deformation of SLM on nanoparticles is lower than the ultimate tensile strain of SLM (6%-11%),[105] so SLM films didn't break during scanning.

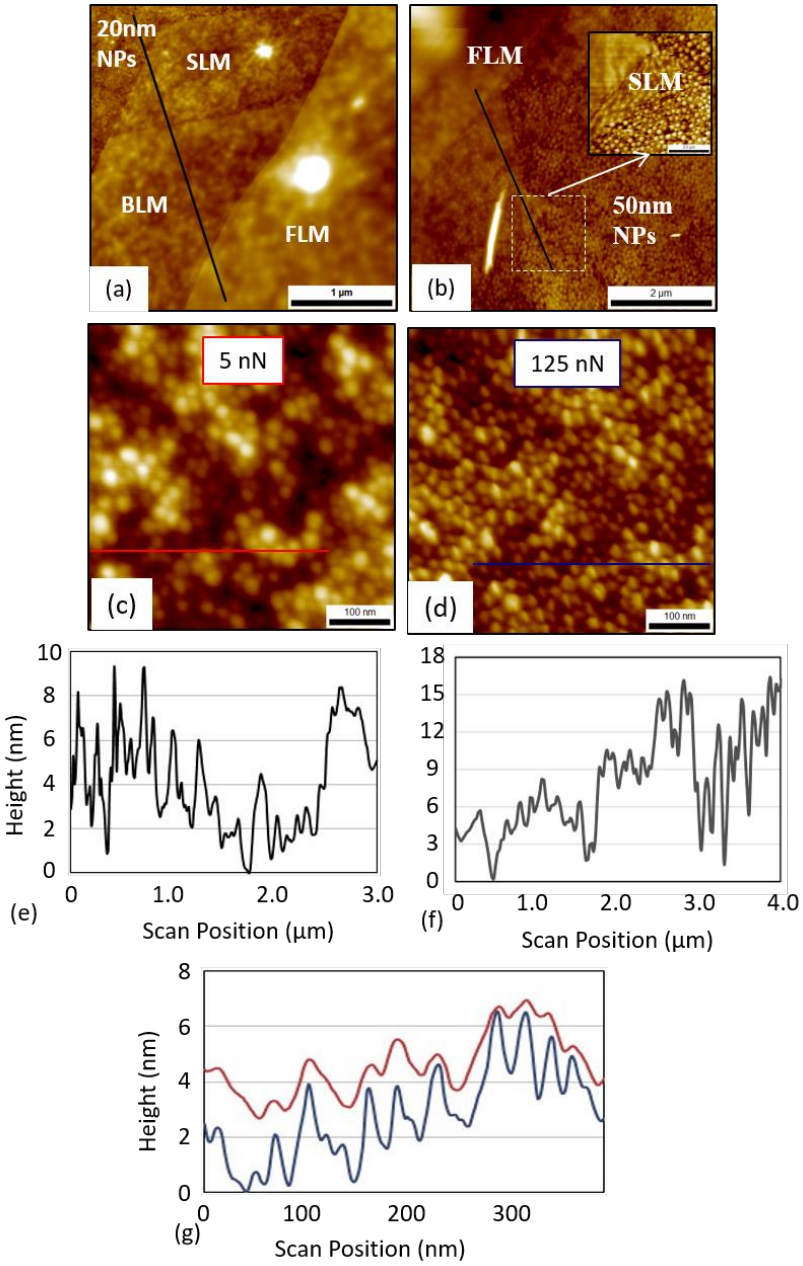

Figure 2.6 (a) The AFM topography image of single and multilayer MoS_2 on 20 nm NPs. The black line is a line profile taken from the surface, as shown in graph (e). (b) The topography of single layer and multilayer MoS_2 on 50 nm NPs. The inserted image is a zoomed-in scan of single layer and bilayer MoS_2. The line proifle was shown in (f). (c) and (d) illustrate the surface of SLM on 20 nm NPs at 5nN and 125nN applied loads, respectively. Line profiles are shown in (g), where the red and blue lines are from (c) and (d), respectively, which reveals that the level of conformity increases with a larger applied load.

Other than making MoS_2 on 20 nm NPs as shown above, exfoliated MoS_2 was also made on a 50 nm silica NP film. The conformity and elastic modulus were studied by AFM. As shown in Figure 2.7(a-b), MoS_2 is partially conformed on the 50 nm NPs and the degree of conformity increases with higher applied loads. According to the stretch of MoS_2 film, the strain was calculated to be 1.0% when using a 5 nN applied load and 2.3% when using a 125 nN applied load. The strain of MoS_2 on 50 nm NPs is larger than that of MoS_2 on 20 nm NPs. That is because of the larger space between 50 nm NPs, so when using 125 nN applied load the tip can press further on the SLM. In addition, because of the larger space between 50 nm NPs, the area of suspended MoS_2 is greater, causing a larger adhesive force between MoS_2 and the substrate. Hereby, the stretching of MoS_2 on 50 nm NPs was larger when using both 5 nN and 125 nN applied load.

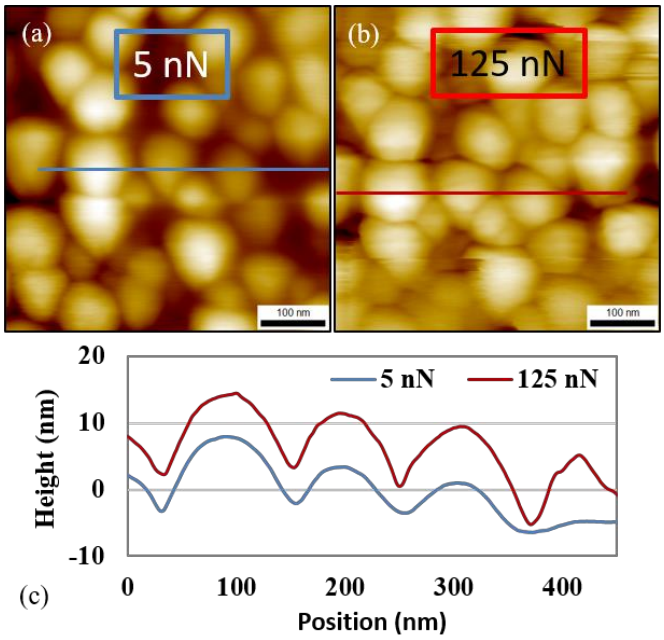

Figure 2.7 (a)-(b) AFM topography images of MoS_2 on 50 nm NPs with scan loads at 5 nN and 125 nN. (c) Line profiles from the blue and red lines in image (a) and (b), showing the stretching behavior of SLM under different applied loads.

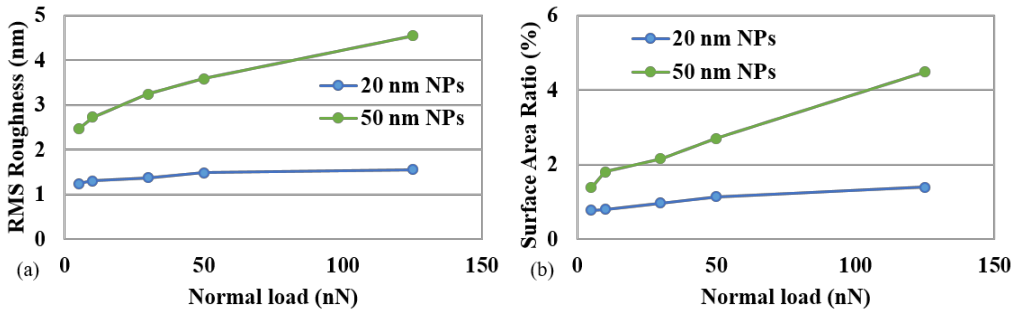

Figure 2.8 (a)-(b) RMS roughness and surface area ratio as a function of the normal load for SLM on 20 nm NP film and 50 nm NP film. The RMS roughness and surface area ratio were averaged over a 0.25 μm^2 scan for each load.

To further investigate the effect of the scanning loads on the surface roughness, the root mean square (RMS) roughness and surface area ratio (%) of SLM on rough

substrates were studied. AFM probes with tip radii of ~30 nm was used to scan exfoliated SLM areas on 20 nm and 50 nm NPs. As shown in Figure 2.8(a-b), SLM showed increased roughness and surface area ratio with higher normal load, indicating the conformity to the rough substrate increased with increased load. It can be seen that, SLM on 50 nm NPs experiences larger RMS roughness and surface area ratio than SLM on 20 nm NPs. This trend is because of the larger degree of conformity for SLM on 50 nm NPs. In addition, the increase of RMS roughness occurred at a slower rate when the normal load became larger due to the larger bending stiffness for strained SLM. From 50 nN to 125 nN, the RMS roughness of SLM on 20 nm NPs only increased 0.07 nm, which indicates the SLM reached its maximum conformity for the size of the tip.

2.3.3 Atomic stick-slip images of SLM and bulk MoS_2 on rough substrates

To investigate the stretch of the crystal lattice of MoS_2 on NPs, AFM was used to collect atomic stick-slip images, and the distances between sulfur atoms was measured. The atomic stick-slip measurements based on the fact that when the tip scans atoms in contact mode, the stick-slip motion causes the tip to oscillate periodically, allowing us to obtain images representative of the periodicity of surface atoms and crystal orientation of the exposed layer. The raw friction images of SLM and bulk MoS_2 are shown in Figure 2.9(a-c), exhibiting the friction signal of forward sliding direction. The friction images demonstrate that the force at which slip occurs on bulk MoS_2 is more organized than that on SLM. This is because of the stretching of SLM pushed by the AFM probe and larger flexibility of SLM. Figure 2.9(d-f) show the corresponding Fourier

transformed images with threefold symmetric pattern,[24, 111] illustrating the sulfur-sulfur (S-S) distances of SLM on top of NPs, SLM in between NPs and bulk MoS_2. The distances of sulfur atoms are taken from three images to calculate the averaged sulfur-sulfur distance of an area. The values are shown in Table 1, which reveals that the average S-S distance is larger for SLM than bulk MoS_2. This is because the stiffness of single layer MoS_2 is lower than that of bulk MoS_2 so SLM can stretch more on the nanoparticles. In addition, the interfacial force of MoS_2-substrate is lower than the interlayer attractive force of MoS_2, so the AFM probe was able to deform SLM more than the top-most layer of bulk MoS_2. The distance between sulfur atoms is the largest for SLM between NPs because of the further deformation of MoS_2 when the AFM tip scanned on the suspended MoS_2. The strain of SLM on NPs and between NPs compared to bulk MoS_2 is 1.9 % and 4.7 %, respectively. These values are larger than the calculated stretch at even 125 nN (1.6%) shown above, which may be caused by the lateral thermal drift of the tip during scanning and the uneven roughness on the substrate.

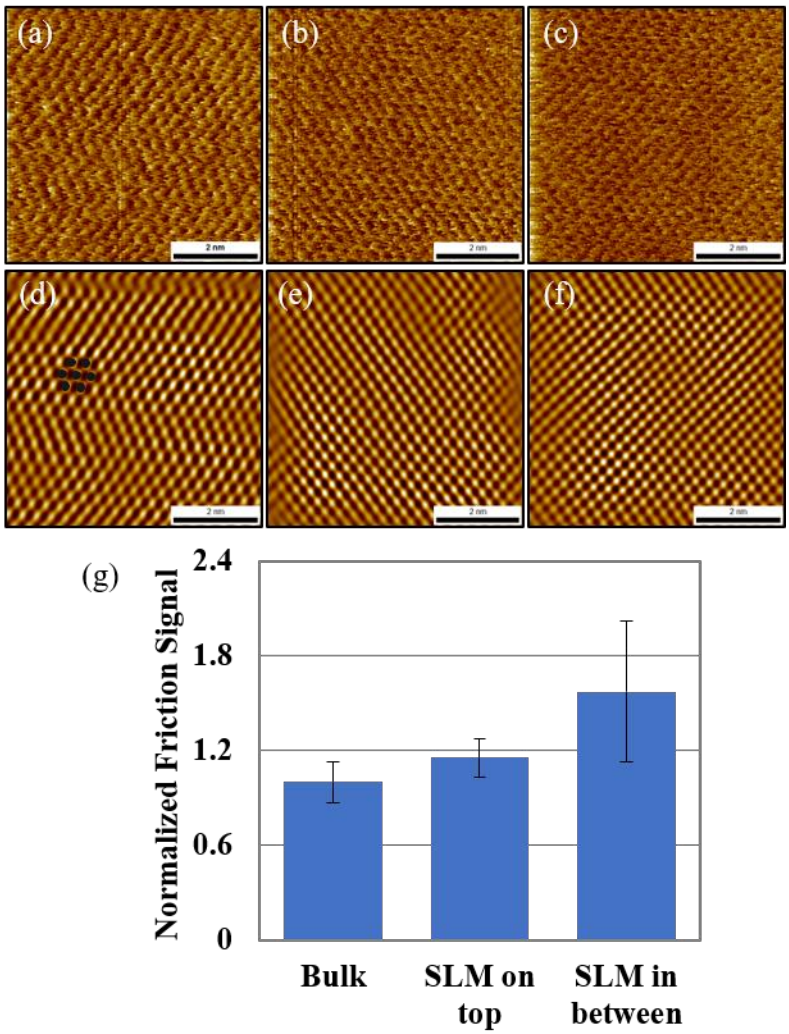

Figure 2.9 (a)-(c) Friction images measured by FFM on bulk-like MoS_2, on SLM suspended between, and on top of 20 nm NPs, respectively. (d)-(f) The corresponding Fourier transformed (FFT) images. (g) The normalized friction signal of bulk-like MoS_2 and SLM, showing the friction is the highest for SLM suspended between NPs.

To figure out the sulfur-sulfur distances and lattice strain of MoS_2 on 50 nm NPs, AFM was used to obtain atomic scale images of the sample. The friction images of bulk MoS_2, SLM on top of NPs and SLM suspended between NPs are shown in Figure 2.10(a-c). The images below are the corresponding filtered images showing the

periodicity of MoS_2 lattice, appearing a threefold symmetric pattern. The friction measurement (Figure 2.10(g)) shows the largest friction on SLM hung between NPs and the lowest friction for bulk-like MoS_2. The friction on SLM suspended between 50 nm NPs is larger than the friction of SLM hung between 20 nm NPs. The possible reason might be the influence of 20 nm NPs on the tip is greater than 50 nm NPs when the AFM probe scanned on the SLM between NPs, making the tip-MoS_2-substrate area greater and resulting in a higher friction during the scan on SLM suspended between NPs. The averaged S-S distances are shown in Table 1. For SLM on 50 nm NPs and suspended between NPs, the strains were calculated to be 4.5% and 6.5%, indicating SLM on 50 nm NPs had larger strain than SLM on 20 nm NPs.

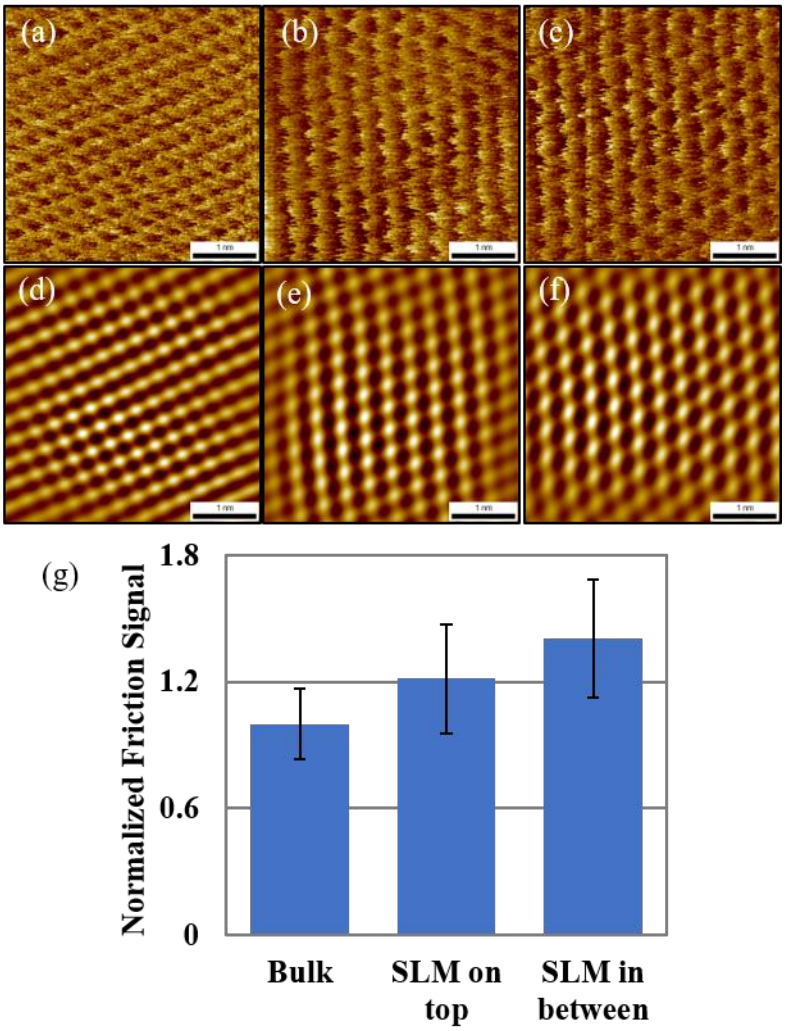

Figure 2.10 (a)-(c) Friction images of bulk-like MoS_2, SLM on the top of 50 nm NPs and SLM suspended between NPs, respectively. (d)-(f) The filtered images correspond to the friction images. (g) The normalized friction signal of bulk-like MoS_2 and SLM on 50 nm NPs. The Frictional signal is normalized to the friction of bulk-like MoS_2.

Table 2.1 Distances between sulfur atoms on bulk-like and single layer MoS_2 measured by AFM.

	Averaged S-S distance (Å) of MoS_2 on 20 nm NPs	Averaged S-S distance (Å) of MoS_2 on 50 nm NPs
Bulk-like MoS_2	3.18 ± 0.16	4.00± 0.10
SLM on top of NPs	3.24 ± 0.20	4.18± 0.13
SLM between NPs	3.33 ± 0.26	4.26± 0.04

2.3.4 Frictional properties of MoS_2 on rough substrates

After studying the conformity and strain of SLM on rough substrates, friction measurements of MoS_2 nanoflakes on rough substrates were also performed using AFM with contact mode silicon tips. The number of layers of MoS_2 was determined by the thickness measured by AFM. The frictional properties were compared between MoS_2 nanosheets on a flat silica substrate, a 20 nm NP film and two 50 nm NP films. The friction images are shown in Figure 2.11(a-c), indicating that MoS_2 can reduce the friction on nanoscopically rough substrates and SLM has higher friction than multi-layer MoS_2. The value of friction was measured on SLM, BLM and bulk MoS_2. Figure 2.11(e) shows the friction signal normalized by the friction of bulk MoS_2 for each sample, demonstrating that the friction decreases with the increase in layer thickness, which is similar to the layer-dependent phenomenon of friction for ultra-thin MoS_2 on flat silica substrates.[24] The possible reason is that asperities on SLM surface will cause more stick-slip motions when the tip scanned the rough surface; resulting in larger friction on thinner MoS_2 layers. Another mechanism is due to the "puckering effect" of the flexible

SLM because the SLM-substrate interaction on rough substrates is smaller than the interaction for SLM on flat substrates, which made the puckering effect easier to occur. These two factors both contributed to the higher friction on thinner MoS_2 layers on rough substrate. When the MoS_2 layers becomes thicker, the RMS roughness drops (Figure 2.11(d)) and the bending stiffness increases, inducing lower friction on the MoS_2 flake. However, the frictional behavior of MoS_2 is different from the frictional properties of graphene on a 20 nm NP film: Graphene on 20 nm NPs did not show a significant frictional difference between single layer graphene (SLG) and bilayer graphene (BLG).[89] That might because of the different stiffness and layer thickness for SLM and SLG. Comparing the friction of MoS_2 on 20 nm and 50 nm NP films, it can be seen that the friction of SLM on 20 nm NPs is larger than its friction on 50 nm NP films despite the larger roughness of SLM on 50 nm NPs (Figure 2.11(d)). The reason might be that there are more asperities within an identically sized area for SLM on 20 nm NPs, which causes more stick slip motions during the scan, resulting in higher friction. The RMS roughness for BLM on 20 nm NPs and 50 nm NPs are very close (Figure 2.11(d)), along with the friction of BLM on these two sizes of NP films. That means the effect of NP sizes was eliminated due to higher stiffness of BLM compared to SLM.

To further study the mechanisms for the layer-dependent of friction, the friction was measured for SLM on top of NPs, SLM in between NPs and bulk MoS_2. The result (Figure 2.10(g)) illustrates SLM on top of NPs has higher friction than bulk MoS_2 due to the deformation cause by the scanning of AFM probe. SLM in between NPs has the highest friction because of the largest contact area between AFM tip and MoS_2

membrane. This result proves that the larger friction of SLM than bulk MoS_2 on NPs is not only because of the larger roughness on SLM surface, but also caused by the deformation of the MoS_2 layer and greater contact area. To figure out the sulfur-sulfur distances and lattice strain of MoS_2 on 50 nm NPs, AFM was used to obtain atomic scale images of the sample. The friction images of bulk MoS_2, SLM on top of NPs and SLM suspended between NPs are shown in Figure 2.10(a-c). The images below are the corresponding filtered images showing the periodicity of MoS_2 lattice, appearing a threefold symmetric pattern. The friction measurement (Figure 2.10(g)) shows the largest friction on SLM hung between NPs and the lowest friction for bulk-like MoS_2. The friction on SLM suspended between 50 nm NPs is larger than the friction of SLM hung between 20 nm NPs. The possible reason might be the influence of 20 nm NPs on the tip is greater than 50 nm NPs when the AFM probe scanned on the SLM between NPs, making the tip-MoS_2-substrate area greater and resulting in a higher friction during the scan on SLM suspended between NPs.

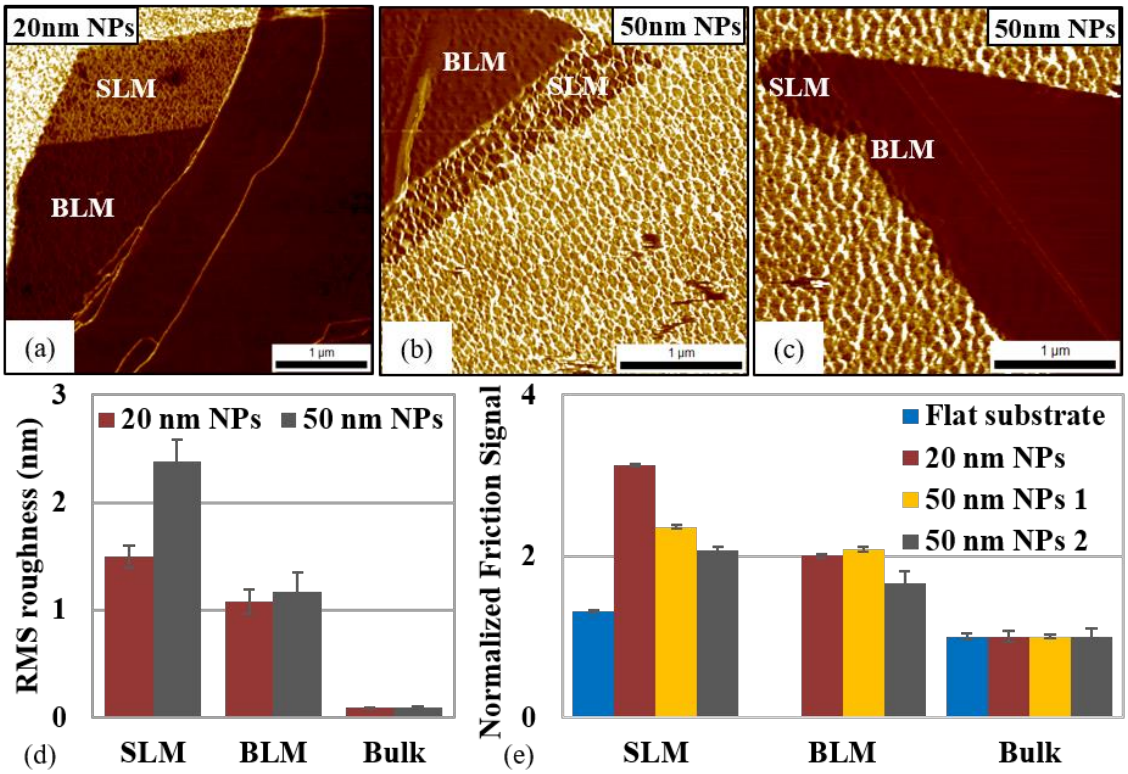

Figure 2.11 (a)-(c) The friction images of single- and multi- layer MoS_2 on 20 nm and 50 nm NP films. d) RMS roughness for SLM, BLM and bulk MoS_2 on 20 nm and 50 nm NP films. (e) The normalized friction signal measured by AFM. The friction signal is normalized to the friction on bulk MoS_2 for each sample.

2.3.5 FTIR of functionalized flat silica substrates

Studies above have shown that the surface roughness influences the frictional properties of MoS_2 nanoflakes. Moreover, since the frictional properties of a supported MoS_2 nanoflake depend on the interfacial interactions, tuning the adhesive force at interfaces might be a useful way to control the frictional response of MoS_2. A method to control the interactions at interface is to modulate the dipole-dipole interactions between MoS_2 and the substrate. Using self-assembled molecules (SAMs) to functionalize the substrates can tune the interfacial interactions.[97, 112-113] Previous studies have shown that

functionalizing probes with various molecules had different adhesive forces with 2D materials,[97] which indicates molecules with various functional groups will affect the adhesive force at MoS_2-substrate interfaces. In this experiment, molecules with different functional groups were used to tune the dipole-dipole interaction at the interface, therefore modulating the frictional properties of supported MoS_2 nanoflakes.

Here, the chemistry of substrates was changed by functionalizing silica surface with APTES and OTS. FTIR was used to identify the molecules on the surface before the transfer of MoS_2. For both the OTS and APTES functionalized substrates, the CH_2 asymmetric (~2920 cm^{-1}) and symmetric (2850 cm^{-1}) stretches of the alkyl chains are shown in their IR spectra (Figure 2.12).

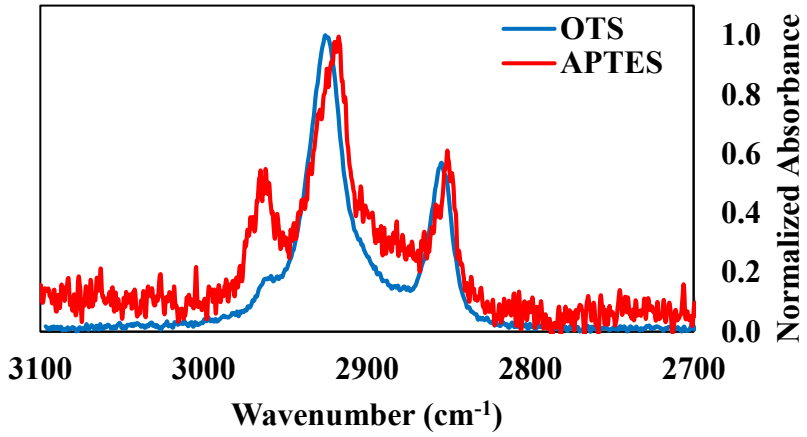

Figure 2.12 FTIR spectra of OTS and APTES functionalized flat SiO_2 substrates. Both molecular films show the CH_2 asymmetric and symmetric stretching band at ~2920 cm^{-1} and ~2850 cm^{-1}, respectively. The spectra are normalized to the CH_2 stretch at ~2920 cm^{-1}.

2.3.6 Frictional properties of MoS_2 on functionalized substrates

Figure 2.13(a-c) are the AFM topography images of single- and multi- layer MoS_2 on unmodified silica substrate, OTS film and APTES film, respectively. Figure 2.13(d-f) are the corresponding friction images, indicating MoS_2 is able to reduce the friction on all the three substrates. As shown in Figure 2.13(g-h), the friction data is normalized to the friction signal of bulk MoS_2 of each sample and exhibits that the APTES and OTS functionalized substrates both have lower friction than bare silica substrates due to the energy dissipation on SAMs. Additionally, the frictional difference between SLM and bulk MoS_2 is more pronounced for MoS_2 on functionalized substrates. The mechanism may be attributed to the smaller adhesive force at SLM-SAM interfaces and the further deformation of SAMs, both resulting in larger shear stress when a tip scans the SLM-SAM composite. Thus, SLM on OTS and APTES films has higher friction than SLM on the unmodified silica substrate.

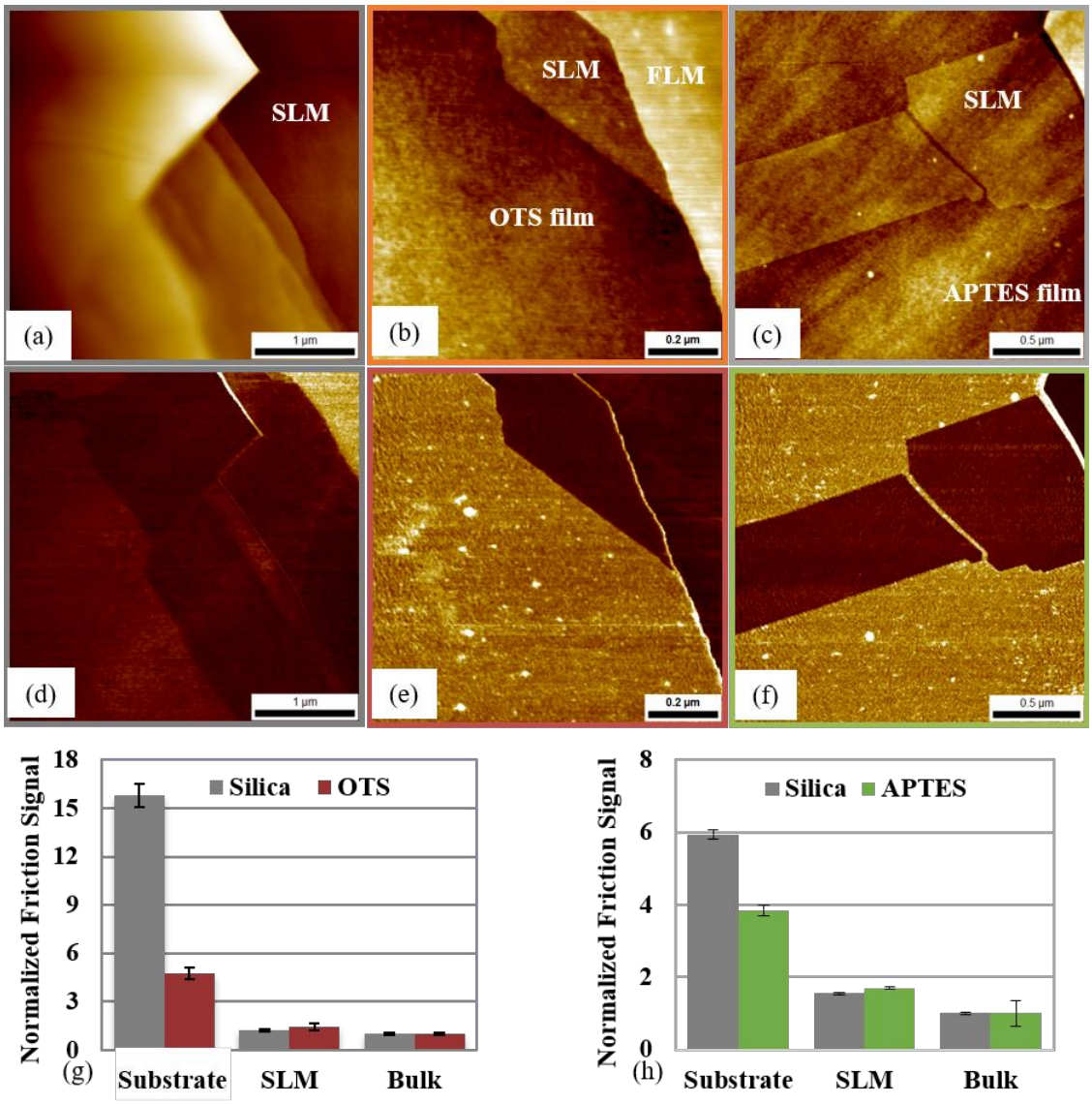

Figure 2.13 (a)-(c) AFM topography images showing single- and multi-layer MoS_2 on silica, OTS and APTES films, respectively. (d)-(f) The corresponding friction images, indicating lower friction on MoS_2 membrane. (g) and (h) The normalized friction signal of MoS2 layers and the substrates.

2.3.7 Raman study of CVD-grown MoS_2 on silica substrate

Studies above have shown studies on atomically thin MoS_2 prepared with exfoliation method. Exfoliated MoS_2 is more pristine and has fewer defects. However,

using exfoliation method to prepare MoS_2 has low production efficiency, which makes it not suitable in real application to make large area membrane. To overcome this limitation, chemical vaper deposition (CVD) method was used for the preparation of ultrathin MoS_2. To study the frictional properties of CVD-grown MoS_2, large area of ultrathin MoS_2 layers were prepared on a flat silica substrate by heating MoO_3 and sulfur powder at 850 ºC for 10 min. Raman spectroscope was used to identify 1-3 layers of MoS_2. As shown in Figure 2.14, it demonstrates the red shift of A_{1g} peak and the blue shift of E_{2g}^1 peak with thicker layers. The distances of peaks on different layers of CVD MoS_2 match the study before,[114] indicating 1 to 3 layers of MoS_2 flakes were successfully made.

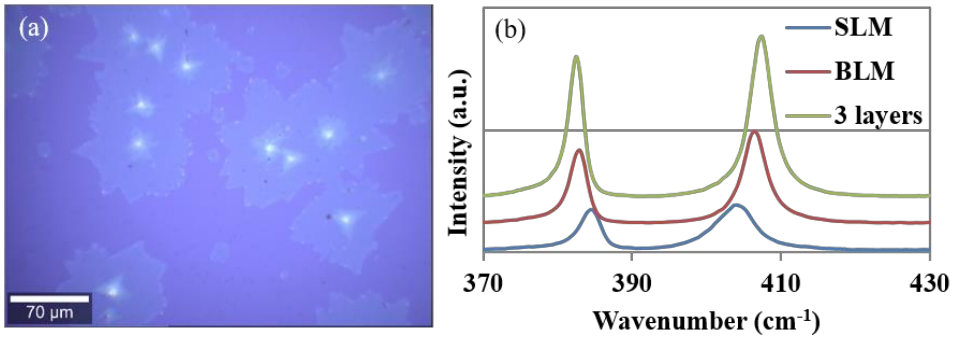

Figure 2.14 (a) The optical image of CVD as-grown single- and multi- layer MoS_2 on a silica substrate. (b) Raman spectra of SLM, BLM and 3 layers MoS_2, showing the shifts of E_{2g}^1 and A_{1g} peaks with the changing of layer thickness.

2.3.8 Friction of as grown MoS_2 on silica substrates by CVD method

According to a study before, CVD-grown MoS_2 adheres more strongly on silica substrate than exfoliated MoS_2 on silica.[19] Since the interfacial interaction affects the frictional response of single- and multi- layer MoS_2, AFM was used to study the friction

of CVD as-grown MoS_2 on silica surface to see if there is a difference compared to MoS_2 made by exfoliation method. As shown in Figure 2.15, the friction on CVD-grown MoS_2 also shows a reducing friction with the larger layer thickness from 1 to 5 layers for both sample-1 and sample-2, which means that the interfacial interaction between CVD as-grown MoS_2 and silica substrate is not high enough to overcome the "puckering effect" during the scan of AFM probe.

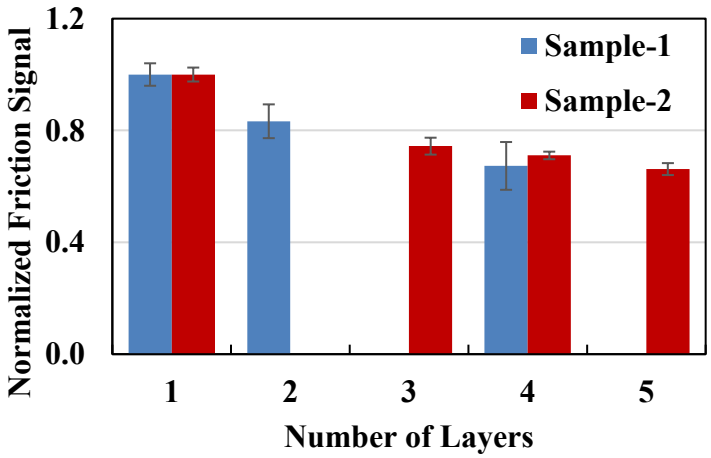

Figure 2.15 Friction measurements of ultrathin CVD-grown MoS_2 with AFM. It shows that the averaged friction on CVD-grown MoS_2 is dependent on layer thickness.

2.4 Conclusion

In summary, MoS_2 nanoflakes were prepared on nanoscopically rough substrates and functionalized silica substrates using the mechanical exfoliation method. Atomically thin MoS_2 flakes were found to be partially conformed on nanoscopically rough substrates and the degree of conformity depends on the layer thickness and applied loads. SLM stretched on rough substrates causes the occurrence of lattice strain. Friction

measurements illustrate a higher friction value for SLM on 20 nm NPs than on 50 nm NPs, which may be due to the presence of more asperities within acertain identical sized area. AFM atomic stick-slip images reveal the stretch of the lattice, which is caused by the deformation of SLM on rough substrates and the pushing of the AFM tip. The friction measurements of single- and multi- layer MoS_2 on OTS and APTES functionalized substrates showed a more pronounced frictional difference between SLM and bulk MoS_2 than MoS_2 on an unmodified flat substrate due to the greater shear stress at tip-SLM interfaces. This study contributes to an in-depth understanding of MoS_2-substrate interactions by investigating the influence of surface morphology and chemistry on the lattice strain and frictional properties. Minimizing the surface friction with MoS_2-SAM composites is expecting be a better method than just MoS_2 nanoflakes because of more energy dissipation routes and tunable adhesive forces at interfaces. Surface nanoscopic roughness helps mimic the behavior of the materials in realistic applications due to the growing interests in ultra-thin MoS_2-based electronic devices. In addition, it opens the possibility to further affect the electronic and catalytic properties caused by lattice strain.

CHAPTER III

EXPLORING THE FRICTIONAL AND ADHESIVE PROPERTIES OF MOS2 WITH MPTMS AND APTES MODIFIED AFM PROBES

3.1 Introduction

While MoS_2 has been used as a solid lubricant and additives in liquid lubricants to reduce friction and alleviate wear since the 1940s,[70-73] the discovery and study of single layer graphene[74] has stimulated interests in the research of atomically thin MoS_2 in recent years. As a 2D material, MoS_2 can be exfoliated to a monolayer, inducing more interesting optical and electronic properties. Studies have shown that bulk MoS_2 is a semiconductor with an indirect band gap (1.2eV).[84-85] However, when exfoliated to a monolayer, it transitions to a direct band gap (1.8eV).[83, 86] The excellent electronic and optical properties of atomically thin MoS_2 make it a promising material in nanoscale devices such as nanotransistors.[87] Thus, studying its mechanical and tribological properties is important for the use of single layer MoS_2 as a solid lubricant and in nanodevices.

The frictional properties of MoS_2 nanoflakes have been studied on amorphous SiO_2 substrates. Changgu Lee, Qunyang Li and coworkers reported that the adhesive force at the MoS_2-SiO_2 interface is relatively small, so the AFM tip deformed thin MoS_2 layers and caused a larger contact area during the scan ("puckering effect"). The "puckering effect" caused by the high flexibility of thin flakes results in the friction of MoS_2 layers increases with decreasing layer thickness.[24] In the case of graphene on atomically flat surfaces such as mica, the layer dependence of friction disappears due to

the strong graphene/substrate interaction.[24, 88] Furthermore, a study using molecular dynamics simulations has shown that the evolution of interfacial commensurability also contributes to the layer dependence of friction.[50] Thus the interaction at interfaces is an important factor for the modulation of the frictional properties of MoS_2 nanoflakes. Seeking methods for modulating the interfacial interactions will be promising for tuning the friction on 2D materials.

A factor that impacts the interactions at interfaces is the surface chemistry. Self-assembled monolayers (SAMs) can be used to alter the MoS_2-substrate dipole-dipole interactions, causing changes of the interfacial adhesion. It has been reported that functionalizing the silica substrates with SAMs can reduce the surface energy and maximize the routes of energy dissipation, resulting in the minimization of friction and wear.[90-94] However, rubbing on SAMs induces irreversible damage of the monolayer.[91] Depositing MoS_2 on the top of SAMs prevents molecules from being shaved away; meanwhile the molecules underneath tune the MoS_2-substrate adhesive force. Bulk MoS_2 is a slightly hydrophilic material with a water contact angle of ~90^o, and single layer MoS_2 is more hydrophilic. It has been reported by Philippe Chow and coworkers that monolayer MoS_2 on SiO_2/Si substrates displays an advancing water contact angle of ~ 83^o.[95] Therefore molecules with hydrophilic functional group are expected to have larger adhesive force with single layer MoS_2 flakes. Varying the chemistry at interfaces affects the frictional properties of 2D materials. Elinski and coworkers functionalized AFM probes with SAMs terminated with -NH_2, -CH_3, and -phenyl to compare the tip-graphene adhesive forces. It was found that the -phenyl terminated tip has the largest

work of adhesion with graphene while -OH terminated tip has the smallest work of adhesion, indicating that interfacial chemistry influences the friction and adhesion measurements on graphene.[97] Lu and coworkers illustrated that the adhesive force between the AFM tip and MoS_2 was changed by functionalizing the AFM probe with octadecyltrichlorosilane (OTS). For bare silicon nitride AFM probes, the interaction forces on pristine and edge faces were not zero, however, for OTS-coated AFM probes, the adhesive force on the edge face became zero.[112] From the studies shown above, we can conclude that using molecules with various functional groups offers a way to tune the hydrophilicity at interfaces, giving rise to the changes of the adhesion and frictional response at MoS_2/tip interfaces.

In this study, two kinds of molecules shown in Figure 3.1, (3-Mercaptopropyl)trimethoxysilane (MPTMS) and (3-Aminopropyl)triethoxysilane (APTES) were chosen to modify silicon AFM probes by forming a monolayer on the tip and tuning the interactions at MoS_2/tip interfaces. It has been reported that thiol (-SH) groups can form covalent bonds with molybdenum due to defects on MoS_2 flakes[115-117], thus the interaction between -SH terminated molecules and MoS_2 was explored. APTES was chosen to tune the MoS_2/tip interaction as amine ($-NH_2$) groups have strong Lewis acid-base interaction with MoS_2 flakes.[118] In this study, single layer MoS_2 was exfoliated onto SiO_2/Si substrates. MPTMS and APTES were used to change the chemical properties of AFM probes. After that, functionalized AFM tips were used to investigate the lubricating properties of MoS_2.

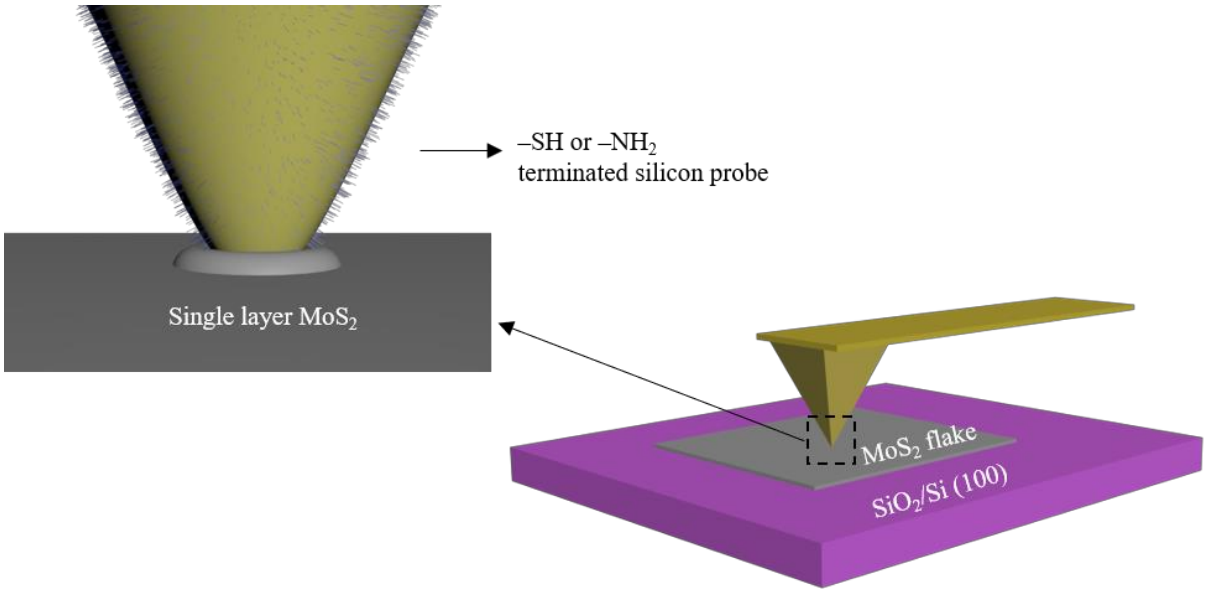

Figure 3.1 The schematic image of functionalized AFM probe on a single layer MoS_2 flake.

3.2 Experimental Method

3.2.1 Sample preparation

To prepare SiO_2/Si(100) substrates with 90 nm thick SiO_2 on the surface, score-cut Si wafers (Virginia Semiconductor) were first cleaned in a base piranha solution of high-purity H_2O (18.2 MΩ cm, Barnstead), H_2O_2 (30%) and concentrated NH_4OH with a 4:1:1 ratio at 85 ^oC for 20 min. Then the wafers were rinsed with high-purity water, ethanol, and dried with streaming N_2. The cleaned wafers were then thermally oxidized in a kiln at 1050 ^oC for 90 min to form 90 nm thick SiO_2 on the surface. The SiO_2/Si substrates were cleaned in base piranha again before MoS_2 (SPI) was transferred onto them. Adhesive tape (Scotch) was used to mechanically exfoliate MoS_2 nanosheets. The tape-MoS_2-substrate samples were annealed at 80 ^oC for 2 min and cooled down to room temperature before peeling the tape off. Heating before removing the tape will release

the gas at the MoS_2-substrate interface, increasing the efficiency of transferred material.[98]

To change the chemistry of AFM probes, silicon tips were functionalized with either (3-Mercaptopropyl)trimethoxysilane (MPTMS, Aldrich, 95%), or (3-aminopropyl)triethoxysilane (APTES, Aldrich, 99%). The tips were first cleaned with base piranha for 40 s and then rinsed with high-purity water, ethanol and dried in air. The cleaned tips were put in a nitrogen tent and the relative humidity was controlled below 0.1%. Here, AFM tips were put in a molecular solution (0.1 mM in toluene) for 12 hr to form a self-assembled monolayer on the surface.

3.2.2 Fourier transform infrared (FTIR) spectroscopy

Silica nanoparticles (20.7 were functionalized in 0.1 mM MPTMS and APTES in toluene solutions and stir for 12 hr to form self-assembled monolayers onto them. The NPs were washed with toluene for one time and ethanol for two times followed by drying in a N_2 tent. A Thermo Nicolet 6700 FTIR equipped with a liquid-nitrogen-cooled MCT (HgCdTe) detector was used to take IR spectra from the functionalized nanoparticles. About 9 mg of the functionalized nanoparticles were mixed in 91 mg of KBr for the transmission IR measurements. Spectra were collected with 256 scans with a resolution of 1 cm^{-1}.

3.2.3 Thermogravimetric analysis (TGA)

The packing density of molecules on silica nanoparticles was explored using a Q-50 thermogravimetric analyzer (TA Instruments). The heating rate was 10 ^{o}C/min from 25 ^{o}C to 800 ^{o}C, and the gas was changed from nitrogen to air at 650 ^{o}C to insure all the carbon parts had been burned off.

3.2.4 Raman microspectroscopy measurements of MoS_2 samples

The Raman spectra were taken with a Raman microscope (Jobin-Yvon HORIBA LabRAM HR800) equipped with a 514.5 nm Ar ion laser. An Olympus BX41 microscope was used to collect scattering light. The grating was set at 1800 gr/mm. The measurements were taken in ambient environment.

3.2.5 Atomic force microscopy measurements of MoS_2 samples

Samples were measured with AFM (Agilent 5500) in nitrogen environment (0.1% RH and 20-25 ^{o}C). Bare and modified contact silicon tips (Mikromasch CSC37) were used. The radii of the silicon tips range from 20 to 50 nm. The spring constant of the cantilever was calculated with calibration method called Sader method.[99-100] Tip radii were measured by via blind tip reconstruction scanning on a Nioprobe sample (Aurora NanoDevices Inc.). The applied load for the friction measurements was 5 nN unless otherwise stated. The friction data was obtained by averaging the friction signal of 3 scans of the same area measured by the same AFM probe.

3.3 Results and Discussion

3.3.1 Characterization of single layer MoS_2

Single layer MoS_2 flakes were prepared on the SiO_2/Si substrates using an exfoliation method. The layer thickness of thin layer MoS_2 was investigated with AFM. The topography image and friction image were taken from the thin layer MoS_2 area (Figure 3.2(b) and Figure 3.2(d)). The layer thickness was measured to be 0.6 nm, indicating it is monolayer MoS_2. Single layer and bulk MoS_2 were examined by Raman spectroscopy to confirm the layer thickness of the MoS_2. In Raman spectra, the displacements and distances of E^1_{2g} and A_{1g} peaks indicate the thickness of MoS_2 nanoflakes.[101-103] Raman spectra of SLM and bulk MoS_2 on silica substrates are shown in Figure 3.2(c). The distances between the E_{2g}^1 and A_{1g} peaks for SLM and bulk MoS_2 are 16.38 cm^{-1} and 25.37 cm^{-1}, respectively. The results agree with previous studies showing a red shift of E_{2g}^1 peak (around 384 cm^{-1}) and a blue shift of A_{1g} (around 405 cm^{-1}) with the increase of layer thickness[79, 102-103].

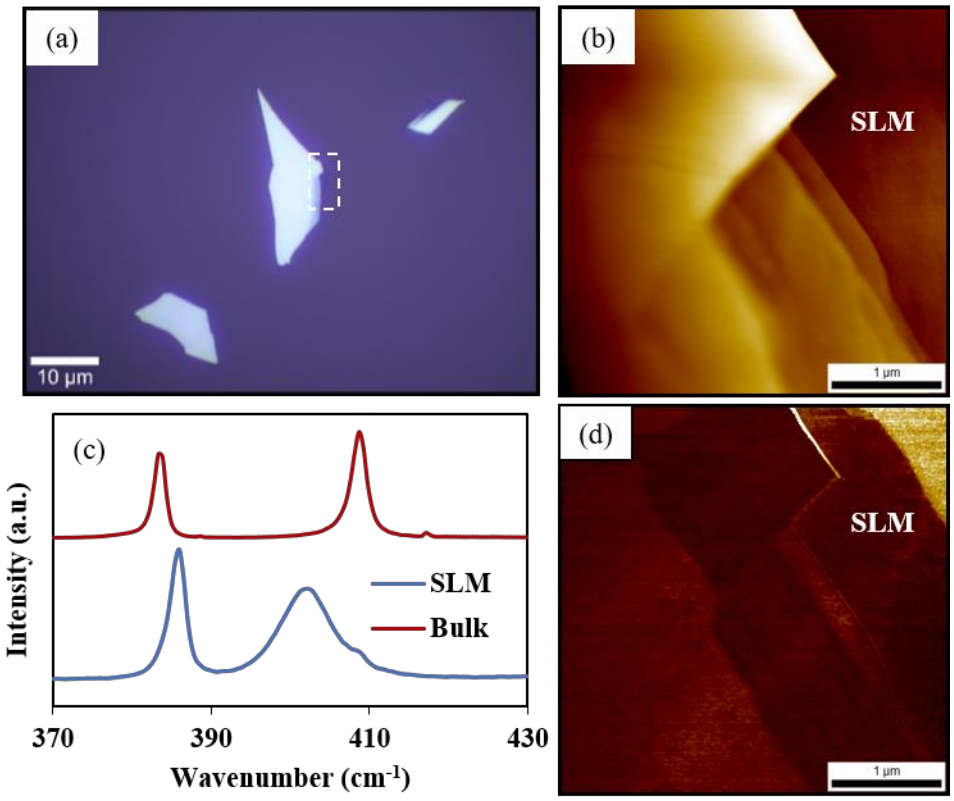

Figure 3.2 The optical image in (a) shows a MoS_2 flake with single layer MoS_2 area on SiO_2/Si substrate. AFM topography (b) and friction (d) images indicates single layer MoS_2 with lower friction than silica substrate. The Raman spectra (c) were taken from single layer and bulk MoS_2 on this flake, indicating that the distance between E_{2g} and A_{1g} peaks increases from single layer MoS_2 to bulk MoS_2.

3.3.2 FTIR of functionalized SiO_2 NPs

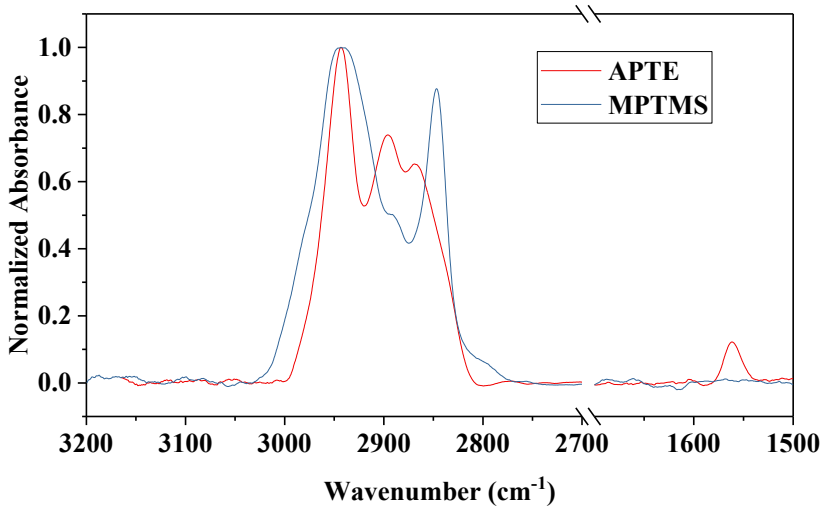

Figure 3.3 FT-IR spectra of MPTMS (blue) and APTES (red) functionalized SiO_2 NPs. The two peaks at around 2920 cm^{-1} and 2985 cm^{-1} are corresponding to the stretches of the $–CH_2$ and $–CH_3$ groups, indicating the successful functionalization of MPTMS and APTES molecules on silica NPs.

Since the frictional properties of a supported MoS_2 flake depend on the interfacial interactions, tuning the adhesive force at interfaces might be a useful way to control the frictional response of single layer MoS_2. In that case, studying the interactions at MoS_2/SAM interfaces becomes significant to explain the behavior of MoS_2 on SAM surface. Here, silicon AFM tips were functionalized with MPTMS and APTES by submersion in 1 mM molecule solutions for 12 hr. To support our assumption that the AFM probes were successfully functionalized, 100 nm silica NPs were functionalized with MPTMS and APTES to mimic modified AFM probes. Here, 100 nm silica NPs were submerged in 1 mM molecule solutions and stir for 12 hr. FT-IR

transmission spectroscopy was subsequently used to confirm the bonding of the molecules on the NP surfaces. The percentage of NPs in the IR window is 9 wt.%. As shown in Figure 3.3, for MPTMS and APTES functionalized NPs, the CH_2 asymmetric (~2940 cm^{-1}) and symmetric (2850 cm^{-1}) stretches of the alkyl chains are shown in their IR spectra (Figure 3.3), which indicates that the molecules are bound to the silica NPs.[119-120] Specifically, for silica NPs modified with APTES, the peak 1562 cm^{-1} correspond to the NH_2 scissor vibration.[121] The FT-IR measurement indicated that silica NPs were functionalized with molecules successfully.

3.3.3 Thermogravimetric analysis of functionalized SiO_2 nanoparticles

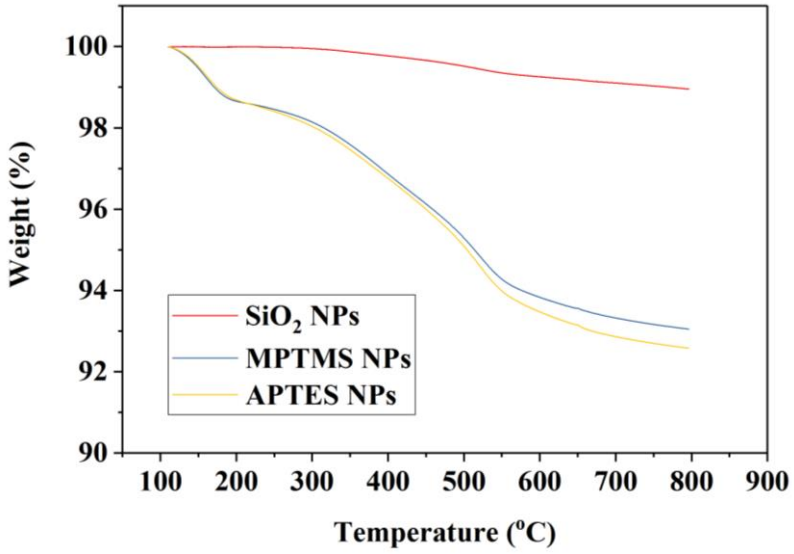

Figure 3.4 TGA thermogram of bare, MPTMS-functionalized and APTES-functionalized SiO_2 NPs from 110 °C to 800 °C with heating rate of 10 °C/min.

To obtain the packing density of molecules on silica NPs, a thermogravimetric analyzer was used to investigate the weight losses of SAMs on the NPs. After heating at

100 ^{o}C for 30 min to evaporate all of the water in the NPs, the mass changes of three types of NPs with increasing temperature are shown in Figure 3.4. The change of weight in unmodified SiO_2 NPs can be ascribed to the elimination of water. Meanwhile, the weight loss between 300 ^{o}C and 800 ^{o}C of the functionalized NPs relates to the decomposition of APTES and MPTMS chains.[122-124] In this temperature range, the weight losses of the MPTMS and APTES functionalized silica NPs were 5.4 wt. % and 5.7 wt. %, respectively. With BET surface analyzer indicating the surface area of 100 nm SiO_2 NPs is 20.7±3 m^2/g, the surface densities of the MPTMS and APTES molecules are calculated to be 0.0203 $mmol/m^2$ and 0.0281 $mmol/m^2$, respectively. The density of surface silanol groups on silica is about 5 OH/nm^2 (0.0083 $mmol/m^2$),[125] indicating that both MPTMS and APTES formed more than one layer of molecules on silica NPs. Studies have demonstrated that the predominated groups on the surface are –SH for MPTMS and $–NH_2$ for APTES.[123, 126-127] For that reason, the tip/sample interactions are mostly the interactions of $–SH/MoS_2$ and $–NH_2/MoS_2$.

3.3.4 Adhesion and friction of single layer and bulk MoS_2 with modified AFM probes

The pull off forces were obtained from force-distance curves and the work of adhesion between the tip and sample was calculated using Eq.1, where the pull-off force (F_p) and tip radius (R) were used. As shown in Figure 3.5(a), the work of adhesion at the interface between the tip and single layer/bulk MoS_2 was increased by the APTES molecules on AFM tips, which is believed to be caused by the strong interaction between the non-pair electrons in the amine group and the molybdenum atoms in MoS_2. In

addition, the MoS_2/MPTMS interface exhibited the largest work of adhesion, which is possible due to the formation of covalent bonds between molecules and defects on MoS_2. It is worth noting that the work of adhesion on SLM and bulk MoS_2 using tips with the same chemistry was very close, which may be due to single layer MoS_2 having 3 layers of atoms allowing it to screen the electronic effects from the substrate. Thus, there is no pronounced difference for the work of adhesion on SLM and bulk MoS_2. Figure 3.5(b) demonstrates the W_a distribution histogram of three tips with different chemistry. As we can see, the work of adhesion measured with the modified AFM probes show a larger W_a distribution range with a smaller force peak. The possible reason might be that the varied distribution of defects on MoS_2 surface[128] has a greater influence on the adhesive properties of -SH and -NH_2 terminated AFM probes.

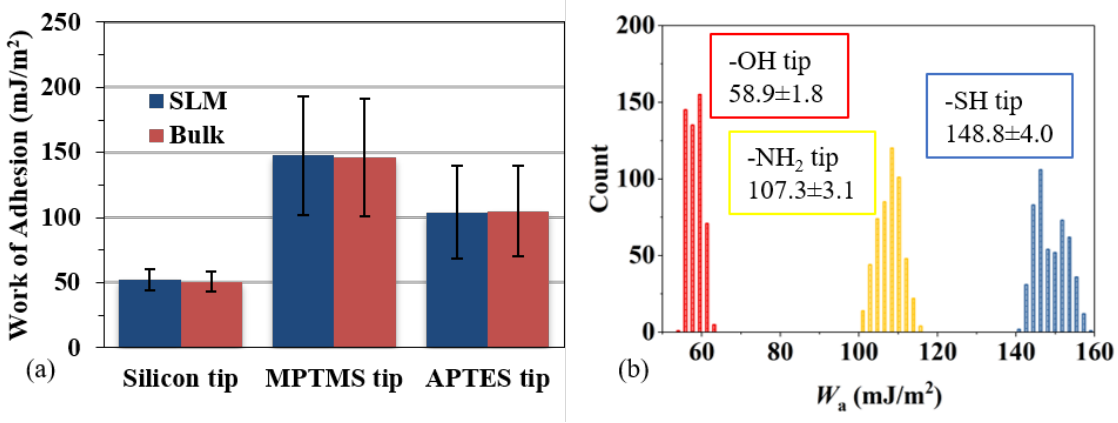

Figure 3.5 Work of adhesion calculated using pull off force on single layer and bulk MoS_2 (a) indicates that both APTES and MPTMS molecules on silicon probes increase the adhesive forces. The work of adhesion distribution histogram for three tips with different chemistry on SLM is shown in (b).

The frictional properties of MoS_2 with modified AFM probes were studied and compared to the tribological properties of MoS_2 flakes measured with unmodified silicon probes. AFM tips were coated with a layer of molecules (MPTMS and APTES) and were used to measure the adhesion and friction on single layer MoS_2 and bulk MoS_2. Figure 3.6(a-c) demonstrate the friction force (F_f) obtained at applied load from 0 to 26 nN (blue lines) and from 26 to -5 nN (orange lines). The friction vs. load curves of loading and unloading trials indicate that during unloading, the friction drops slower with reduced loads, which might be due to the adhesive force at the tip/sample interface, making the tip adhere to the single layer MoS_2, resulting in a larger contact area during the unloading process. It can be seen from the friction vs. load curves that as the normal load increases, the friction increased as well. However, the increase of friction with higher applied load was not linear, which means that Amonton's law in which the friction force is proportional to the normal load, does not apply to our system. Here, assuming the tip/SLM contact area meets all of the required conditions,[129] intermediate JKR (Johnson-Kendall-Roberts) – DMT (Derjaguin-Muller-Toporov) model was used for determining the contact area (Eq. 2) and for the calculation of friction forces (Eq. 4).

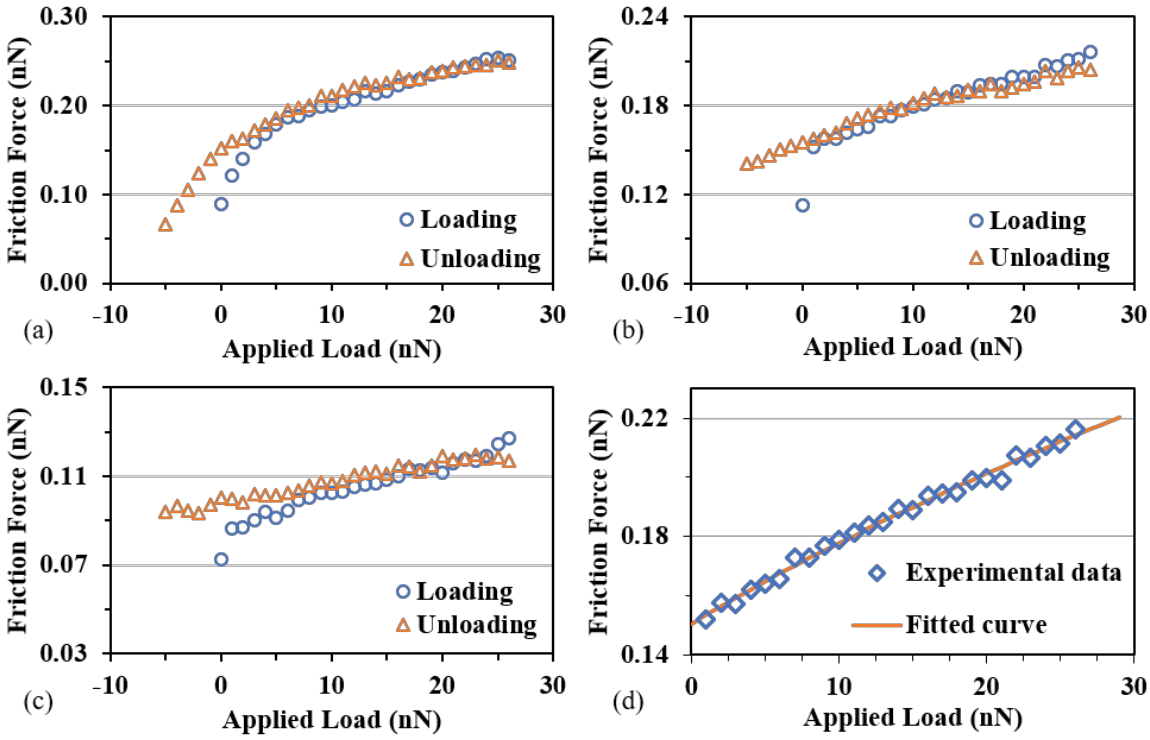

Figure 3.6 Friction vs. load graphs of loading and unloading trials with a silicon AFM probe (a), an MPTMS-modified AFM probe (b) and an APTES-modified AFM probe (c) on SLM illustrate the hysteretic effect of friction. Graph (d) shows the experimental friction vs. load data of a MPTMS-modified AFM tip on SLM and the fitted curve using the intermediate model.

$$W_a = -\frac{2F_p}{3\pi R} \quad (1)$$

$$a = a_0 \left(\frac{\alpha + \sqrt{1+\frac{F_L}{F_p}}}{1+\alpha}\right)^{2/3} \quad (2)$$

$$F_f = \sigma A + \mu F_L \quad (3)$$

$$F_f = \frac{F_{f0}}{\pi a_0^2} a^2 + \mu F_L = F_{f0} \left(\frac{\alpha + \sqrt{1+\frac{F_L}{F_p}}}{1+\alpha}\right)^{4/3} + \mu F_L \qquad (4)$$

$$\sigma = \frac{F_{f0}}{\pi a_0^2} \qquad (5)$$

Using the intermediate model, an example of the transition fitted curve is shown in Figure 3.6(d). Eq. 2 was applied to calculate the contact radius (a) for which the applied load (F_L), pull off force (F_p), contact area at zero load (a_0) and transition parameter (α, where α=1 means it follows JKR model and α=0 means it follows DMT model) were used. The friction force was calculated using the combination of Amonton's law and the single asperity law (Eq. 3). The friction vs. load data was fitted in the intermediate model in which the friction force at zero (F_{f0}), α, F_p and the friction coefficient (μ) are set to be free parameters, meanwhile the tip radius was set as the calibrated value. After fitting all of the friction vs. load data in the equation, it was found that the α values are very close to 1 and friction coefficients range from 10^{-12} to 10^{-8}. This indicates that the MoS_2/SiO_2 and MoS_2/SAM interfaces in our study follow the JKR model and the friction coefficients are negligible values.

Figure 3.7(a) demonstrates the shear strength at the MoS_2/silica, MoS_2/MPTMS and MoS_2/APTES interfaces. The shear strength was calculated by dividing the calculated frictional force at zero load by the contact area at zero applied load (Eq. 5). Despite the much larger work of adhesion caused by the amine and thiol groups, the frictional shear strength didn't show as much of an increase. The possible reason might

be that the frictional shear strength is dependent on more than one factor. Not only does the interfacial adhesion affect the friction, the stick-slip motion and surface evolution also influence the friction at interfaces.

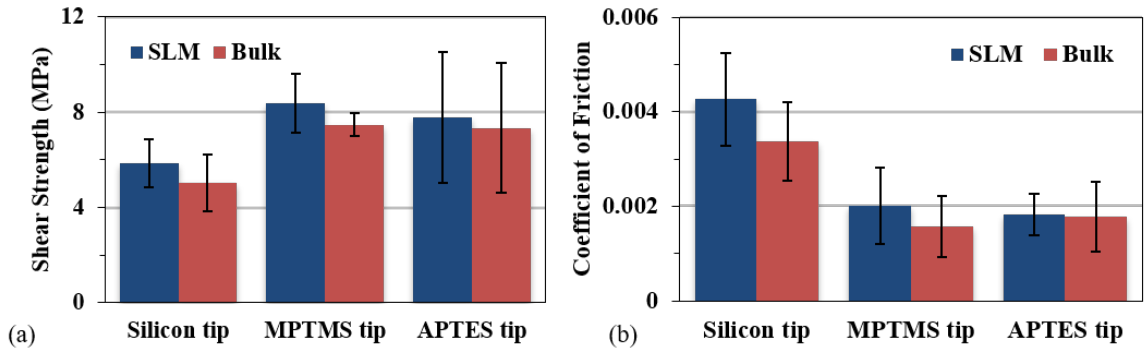

Figure 3.7 The shear strengths (a) and friction coefficients (b) on SLM and bulk MoS_2 surfaces with different AFM tips, showing that functionalized AFM probes magnified the shear strengths while reduced the friction coefficients.

Even though the friction data fitted better in the single asperity law, it is useful to use Amonton's law to calculate μ to compare the rate of increase in friction with higher applied loads for different tips. The friction coefficient was obtained using the friction data from applied loads of 5 nN to 26 nN, where the friction changes were closer to being linear. As shown in Figure 3.7(b), the friction coefficient is the largest at silica/MoS_2 interfaces. This can be explained by Eq. 4, in which if F_p is larger, the increase of F_f will be slower with higher F_L. The possible mechanism is that because functionalized AFM tips have larger adhesion and relatively large contact area at low load. When increasing the load, the changes in contact area would be relatively small compared to unmodified silicon probes. Another phenomenon that draws our attention is

that μ on SLM is larger than that on bulk MoS_2, which can be explained by the lower SLM/substrate interaction resulting in larger deformation of SLM with applied load.

3.4 Conclusion

To conclude, friction and adhesion on single layer MoS_2 and bulk MoS_2 were studied with unmodified silicon probes, MPTMS and APTES modified AFM probes. The friction vs. load data was fitted using an intermediate JKR-DMT model with R^2 more than 0.98 for all samples. The pull-off forces were used to get the work of adhesion for 3 different types of functionalized tips on SLM and bulk MoS_2. APTES functionalized AFM tips exhibited larger work of adhesion on the MoS_2 surface than unmodified silicon tips because of the strong Lewis acid-base interaction between the amine and transition metal. In addition, MPTMS functionalized tips exhibited the greatest work of adhesion, which might be due to the interactions between –SH group and defects on MoS_2 surfaces. The shear strength at the tip/MoS_2 interface was found to be influenced by the interfacial adhesion where the functionalized AFM tips had higher shear strength on MoS_2; however, the difference in shear strength was not as large as the difference in the work of adhesion between tips. The reason is that the shear strength is affected by multiple factors (e.g. adhesion at interface, stick-slip motion, surface evolution and roughness). This work explored the adhesion and friction between MoS_2 and different molecules, showing the potential of tuning the adhesive force at MoS_2/substrate interface with SAMs and opening up the possibility of modulating the tribological properties on 2D materials.

CHAPTER IV

REACTIVITY OF 4-NBD WITH MONOLAYER AND MULTILAYER MOS_2 ON AU(111)

4.1 Introduction

The interests in the researches of 2D materials was retrieved following the discovery and pioneering work on graphene since 2004. Graphene, however, is not suitable in many technological applications due to the absence of a band gap.[130-134] To overcome this limitation when developing nanoelectronic devices, semiconducting 2D materials such as MoS_2 are explored. Monolayer MoS_2 is favored in electronic devices such as nanotransistors.[135-138] Other than its outstanding electronic properties, MoS_2 is also discovered to have excellent lubricious properties. Studies since last century have proven the applications of MoS_2 as additives in oil and as boundary lubricants for minimizing friction.[52, 139-145] The study of optical, mechanical, tribological, and chemical properties on MoS_2 has been a hot topic recently due to the outstanding electrical and lubricating properties of MoS_2.[56, 146-148]

MoS_2 is a layered material composed of vertically stacked Mo atoms sandwiched with S atoms layers, and the layers of MoS_2 are held together weakly by van der Waals forces. Single layer MoS_2, 6.5 Å thick, can be extracted from MoS_2 crystal with exfoliation methods or chemical/physical composition methods. The layer-dependent properties of MoS_2 have drawn plenty of attention. As an example, it has been reported that exfoliating bulk MoS_2 into monolayer makes it transition from indirect band gap

(1.2eV) [84-85] to direct band gap (1.8eV). [83, 86] The direct band gap results in photoluminescence from single layer MoS_2, which makes it promising to use in many optoelectronic applications. Hereby, studying the mechanical and chemical properties of single- and multi-layer MoS_2 on different substrates including conductive surface is necessary to predict the behavior of MoS_2 in real devices. In this experiment, gold substrates were used because gold is inert and conductive metals are commonly seen in electronic technologies. A newly developed exfoliation method by our group using thermal-release tape was executed for depositing MoS_2 on the gold substrates. Large areas up to over a millimeter of single layer MoS_2 was able to be prepared on gold surface due to the strong adhesion at Au/MoS_2 interface.

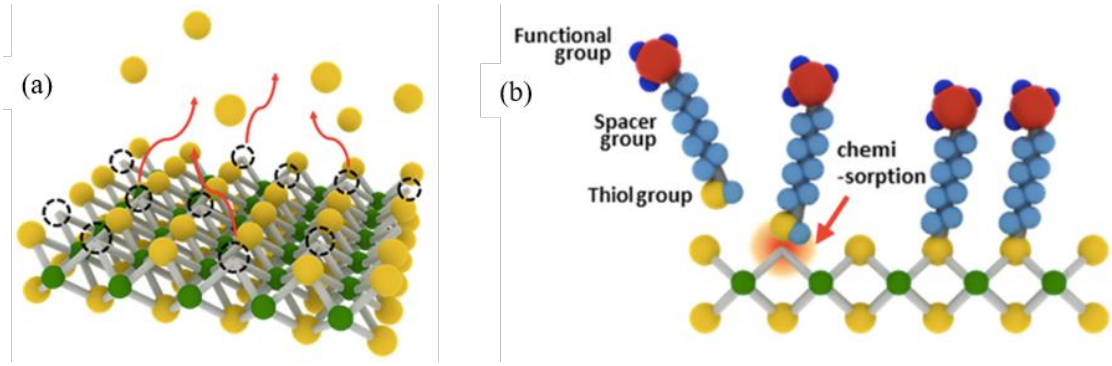

Figure 4.1 Schematic showing induced sulfur vacancies on MoS_2 surface after annealing at 250 °C. (b) Schematic of chemically absorbed thiol molecules onto MoS_2 surface. Adapted with permission from Sim *et al.*[149] Copyright 2015 by ACS Publications.

Modifying the MoS_2 surface through chemical reactions is considered a promising way to tune its mechanical and chemical properties. The surface of natural MoS_2 is 2H-phase, which is an inert basal plane in MoS_2.[150-153] Hereby, highly reactive

sites such as S vacancies are usually needed in MoS_2 modification. Sulfur-containing functional groups can subsequently generate covalent bonds with these sulfur vacancies or unsaturated molybdenum edges. [115-117] Sim and coworkers annealed MoS_2 samples at 250^oC in air for 1h to create binding sites for molecular attachment (Figure 4.1(a)). Then thiolated ligands were chemically absorbed on the MoS_2 sheet, as shown in Figure 4.1(b). Thiols are organic molecules that can form self-assembled monolayers on inorganic substrates. It was revealed in their study that both mercaptothylamine (NH_2-terminated thiol, MEA) and 1H,1H,2H,2H-perfluorodecanethiol (CF3-terminated thiol, FDT) were tightly bond on the MoS_2 surface via the strong interaction between thiol and sulfur vancancies.[154] Sulfur vacancies are not abundant in natural MoS_2 crystals. [128] Annealing the sample in high temperature or sputtering the surface with argon atoms allows to get MoS_2 surfaces rich of S vacancies.[155-159] However, it is difficult to control the density of defects with high temperature and it generates other defects on the surface of MoS_2 with argon plasma bombardment. Chemically bonding thiols on MoS_2 needs abundant sulfur vacancies, therefore it is difficult to get a high degree of functionalization with thiol molecules.

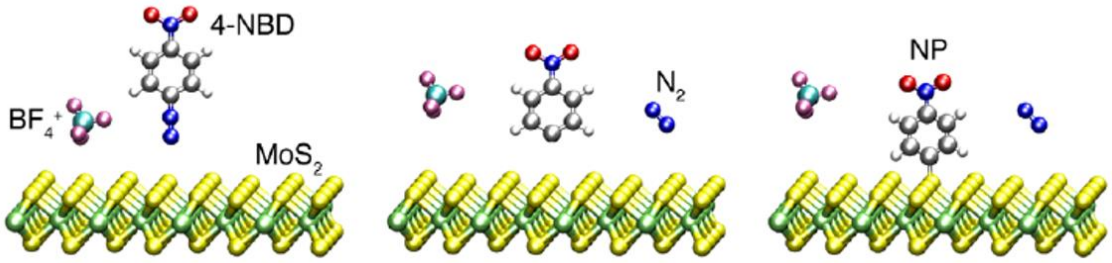

Figure 4.2 Schematic indicates the reaction between MoS_2 and 4-NBD. Nitrogen (N_2) molecules break from the molecule because of charges on MoS_2 surface. As a result, nitrobenzene radical forms a C-S bond with the MoS_2 surface. Adapted with permission from Chu *et al.* [160] Copyright 2018 by ACS Publications.

To get a controlled degree of functionalization, other modifying methods were pursued. The study carried out by Ximo S. Chu and coworkers has explored the reaction between 4-nitrobenzenediazonium tetrafluoroborate (4-NBD) and MoS_2 on SiO_2/Si substrates, revealing the formation of covalent C-S bonds (Figure 4.2). In addition, the molecular coverage is related to reaction time, layer thickness and defects of MoS_2.[160] However, the thickness of molecular film and the force required to wear away the molecules were not well studied. Here, as shown in Figure 4.3, single- and multi- layer MoS_2 on gold samples were modified with 4-NBD in aqueous solution. The bonding between nitrobenzene molecules and the surface of MoS_2 was studied with Raman spectroscopy, XPS, STM, and AFM.

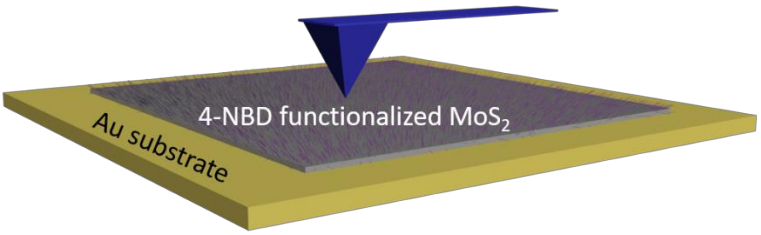

Figure 4.3 Schematic of MoS_2 on Au substrate after 4-NBD treatment. AFM was used to study the topography and sliding wear behavior of the surface.

4.2 Experimental Methods

4.2.1 Sample preparation

The MoS_2 on gold samples were made with a modified exfoliation method. Before transferring MoS_2 on Au substrates, the Au on mica substrates (Phasis, 200 nm thick Au thin films on mica, flame annealed) were cleaned with UV ozone for 15 minutes, then washed by water and rinsed with ethanol, then dried with steaming N_2. Thermal-released tape was used to peel off a thin layer of MoS_2 from MoS_2 crystal (SPI Supplies) and transferred onto Au (111) substrates. After manually pressing the MoS_2 to increase the adhesive force, the tape/MoS_2/Au sandwich was put on a heating plate to anneal it at 100 ^oC. At this temperature, the tape was released from the sample, and tweezers were used afterwards to carefully peel off bulk MoS_2 from gold substrates and large clean monolayer MoS_2 was left on the gold surface. The size of thin layer MoS_2 can reach up to one millimeter. Figure 4.4 demonstrates the procedures in sample preparation.

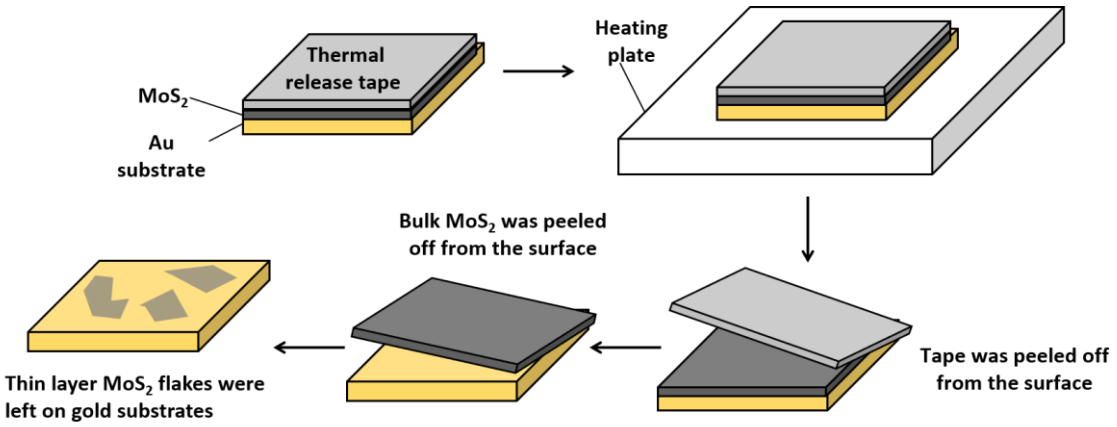

Figure 4.4 Modified thermal-released tape method. After heating the sample to remove the tape, the bulk MoS_2 flake was peeled off from the surface with tweezers instead of sonication.

4.2.2 Modification of MoS_2 with 4-NBD

The reaction of MoS_2/Au samples and 4-NBD was executed in a nitrogen tent. MoS_2/Au samples were immersed in 4-NBD aqueous solutions that were heated in a water bath to 35 ^oC for 20 min. The vial was covered with aluminum foil to avoid light and swirled continuously. After the reaction finished, the modified MoS_2 on gold samples were washed with nanopure water and ethanol, then dried with flowing N_2.

4.2.3 Raman spectroscopy of MoS_2 on gold samples

Raman spectra of MoS_2 were obtained before and after modification. A confocal Raman microscope (WITec alpha 300 RA, Germany) with an EC Epiplan-NEOFLUAR (ZEISS, Oberkochen, Germany) 100× objective (NA = 0.9, DIC) was used to explore the sample surface at room temperature. Each spectrum was taken using a 532 nm

coherent compass sapphire laser (WITec, Ulm, Germany). The results were processed using WITec's Project FOUT software to get Raman spectra of each sample.

4.2.4 XPS investigation of MoS_2 samples

A Scientia Omicron ESCA+ X-ray photoelectron spectrometer equipped with a Mg Kα (1253.6 eV) source (300 W) was implemented for XPS measurements. During the measurement, the base pressure for XPS data collection was preserved in the $\sim 10^{-10}$ mbar range. The energy resolution was about 0.9 eV and the beam size was about 54 μm. Survey scans were performed at a passing energy of 100 eV at 1.0 eV step and 0.1 s dwell time. The survey results were averaged from 3 scans at the same area. In addition, High-resolution scans of Mo 3d, Mo 3p and S 2p were carried out at a passing energy of 20 eV at 0.05 eV step and 0.1 s dwell time. The spectra showing Mo, S, N-C and N-O peaks were averaged from 50 scans of each. All the peaks were calibrated by the Au $4f_{7/2}$ at 84 eV binding energy.

4.2.5 STM studies of MoS_2 surface

An Omicron VT-STM system using mechanically cut Pt/Ir (80/20) tips with a base pressure less than 1×10^{-10} mbar was used to collect STM images. STM images were obtained using constant-current mode at a tip biasing and sample grounding configuration. The details of bias voltages and tunneling currents are reported with each corresponding STM image. The images were analyzed with Scanning Probe Image Processor software (version 6.7.2, Image Metrology, Lyngby, Denmark).

4.2.6 AFM measurements for morphology and wear properties

Contact mode AFM (Agilent 5500) was used in the measurement. In this study, silicon tips (Mikromasch CSC37) was used in nitrogen environment (0.1% relative humidity). The radii of the silicon tips are ~10 nm. The spring constant of the cantilever was calculated with the Sader Method[161] and tip radii were measured via scanning on a Nioprobe sample (Aurora NanoDevices Inc.). All the AFM topography and friction images, tip radii, tuning curves and force distance curves were analyzed with Scanning Probe Image Processing software (Image Metrology, Denmark).

4.3 Results and Discussion

4.3.1 Raman spectroscopy and XPS characterizations of MoS_2 on gold sample before and after modification with 4-NBD

Single- and multi-layer MoS_2 were deposited on Au(111) surfaces with the thermal-released tape method (Figure 4.4). The optical image of exfoliated MoS_2 on Au sample is shown in Figure 4.5(a), showing that there are both multilayer and single layer MoS_2 on the surface. Raman spectroscopy was used to determine the layer thickness of MoS_2 and to study the formation of the surface after functionalization with 4-NBD. Raman spectra of pristine single layer MoS_2 and multilayer MoS_2 are shown as red and blue lines in Figure 4.5(b), respectively. The distances between E^1_{2g} and A_{1g} peaks are 18.39 cm^{-1} for the thinner MoS_2 area and 25.71 cm^{-1} for the thicker MoS_2 area. The distance of the two Raman peaks at thinner the MoS_2 area indicates that it is monolayer

MoS_2.[79, 101, 103-104] The splitting of the E^1_{2g} peak on monolayer MoS_2 is induced from the tensile strain on the MoS_2 bubbles.[76, 162-163] After modification with 4-NBD molecules, Raman spectroscopy was used to characterize single- and multi-layer MoS_2 again. The Raman spectra show that the E^1_{2g} and A_{1g} peaks of MoS_2 are at the same positions before and after 4-NBD modification. There is no shift or extra splitting of peaks, indicating that there might be no chemical reaction between MoS_2 and 4-NBD.

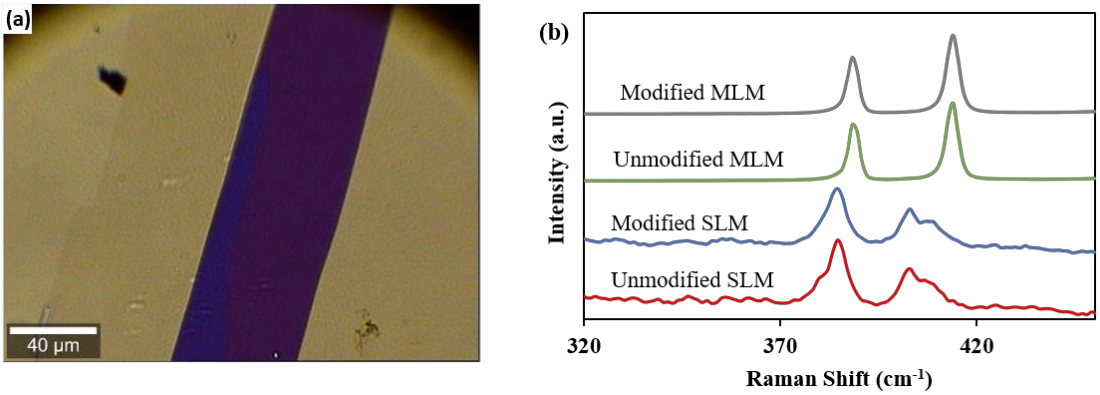

Figure 4.5 (a) Optical image of multi- and single- layer MoS_2 on Au substrate. (b) Raman spectra of single layer MoS_2 (SLM) and multilayer MoS_2 before (red) and after (blue) 4-NBD functionalization. There is no shift or extra splitting of the Raman peaks of MoS_2 after modification.

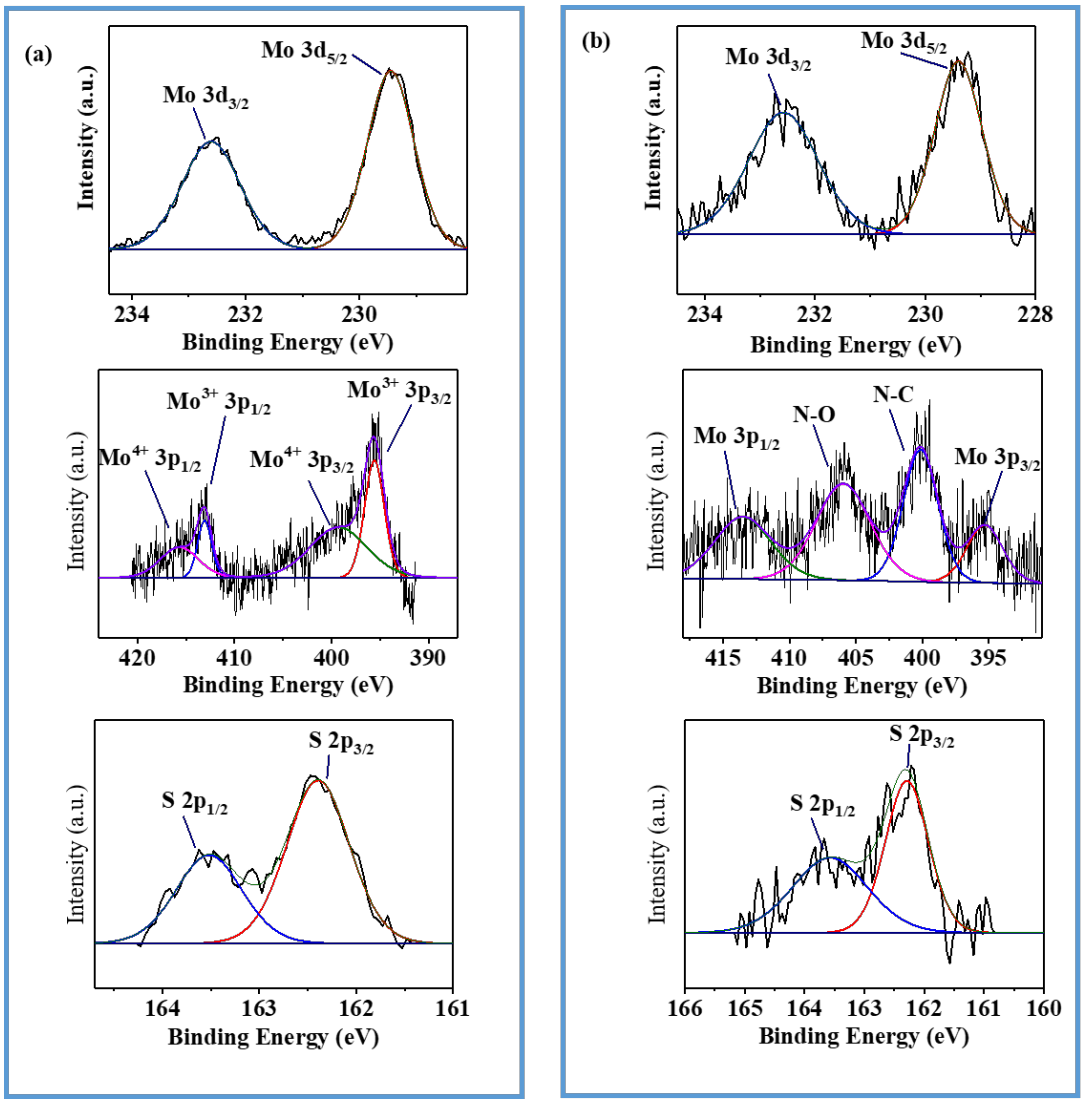

Figure 4.6 (a) and (b) are XPS spectra of MoS_2 on Au(111) sample before and after being modified with 4-NBD, respectively. (d) shows the existing of N-O and N-C peaks after 4-NBD modification, however, there is no S-C peak.

To gain a better understanding of the surface chemistry, XPS was used to characterize the surface of MoS_2 on gold samples before and after functionalization with 4-NBD. Figure 4.6 (a) and (b) indicate the XPS spectra on single layer MoS_2 before and after modification. It shows that for both spectra pre and post modification, there are two

peaks that are corresponding to Mo 3d (232.5 eV, 229.4 eV) and two peaks for S 2p (163.5 eV, 162.4 eV). As shown in the middle graph of Figure 4.6 (a), the XPS spectrum for as-exfoliated MoS_2 show peaks for Mo^{3+} and Mo^{4+}. While after modification (Figure 4.6 (b)), there are not only peaks that are corresponding to Mo 3p at 413.7 eV and 395.3 eV, but also peaks that are corresponding to N-O (405.9 eV) and N-C (400.2 eV). This indicates that there are nitrobenzene molecules adsorbed on MoS_2 surface, which is also demonstrated in the STM and AFM images shown below. However, there is no C-S peak at 163-164 eV, indicating that there is no reaction between 4-NBD and the surface of MoS_2.

4.3.2 Explore the surface of unmodified and modified MoS_2 with STM

Scanning tunneling microscopy (STM) was used to study the surface properties of MoS_2/Au(111) before and after the functionalization of 4-NBD molecules. As shown in Figure 4.7 (a) and (b), before modification, monolayer MoS_2 surface is clean and S atoms can be observed in the atomic resolution image. Moiré patterns can be seen at small scanning area due to the mismatch of MoS_2 and Au lattices.[164-165] The exhibition of moiré patterns indicates that this is single layer MoS_2 on Au(111). In addition, bubble structures on MoS_2 are shown as bright spots in STM topography images. Meanwhile, after modification, STM topography images (Figure 4.7 (c) and (d)) show that the surface of monolayer MoS_2 is covered with molecules. We also noticed that 4-NBD molecules desorb from the MoS_2 surface after several scans by STM in ultra-high vacuum (UHV, base pressure 10^{-10} mbar). The possible desorption mechanism could be

the multiple-vibrational excitation by tunneling electrons at low bias regions.[166] Such a phenomenon indicates 4-NBD physically adsorbs onto the MoS_2 surface without forming a covalent bond.

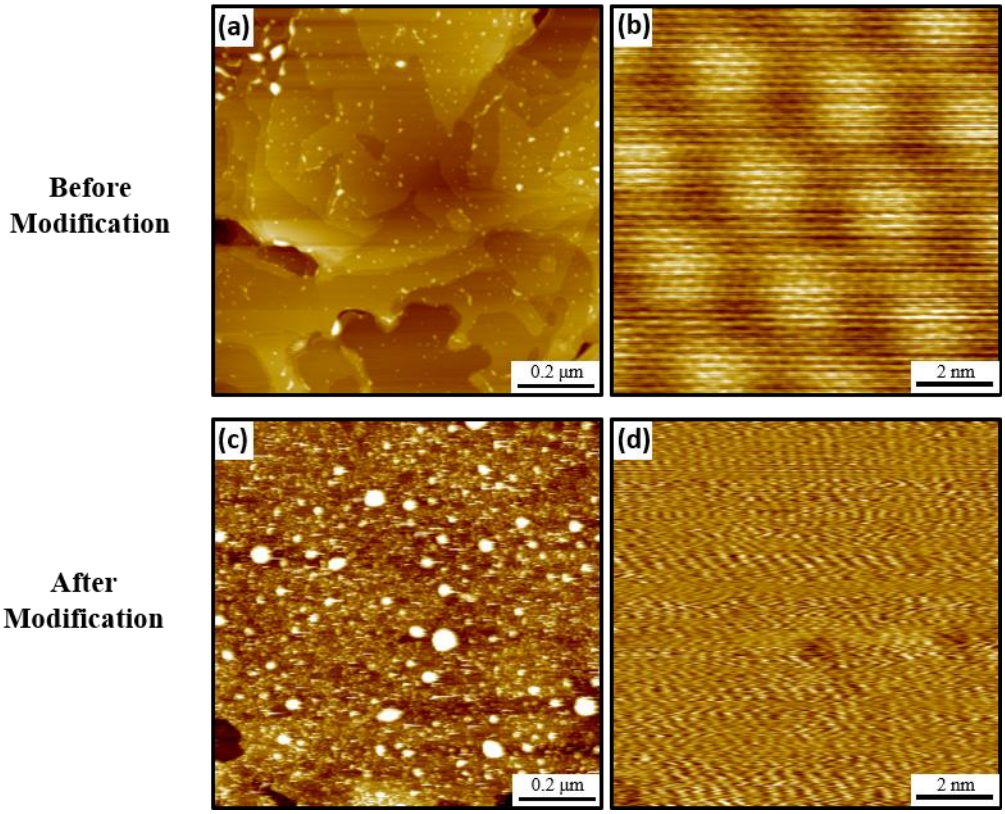

Figure 4.7 (a) STM image (0.2 V, 500 pA) of MoS_2 on Au(111). (b) Atomic resolution STM image (0.05 V, 500 pA) of MoS_2 on Au(111). (c) STM image showing the surface of MoS_2/Au(111) sample after modified with 4-NBD solution. (d) STM image of a 15 nm area of the modified monolayer MoS_2 surface. The scanning parameters for c and d are 1 V, 10 pA.

4.3.3 AFM study on the MoS_2 surface before and after functionalization

After transferring large-scale MoS_2 on Au(111) substrates, the surface of MoS_2 was explored by contact mode AFM to obtain the topographic and friction properties. We first tried the old thermal-release tape exfoliation method. The procedure of this method is shown in Figure 1.5. Instead of peeling bulk MoS_2 with tweezers, samples are sonicated to get rid of bulk MoS_2 layers. The AFM topography image shown in Figure 4.8(a) demonstrates that the MoS_2 surface is not flat, there are bubbles everywhere on the MoS_2 surface. The gold steps can be seen on gold surface and through monolayer MoS_2 in the topography images. The friction images on the sample surface are shown in Figure 4.8(b), indicating reduced friction on MoS_2 surface. It can also be seen that both the MoS_2 and the gold surface is clean without tape residue. From the friction images and STM study, the bubbles are determined to be MoS_2, and these bubbles can be eliminated using a large applied load. As shown in Figure 4.9(a) and (b), after using 30 nN and 50 nN loads to scan the surface, the bubbles gradually disappeared and the tip could press down the gold more at the bubble area because there were holes at the areas where the bubbles were. Using 1 nN load to scan the same area after compressing down the bubbles (Figure 4.9(c)) shows that the some most of the bubbles reappear. The bubbles on MoS_2 surface indicate that the MoS_2 flakes is not completely adhered on the gold substrate. The gold vacancies beneath the MoS_2 bubbles can be explained by vacancies on Au surface. This phenomenon also proves the bubbles might be produced by air or organic assembles trapped underneath MoS_2.

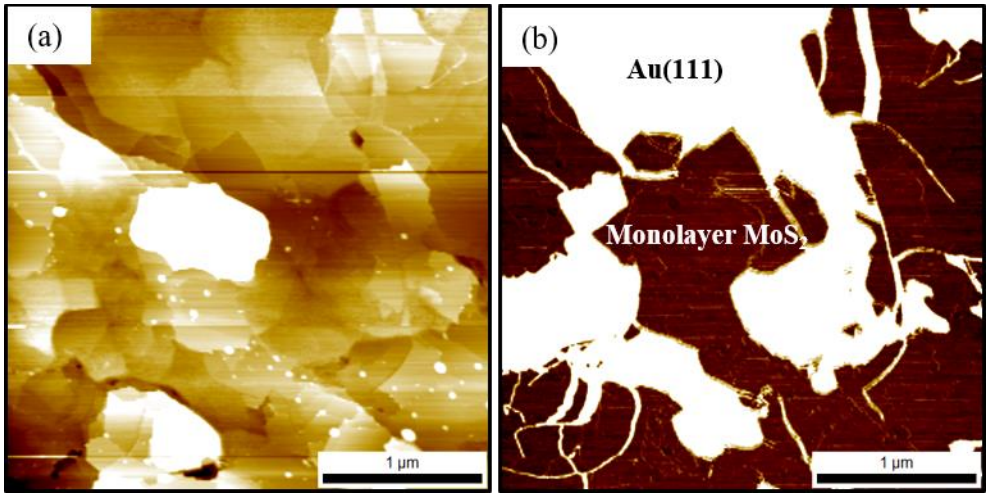

Figure 4.8 (a) AFM topography image of monolayer MoS_2 on Au(111). (b) Corresponding friction image showing MoS_2 has lower friction than Au substrate.

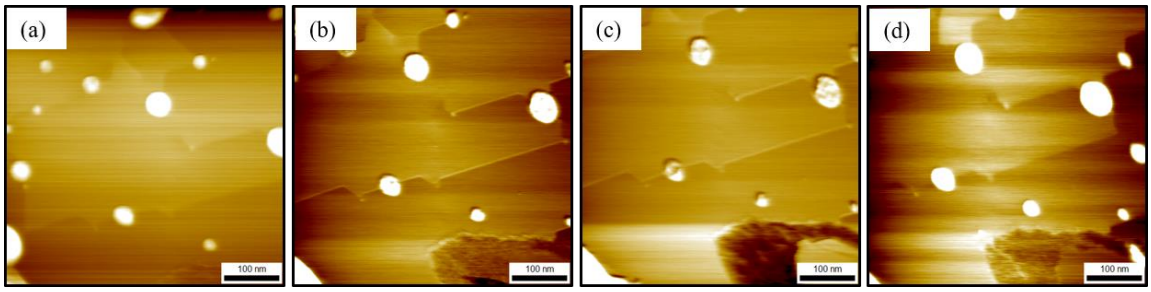

Figure 4.9 (a) Topography image of monolayer MoS_2 on Au(111) with 1 nN applied load. (b) and (c) are the same area with 30 nN and 50 nN applied load, respectively. (d) Topography image of the same area after scanning with 50 nN applied load.

With our newly developed tweezers-peeled exfoliation method. AFM was used to get the topography and wear properties on sample surfaces before and after modification of 4-NBD. Results show that large-scale continuous monolayer MoS_2 can be obtained. The AFM topography image shown in Figure 4.10 (a) demonstrates that the MoS_2 surface is not flat. There are bubbles on the MoS_2 surface, which is due to air

trapped between MoS_2 and gold substrate. This MoS_2 sample was put in a 10 mM 4-NBD solution for 20 mins, followed by rinsing with water, ethanol and drying with nitrogen. Here, the morphology of 4-NBD modified MoS_2 on gold samples was studied for the first time. As shown in Figure 4.10, AFM was used to image the MoS_2 surface after functionalization. The thickness of the multilayer MoS_2 flake was determined to be ~9 layers with AFM topography imaging. The AFM images illustrate that both mono- and multi- layer MoS_2 surfaces are covered with a layer of molecules. As shown in Figure 4.10(d), on multilayer MoS_2 surface, the organic molecules were clustered to form discontinuous islands of molecules. Meanwhile, single layer MoS_2 was mostly covered with nitrobenzene molecules, with only some pores all over the surface showing uncovered MoS_2 area that has lower friction in the friction image. This phenomenon can be seen more clearly in zoom-in topography and friction images of mono- and multi-layer MoS_2 in Figure 4.11 (a), (b), (e) and (f).

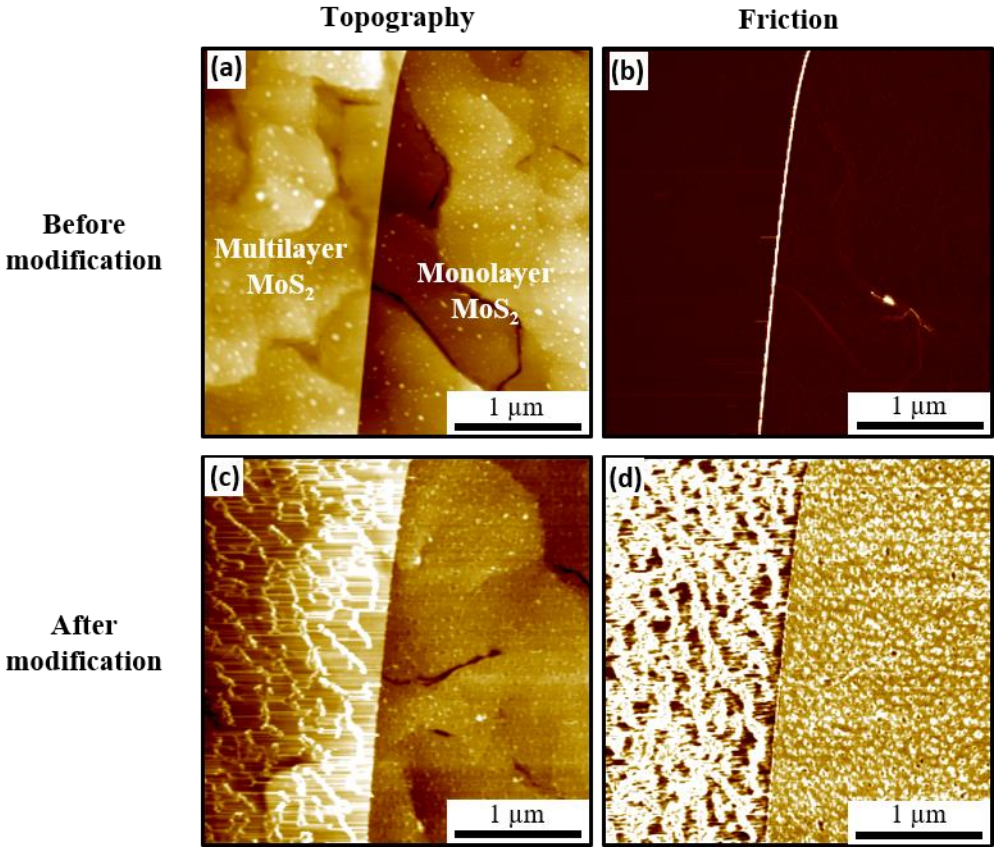

Figure 4.10 (a) AFM topography image of the multi and single layer MoS_2, showing that the MoS_2 surface prepared is not totally flat. There are bubbles all over the surface. (b) AFM topography image after modification. It exhibits molecules assembled on MoS_2. (c) and (d) are the friction images before and after modification. According to the friction images, the MoS_2 surface is not totally covered with nitrobenzene molecules and the area covered with molecules has higher friction. The color scale for both topography images is $\Delta z = 10$ nm, and the color scale for both friction images is $\Delta F_f = 20$ mV.

To study the wear properties of nitrobenzene molecules on MoS_2 surface, four different applied forces of 1 nN, 3 nN, 5 nN and 10 nN were used to wear away molecules attached to MoS_2 surface. A 1.5 µm image was scanned at 0.3 nN load before and after scratching the surface with different loads. As shown in Figure 4.11 (g) and (h), on multilayer MoS_2, the molecule clusters can be easily removed by the AFM tip at

3 nN. However, for molecules on single layer MoS_2, even at 5 nN load, there are still molecule assembles on monolayer MoS_2 surface. Only at 10 nN applied load, the congregated molecules on MoS_2 single layer are completely worn away. The greater degree of coverage and stronger connections of nitrobenzene molecules on single layer MoS_2 is possibly due to the influence of electron-donating Au substrate. This is opposite to what was observed on MoS_2 deposited on SiO_2/Si substrate.[160] Clusters of nitrobenzene molecules are removed from the MoS_2 surface with the applied load as little as 3 nN. The reason for the easy removal of nitrobenzene molecules on MoS_2 is because of the physisorption between molecules and MoS_2 surface. Additionally, the thickness of the molecule films is also measured with AFM. The line profiles shown in Figure 4.12 (a) and (b) reveal that the thickness of the molecule layers is ~1.5 nm for both monolayer MoS_2 and multilayer MoS_2.

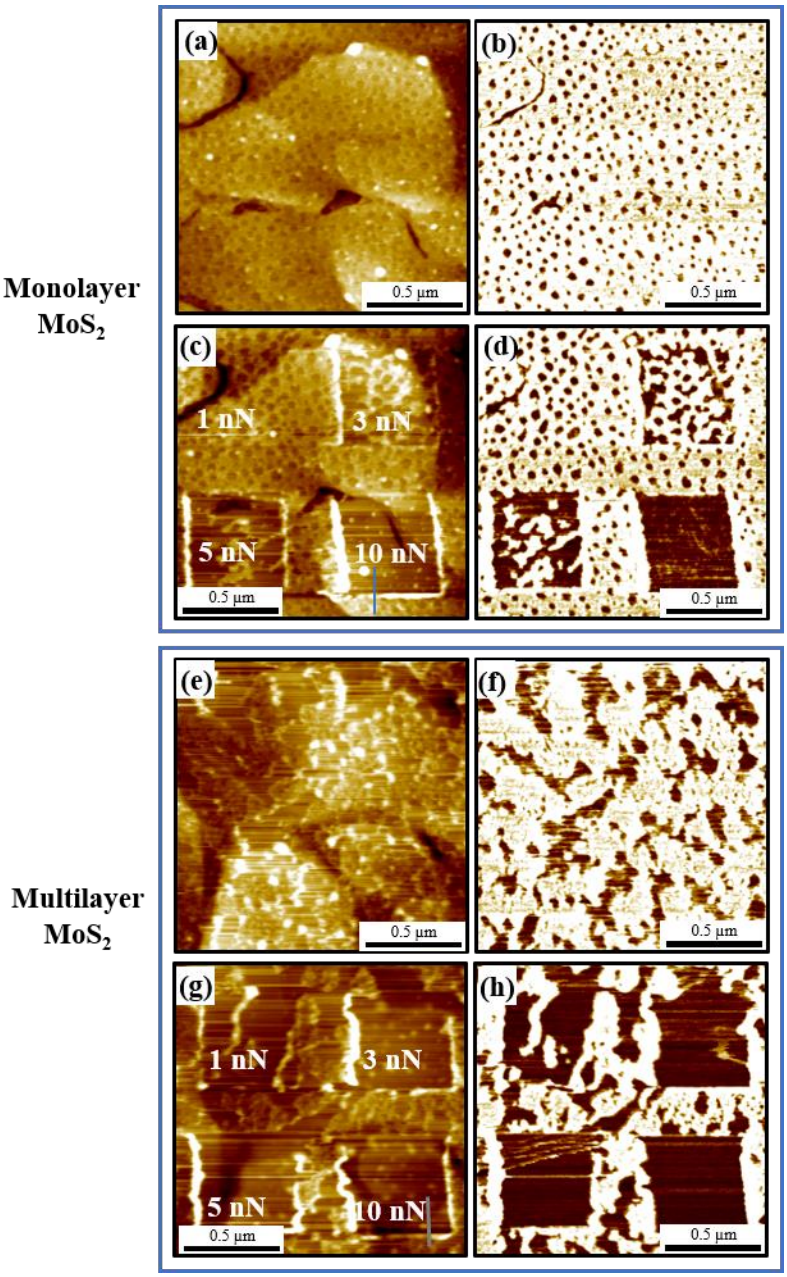

Figure 4.11 (a) and (b) are AFM topography and friction images with a scan size of 1.5 × 1.5 µm^2 on single layer MoS_2. (e) and (f) are AFM topography and friction images on multilayer MoS_2. These images reveal that the degree of functionalization of nitrobenzene molecules on single layer MoS_2 is higher than that on multilayer MoS_2. (c) and (d) are the topography and friction images after using four different loads (1 nN, 3 nN, 5 nN and 10 nN) to scan at 0.5 × 0.5 µm^2 squares on modified monolayer MoS_2. (g) and (h) are the topography and friction images on multilayer MoS_2 after rubbing the surface with various loads.

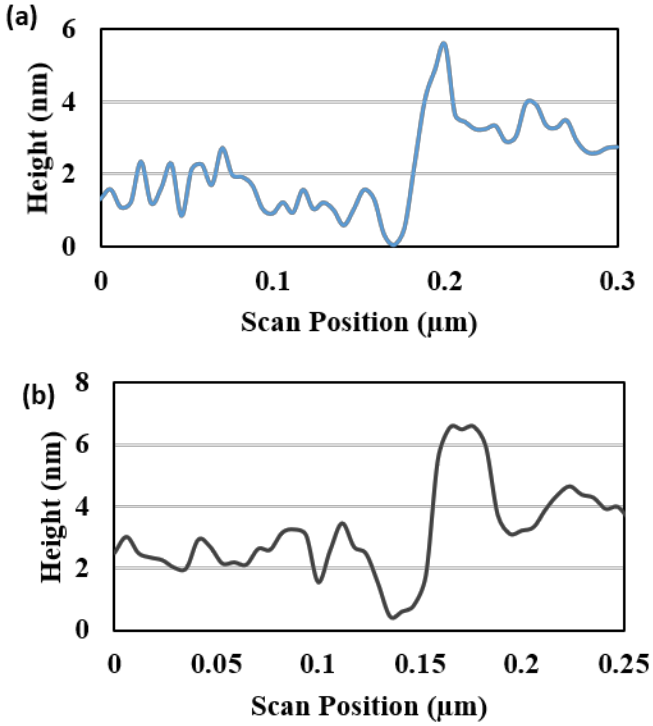

Figure 4.12 (a) and (b) are the line profiles from Figure 4.11(e) and (g), respectively, indicating the thickness of the molecule films is ~1.5nm for both single- and multi-layer MoS_2. The color scale for all topography images is Δz = 8 nm, and the color scale for all friction images is ΔFf = 7 mV.

4.3.4 The influence of the concentration of 4-NBD solutions on the coverage and wear properties of molecule films on monolayer MoS_2 surface

To study how the concentration of 4-NBD solutions impacts the coverage and wear properties of nitrobenzene molecules on monolayer MoS_2, 4-NBD solutions with the concentration of 5 mM, 10 mM and 20 mM were used. The reaction time was set to be 20 min to immerse three exfoliated MoS_2/Au samples into each solution separately. The AFM topography and friction images of monolayer MoS_2 modified with a 5 mM

solution are shown in Figure 4.13 (a) and (d). The molecule film formed on MoS_2 has larger holes on it compared to the sample put in a 10 mM 4-NBD solution shown in Figure 4.13 (b) and (e). Figure 4.13 (c) and (f) are the topography and friction images on a monolayer MoS_2 sample modified in a 20 mM solution. The exposed MoS_2 spots on this sample are fewer and smaller than the other two samples. It indicates that the coverage of organic molecules on the MoS_2 surface increases with an increasing diazonium concentration from 5 mM to 20 mM.

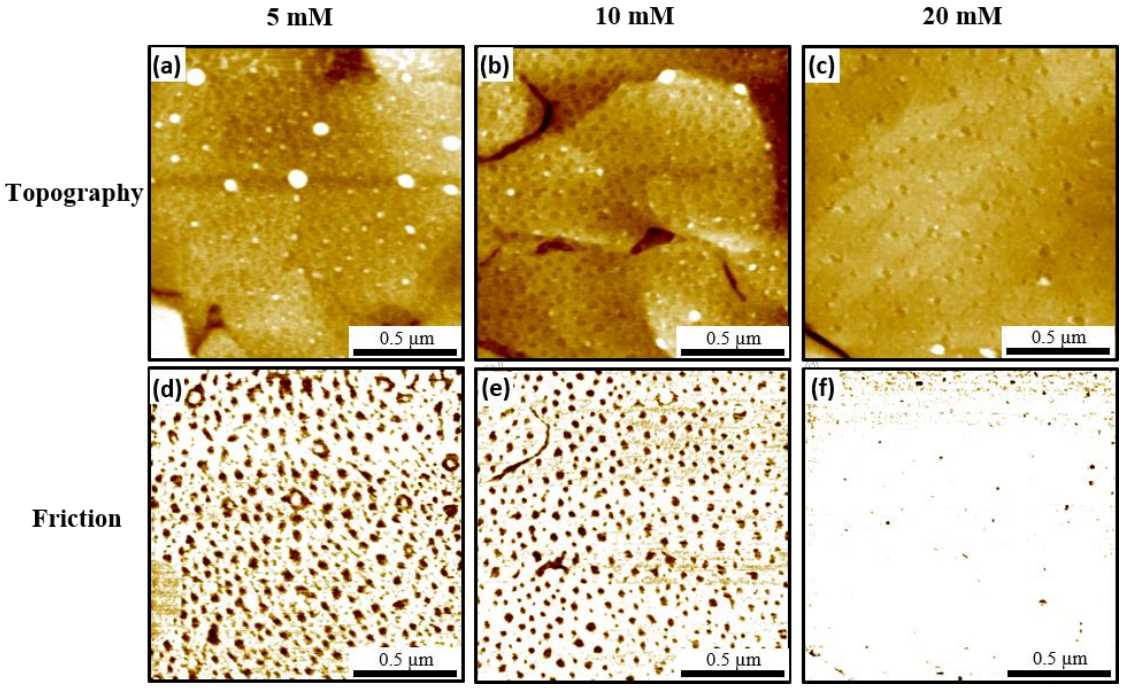

Figure 4.13 (a), (b), and (c) are the AFM topography images of single layer MoS_2 surface modified with 5 mM, 10 mM, and 20 mM 4-NBD solutions for 20 min, respectively. (d), (e) and (f) are the corresponding friction images. The color scale for all topography images is $\Delta z = 8$ nm, and the color scale for all friction images is $\Delta F_f = 7$ mV.

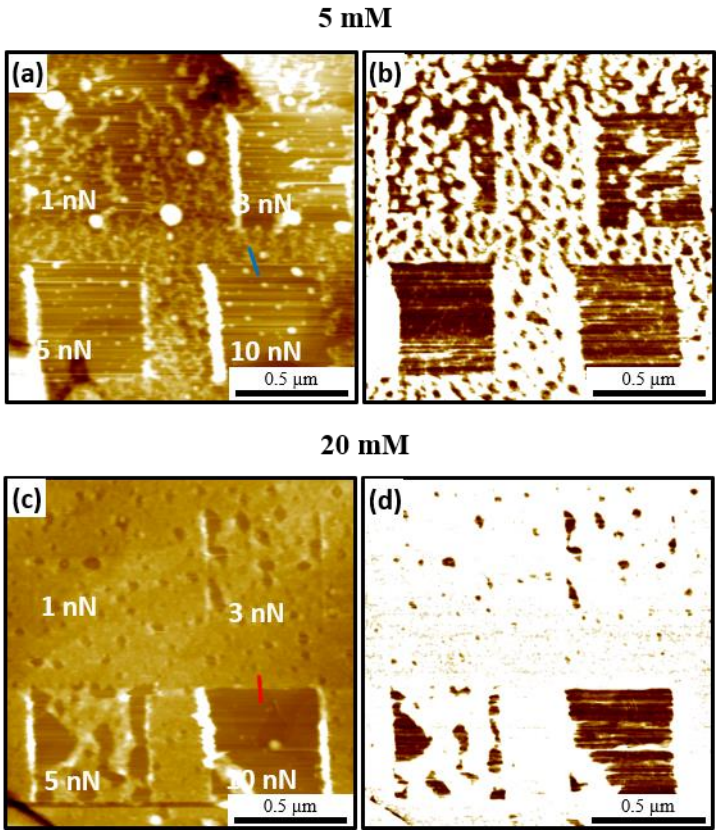

Figure 4.14 (a) and (c) are the AFM topography images after the modification of MoS_2 on Au(111) samples with 5 mM and 20 mM 4-NBD solutions, respectively. (b) and (d) are the corresponding friction images. The color scale for both topography images is $\Delta z = 8$ nm, and the color scale for both friction images is $\Delta F_f = 7$ mV.

Normal loads of 1 nN, 3 nN, 5 nN and 10 nN were also applied on the samples functionalized with 5 mM and 20 mM solutions. Figure 4.14 (a) and (b) are the AFM topography and friction images for the MoS_2 on Au sample functionalized with a 5 mM 4-NBD solution. It can be seen that most of the molecule clusters were worn away at a 3 nN applied force. Meanwhile, Figure 4.14 (c) and (d) indicates that for MoS_2 on gold sample reacted in a 20 mM 4-NBD solution, even at 5 nN applied load, the surface of MoS_2 is still mostly covered with nitrobenzene molecules. However, for monolayer

MoS_2 reacted with a 10 mM 4-NBD solution, molecules were mostly worn away at 5 nN (Figure 4.11 (c) and (d)). It indicates that the concentration of 4-NBD solutions also affects the wear properties of molecular films formed on monolayer MoS_2. The higher the concentration, the more difficult it is for the molecules to be worn away. Furthermore, line profiles were taken to study the thickness of molecule layers on these two samples. As shown in Figure 4.15 (a) and (b), the thickness of the molecules formed on monolayer MoS_2 was measured to be ~1.5 nm, which implies that the thickness of nitrobenzene molecular films on MoS_2 surface does not change with the concentration of 4-NBD solutions.

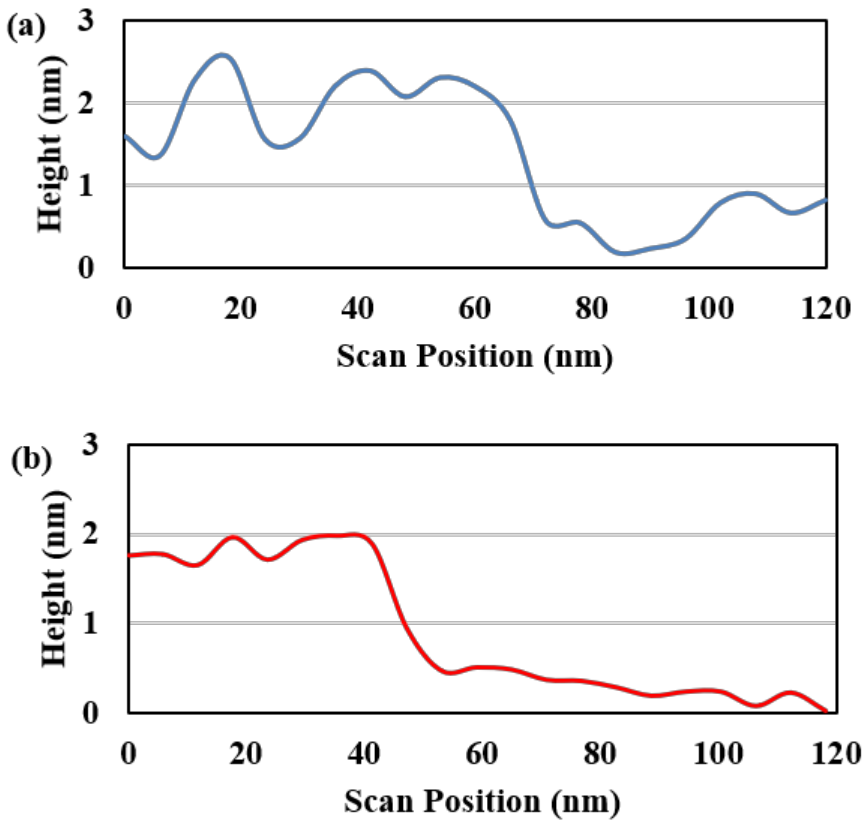

Figure 4.15 (a) and (b) are the line profiles showing the thickness of molecule films with 5 mM and 20 mM solutions, respectively, indicating the thickness of organic molecules is not dependent on the 4-NBD concentration.

4.4 Conclusion

In conclusion, we have studied the reaction between mono- and multi- layer MoS_2 with 4-NBD solutions. MoS_2 on Au samples modified with 4-NBD solutions were characterized with XPS, Raman spectroscopy STM, and AFM. In XPS measurement, although N-O and N-C peaks appear, there is no S-C peak in XPS spectra, indicating there is no chemical reaction. Additionally, Raman spectra show no shifts or splits of both E^1_{2g} and A_{1g} peaks on single- and multi- layer MoS_2 after modification with diazonium solutions. From XPS and Raman studies, it can be concluded that

nitrobenzene molecules are physically adsorbed on MoS_2/Au surface, and there is no S-C bond between them. In addition, AFM was used to study the wear properties of nitrobenzene molecule films on MoS_2. It shows that molecules aggregated on multilayer MoS_2 can be totally worn away at 3nN, while it needs more than 5 nN to completely wear off the molecules on monolayer MoS_2. Moreover, the concentration of solutions was observed to play a particular role in the coverage of molecules and the force that is required to diminish nitrobenzene molecules on monolayer MoS_2. With higher 4-NBD concentration, the coverage of molecules increases, and it needs larger applied load to wear away organic molecules. Our experiments revealed the chemical, optical and wear properties of the surface of MoS_2 on Au samples after the reaction with 4-NBD solutions. These findings shed light on the understanding of the reaction between 4-NBD and MoS_2.

CHAPTER V

SUMMARY AND OUTLOOK

5.1 Summary

In this work, different methods to tune the tribological properties of MoS_2 have been explored. It has been reported that the interfacial interactions between 2D materials and substrates is a significant factor that influences their frictional behavior. This is because of "puckering" effect as well as evolution of 2D materials during sliding. The out of plane flexibility of 2D materials plays an important role in the "puckering" effect. Here, we changed the surface roughness and chemistry to modulate the interfacial interactions for MoS2 on SiO_2 substrates. In addition, methods were explored to change the chemical properties on MoS_2 surface by forming covalent bonds.

The first study demonstrated in Chapter II modulated the surface roughness and chemistry to control frictional and mechanical properties of single- and multi- layer MoS_2. Depositing various sizes of SiO_2 nanoparticles on substrates is a way to change surface roughness. Here, we chose 20 nm and 50 nm SiO_2 nanoparticles and spin coat them separately on freshly cleaned Si wafers to adjust surface morphology. AFM topography images indicate thin MoS_2 layers are partially conformed on nanoscopically rough substrates, which is attributed to the flexibility of thin layer MoS_2 nanosheets. AFM atomic resolution studies have revealed that S-S distances in atomic scale images of MoS_2 are affected by surface roughness. This is caused by different strain of MoS_2 on 20 nm and 50 nm NPs. In addition, friction studies indicate the friction on monolayer MoS_2 surface is also influenced by nanoscopic roughness of substrates. In further

studies, molecules that can form covalent bonds with SiO_2/Si substrates were used to modulate surface chemistry and interfacial interactions between MoS_2 and substrates. Results exhibit larger friction on MoS_2/SAM surfaces due to ease of sliding of MoS_2 on SAM, resulting in larger puckering effect. Studies in Chapter I relate the interfacial forces with the tribological properties of atomically thin MoS_2 nanoflakes.

A further study on the interaction between MoS_2 and organic molecules was executed and demonstrated in Chapter III. In Chapter II, the friction on the MoS_2/SAM composites was studied, however, it did not research on the interactions between MoS_2 and organic molecules. It is difficult to directly measure the adhesion between MoS_2 and the substrate, instead, molecules was put on AFM tips. In Chapter III, AFM tips were coated with MPTMS and APTES to change their chemical properties, followed by measure the frictional and adhesive properties from MoS_2 surfaces. The results elucidate that molecules coated on AFM tips give rise to different tribological properties at tip/MoS_2 interfaces. Diverse functional groups in MPTMS and APTES contribute to changes in adhesion between AFM tips and MoS_2, inducing difference in friction. Works presented in Chapter II and Chapter III have proofed that the interfacial interactions, including adhesion have influences on the tribological properties of supported MoS_2 nanoflakes. Hereby, tuning the interactions at interfaces is considered a functional method for modulating surface friction.

Chapter IV shows an attempt to tune the tribological response of MoS_2 using a different method, which is to change the chemistry on MoS_2 surface. Effort has been paid to search for molecules that can form covalent bonds with MoS_2 to alter its surface

friction. Moreover, breaking the lattice of MoS_2 may produce more reaction sites on its surface and improve its catalytic properties. Studies before has shown the chemical reaction between 4-NBD and MoS_2. Here we also immersed MoS_2 in 4-NBD solution to make the reaction take place. However, according to Raman, XPS and AFM characterizations, there is no chemical bond between MoS_2 and nitrobenzene molecules. Nitrobenzene molecules only polymerized and formed a ~1.5 μm molecular film on MoS_2 surface. We figured out that the layer thickness of MoS_2 and the concentration of 4-NBD solution both affects the coverage and wear properties of nitrobenzene films. Although there is no chemical reaction between MoS_2 and 4-NBD, the friction on MoS_2 surface is changed by the covered molecules.

5.2 Outlook

This research focuses on studying various factors that affects the tribological properties of MoS_2. It has been proved that there might not be any reaction between 4-NBD and MoS_2. Future studies can explore creating defects on MoS_2 and see if MoS_2 with abundant defects will form enough covalent bonds with nitrobenzene molecules to be detected by characterization methods. Additionally, after chemically bond molecules on MoS_2 surface, the optical, electronic and catalytic properties of MoS_2 can be investigated. Further work on MoS_2 may also expand to studying its oxidation process on surfaces. We are now able to make MoS_2 on different substrates. The influence of substrates, humidity and temperature is interesting to exploit.

There are other newly developed 2D materials that are not well studied yet. Such as MXenes. MXenes are mostly metal carbides or metal nitrides that can be exfoliated from MAX. Materials in MXene family have metallic conductivity and are promising for applications in optoelectronic devices.[167-170] Therefore, studying its tribological properties on different substrates can be useful for its possible applications.

REFERENCES

(1) Holmberg, K.; Erdemir, A., Influence of Tribology on Global Energy Consumption, Costs and Emissions. *Friction* **2017,** *5* (3), 263-284.

(2) Mate, C. M., *Tribology on the Small Scale*. 2008.

(3) Spear, J. C.; Ewers, B. W.; Batteas, J. D., 2d-Nanomaterials for Controlling Friction and Wear at Interfaces. *Nano Today* **2015,** *10* (3), 301-314.

(4) Berman, D.; Erdemir, A.; Sumant, A. V., Approaches for Achieving Superlubricity in Two-Dimensional Materials. *ACS Nano* **2018,** *12* (3), 2122-2137.

(5) Woods, C. R.; Britnell, L.; Eckmann, A.; Ma, R. S.; Lu, J. C.; Guo, H. M.; Lin, X.; Yu, G. L.; Cao, Y.; Gorbachev, R. V.; Kretinin, A. V.; Park, J.; Ponomarenko, L. A.; Katsnelson, M. I.; Gornostyrev, Y. N.; Watanabe, K.; Taniguchi, T.; Casiraghi, C.; Gao, H. J.; Geim, A. K.; Novoselov, K. S., Commensurate–Incommensurate Transition in Graphene on Hexagonal Boron Nitride. *Nature Physics* **2014,** *10* (6), 451-456.

(6) Dong, Y.; Duan, Z.; Tao, Y.; Wei, Z.; Gueye, B.; Zhang, Y.; Chen, Y., Friction Evolution with Transition from Commensurate to Incommensurate Contacts between Graphene Layers. *Tribology International* **2019,** *136*, 259-266.

(7) Novoselov, K. S.; Geim, A. K.; Morozov, S. V.; Jiang, D.; Zhang, Y.; Dubonos, S. V.; Grigorieva, I. V.; Firsov, A. A., Electric Field Effect in Atomically Thin Carbon Films. *Science* **2004,** *306*, 666-669.

(8) Castro Neto, A. H.; Guinea, F.; Peres, N. M. R.; Novoselov, K. S.; Geim, A. K., The Electronic Properties of Graphene. *Reviews of Modern Physics* **2009,** *81* (1), 109-162.

(9) Balandin, A. A.; Ghosh, S.; Bao, W.; Calizo, I.; Teweldebrhan, D.; Miao, F.; Lau, C. N., Superior Thermal Conductivity of Single-Layer Graphene. *Nano Lett* **2008,** *8* (3), 902-907.

(10) Deng, S.; Berry, V., Wrinkled, Rippled and Crumpled Graphene: An Overview of Formation Mechanism, Electronic Properties, and Applications. *Materials Today* **2016,** *19* (4), 197-212.

(11) Ugeda, M. M.; Bradley, A. J.; Shi, S. F.; da Jornada, F. H.; Zhang, Y.; Qiu, D. Y.; Ruan, W.; Mo, S. K.; Hussain, Z.; Shen, Z. X.; Wang, F.; Louie, S. G.; Crommie, M. F., Giant Bandgap Renormalization and Excitonic Effects in a Monolayer Transition Metal Dichalcogenide Semiconductor. *Nat Mater* **2014,** *13* (12), 1091-5.

(12) Wang, Z.; Ki, D.-K.; Khoo, J. Y.; Mauro, D.; Berger, H.; Levitov, L. S.; Morpurgo, A. F., Origin and Magnitude of 'Designer' Spin-Orbit Interaction in Graphene on Semiconducting Transition Metal Dichalcogenides. *Physical Review X* **2016,** *6* (4).

(13) Shi, Y.; Li, H.; Li, L. J., Recent Advances in Controlled Synthesis of Two-Dimensional Transition Metal Dichalcogenides Via Vapour Deposition Techniques. *Chem Soc Rev* **2015,** *44* (9), 2744-56.

(14) Shi, W.; Ye, J.; Zhang, Y.; Suzuki, R.; Yoshida, M.; Miyazaki, J.; Inoue, N.; Saito, Y.; Iwasa, Y., Superconductivity Series in Transition Metal Dichalcogenides by Ionic Gating. *Sci Rep* **2015,** *5*, 12534.

(15) Lv, R.; Robinson, J. A.; Schaak, R. E.; Sun, D.; Sun, Y.; Mallouk, T. E.; Terrones, M., Transition Metal Dichalcogenides and Beyond: Synthesis, Properties, and Applications of Single- and Few-Layer Nanosheets. *Acc Chem Res* **2015,** *48* (1), 56-64.

(16) Nguyen, H.; Huang, C.-F.; Luo, W.; Xia, G.; Chen, Z.; Li, Z.; Raymond, C.; Doyle, D.; Zhao, F., Synthesis of Large-Scale 2-D MoS_2 Atomic Layers by Hydrogen-Free and Promoter-Free Chemical Vapor Deposition. *Materials Letters* **2016,** *168*, 1-4.

(17) Kim, Y.; Bark, H.; Ryu, G. H.; Lee, Z.; Lee, C., Wafer-Scale Monolayer MoS_2 Grown by Chemical Vapor Deposition Using a Reaction of Moo3 and H_2S. *J Phys Condens Matter* **2016,** *28* (18), 184002.

(18) Liu, K.; Yan, Q.; Chen, M.; Fan, W.; Sun, Y.; Suh, J.; Fu, D.; Lee, S.; Zhou, J.; Tongay, S.; Ji, J.; Neaton, J. B.; Wu, J., Elastic Properties of Chemical-Vapor-Deposited Monolayer MoS_2, Ws_2, and Their Bilayer Heterostructures. *Nano Lett* **2014,** *14* (9), 5097-103.

(19) Plechinger, G.; Mann, J.; Preciado, E.; Barroso, D.; Nguyen, A.; Eroms, J.; Schüller, C.; Bartels, L.; Korn, T., A Direct Comparison of Cvd-Grown and Exfoliated MoS_2 using Optical Spectroscopy. *Semiconductor Science and Technology* **2014,** *29* (6), 064008.

(20) Wan, Y.; Zhang, H.; Zhang, K.; Wang, Y.; Sheng, B.; Wang, X.; Dai, L., Large-Scale Synthesis and Systematic Photoluminescence Properties of Monolayer MoS_2 on Fused Silica. *ACS Appl Mater Interfaces* **2016,** *8* (28), 18570-6.

(21) Botas, C.; Álvarez, P.; Blanco, C.; Santamaría, R.; Granda, M.; Gutiérrez, M. D.; Rodríguez-Reinoso, F.; Menéndez, R., Critical Temperatures in the Synthesis of Graphene-Like Materials by Thermal Exfoliation–Reduction of Graphite Oxide. *Carbon* **2013,** *52*, 476-485.

(22) Viculis, L. M.; Mack, J. J.; Mayer, O. M.; Hahn, H. T.; Kaner, R. B., Intercalation and Exfoliation Routes to Graphite Nanoplatelets. *Journal of Materials Chemistry* **2005,** *15* (9).

(23) Li, H.; Wu, J.; Yin, Z.; Zhang, H., Preparation and Applications of Mechanically Exfoliated Single-Layer and Multilayer Mos(2) and Wse(2) Nanosheets. *Acc Chem Res* **2014,** *47* (4), 1067-75.

(24) Lee, C.; Li, Q.; Kalb, W.; Liu, X. Z.; Berger, H.; Carpick, R. W.; Hone, J., Frictional Characteristics of Atomically Thin Sheets. *Science* **2010,** *328* (5974), 76-80.

(25) Yuan Huang, E. S., Norman N. Shi, Jiabao Zheng, Tianzhong Yang, Dirk Englund, Hong-Jun Gao, and Peter Sutter., Reliable Exfoliation of Large-Area High-Quality Flakes of Graphene and Other Two-Dimensional Materials. *ACS Nano* **2015,** *9* (11), 10612-10620.

(26) Magda, G. Z.; Peto, J.; Dobrik, G.; Hwang, C.; Biro, L. P.; Tapaszto, L., Exfoliation of Large-Area Transition Metal Chalcogenide Single Layers. *Sci Rep* **2015,** *5*, 14714.

(27) Castellanos-Gomez, A.; Buscema, M.; Molenaar, R.; Singh, V.; Janssen, L.; van der Zant, H. S. J.; Steele, G. A., Deterministic Transfer of Two-Dimensional Materials by All-Dry Viscoelastic Stamping. *2D Materials* **2014,** *1* (1).

(28) Berman, A. D.; Ducker, W. A.; Israelachvili, J. N., Origin and Characterization of Different Stick-Slip Friction Mechanisms. *Langmuir* **1996,** *12*, 4559-4563.

(29) Lee, D. W.; Banquy, X.; Israelachvili, J. N., Stick-Slip Friction and Wear of Articular Joints. *Proc Natl Acad Sci U S A* **2013,** *110* (7), E567-74.

(30) Kim, Y.; Lee, J.; Yeom, M. S.; Shin, J. W.; Kim, H.; Cui, Y.; Kysar, J. W.; Hone, J.; Jung, Y.; Jeon, S.; Han, S. M., Strengthening Effect of Single-Atomic-Layer Graphene in Metal-Graphene Nanolayered Composites. *Nat Commun* **2013,** *4*, 2114.

(31) Mandelli, D.; Vanossi, A.; Invernizzi, M.; Paronuzzi, S.; Manini, N.; Tosatti, E., Superlubric-Pinned Transition in Sliding Incommensurate Colloidal Monolayers. *Physical Review B* **2015,** *92* (13).

(32) Bohlein, T.; Mikhael, J.; Bechinger, C., Observation of Kinks and Antikinks in Colloidal Monolayers Driven across Ordered Surfaces. *Nat Mater* **2011,** *11* (2), 126-30.

(33) Wang, W.; Shen, J.; He, Q. C., Microscale Superlubricity of Graphite under Various Twist Angles. *Physical Review B* **2019,** *99* (5).

(34) Yang, J.; Liu, Z.; Grey, F.; Xu, Z.; Li, X.; Liu, Y.; Urbakh, M.; Cheng, Y.; Zheng, Q., Observation of High-Speed Microscale Superlubricity in Graphite. *Phys Rev Lett* **2013,** *110* (25), 255504.

(35) Liu, S. W.; Wang, H. P.; Xu, Q.; Ma, T. B.; Yu, G.; Zhang, C.; Geng, D.; Yu, Z.; Zhang, S.; Wang, W.; Hu, Y. Z.; Wang, H.; Luo, J., Robust Microscale Superlubricity

under High Contact Pressure Enabled by Graphene-Coated Microsphere. *Nat Commun* **2017,** *8*, 14029.

(36) Berman, D.; Deshmukh, S. A.; Sankaranarayanan, S. K. R. S.; Erdemir, A.; Sumant, A. V., Macroscale Superlubricity Enabled by Graphene Nanoscroll Formation. *Science* **2015,** *348* (6239), 1118-1122.

(37) Spikes, H., Friction Modifier Additives. *Tribology Letters* **2015,** *60* (1).

(38) Lin, J.; Wang, L.; Chen, G., Modification of Graphene Platelets and Their Tribological Properties as a Lubricant Additive. *Tribology Letters* **2010,** *41* (1), 209-215.

(39) Gong, K.; Wu, X.; Zhao, G.; Wang, X., Nanosized MoS_2 Deposited on Graphene as Lubricant Additive in Polyalkylene Glycol for Steel/Steel Contact at Elevated Temperature. *Tribology International* **2017,** *110*, 1-7.

(40) Dou, X.; Koltonow, A. R.; He, X.; Jang, H. D.; Wang, Q.; Chung, Y. W.; Huang, J., Self-Dispersed Crumpled Graphene Balls in Oil for Friction and Wear Reduction. *Proc Natl Acad Sci U S A* **2016,** *113* (6), 1528-33.

(41) Gulzar, M.; Masjuki, H. H.; Kalam, M. A.; Varman, M.; Zulkifli, N. W. M.; Mufti, R. A.; Zahid, R., Tribological Performance of Nanoparticles as Lubricating Oil Additives. *Journal of Nanoparticle Research* **2016,** *18* (8).

(42) Hu, K. H.; Liu, M.; Wang, Q. J.; Xu, Y. F.; Schraube, S.; Hu, X. G., Tribological Properties of Molybdenum Disulfide Nanosheets by Monolayer Restacking Process as Additive in Liquid Paraffin. *Tribology International* **2009,** *42* (1), 33-39.

(43) Huang, H. D.; Tu, J. P.; Zou, T. Z.; Zhang, L. L.; He, D. N., Friction and Wear Properties of If– MoS_2 as Additive in Paraffin Oil. *Tribology Letters* **2005,** *20* (3-4), 247-250.

(44) Kalin, M.; Kogovšek, J.; Remškar, M., Mechanisms and Improvements in the Friction and Wear Behavior Using MoS_2 Nanotubes as Potential Oil Additives. *Wear* **2012,** *280-281*, 36-45.

(45) Tang, G.; Zhang, J.; Liu, C.; Zhang, D.; Wang, Y.; Tang, H.; Li, C., Synthesis and Tribological Properties of Flower-Like MoS_2 Microspheres. *Ceramics International* **2014,** *40* (8), 11575-11580.

(46) Chen, K.; Wan, X.; Wen, J.; Xie, W.; Kang, Z.; Zeng, X.; Chen, H.; Xu, J.-B., Electronic Properties of MoS_2–WS_2 Heterostructures Synthesized with Two-Step Lateral Epitaxial Strategy. *ACS Nano* **2015,** *9* (10), 9868-9876.

(47) Luo, S.; Hao, G.; Fan, Y.; Kou, L.; He, C.; Qi, X.; Tang, C.; Li, J.; Huang, K.; Zhong, J., Formation of Ripples in Atomically Thin MoS_2 and Local Strain Engineering of Electrostatic Properties. *Nanotechnology* **2015,** *26* (10), 105705.

(48) Zheng, C.; Xu, Z.-Q.; Zhang, Q.; Edmonds, M. T.; Watanabe, K.; Taniguchi, T.; Bao, Q.; Fuhrer, M. S., Profound Effect of Substrate Hydroxylation and Hydration on Electronic and Optical Properties of Monolayer MoS_2. *Nano Letters* **2015,** *15* (5), 3096-3102.

(49) S. Bertolazzi, J. B., and A. Kis, Stretching and Breaking of Ultrathin MoS_2. *ACS Nano* **2011,** *12*, 9703-9709.

(50) Li, S.; Li, Q.; Carpick, R. W.; Gumbsch, P.; Liu, X. Z.; Ding, X.; Sun, J.; Li, J., The Evolving Quality of Frictional Contact with Graphene. *Nature* **2016,** *539* (7630), 541-545.

(51) Quereda, J.; Castellanos-Gomez, A.; Agraït, N.; Rubio-Bollinger, G., Single-Layer MoS_2 Roughness and Sliding Friction Quenching by Interaction with Atomically Flat Substrates. *Applied Physics Letters* **2014,** *105* (5), 053111.

(52) Li, M.; Shi, J.; Liu, L.; Yu, P.; Xi, N.; Wang, Y., Experimental Study and Modeling of Atomic-Scale Friction in Zigzag and Armchair Lattice Orientations of MoS_2. *Sci Technol Adv Mater* **2016,** *17* (1), 189-199.

(53) Onodera, T.; Morita, Y.; Suzuki, A.; Koyama, M.; Tsuboi, H.; Hatakeyama, N.; Endou, A.; Takaba, H.; Kubo, M.; Dassenoy, F.; Minfray, C.; Joly-Pottuz, L.; Martin, J.-M.; Miyamoto, A., A Computational Chemistry Study on Friction of H- MoS_2. Part I. Mechanism of Single Sheet Lubrication. *J. Phys. Chem. B* **2009,** *113*, 16526-16536.

(54) Liang, T.; Sawyer, W. G.; Perry, S. S.; Sinnott, S. B.; Phillpot, S. R., First-Principles Determination of Static Potential Energy Surfaces for Atomic Friction In MoS_2 and MoO_3. *Physical Review B* **2008,** *77* (10).

(55) Levita, G.; Cavaleiro, A.; Molinari, E.; Polcar, T.; Righi, M. C., Sliding Properties of MoS_2 Layers: Load and Interlayer Orientation Effects. *The Journal of Physical Chemistry C* **2014,** *118* (25), 13809-13816.

(56) Zhao, X.; Perry, S. S., The Role of Water in Modifying Friction within MoS_2 Sliding Interfaces. *ACS Appl Mater Interfaces* **2010,** *2* (5), 1444-8.

(57) Chen, Z.; He, X.; Xiao, C.; Kim, S., Effect of Humidity on Friction and Wear—a Critical Review. *Lubricants* **2018,** *6* (3).

(58) Gradt, T.; Schneider, T., Tribological Performance of MoS_2 Coatings in Various Environments. *Lubricants* **2016,** *4* (3).

(59) Wang, C.; Li, H.; Zhang, Y.; Sun, Q.; Jia, Y., Effect of Strain on Atomic-Scale Friction in Layered MoS_2. *Tribology International* **2014,** *77*, 211-217.

(60) Castellanos-Gomez, A.; Poot, M.; Steele, G. A.; Zant, H. S. v. d.; Agraït, N.; Rubio-Bollinger, G., Mechanical Properties of Freely Suspended Semiconducting Graphene-Like Layers Based on MoS_2. *Nanoscale Research Letters* **2012,** *7* (233).

(61) Barboza, A. P.; Chacham, H.; Oliveira, C. K.; Fernandes, T. F.; Ferreira, E. H.; Archanjo, B. S.; Batista, R. J.; de Oliveira, A. B.; Neves, B. R., Dynamic Negative Compressibility of Few-Layer Graphene, H-Bn, and MoS_2. *Nano Lett* **2012,** *12* (5), 2313-7.

(62) Binnig, G.; Quate, C. F.; Gerber, C., Atomic Force Microscope. *Physical Review Letters* **1986,** *56* (9), 930-933.

(63) Marturi, N., Vision and Visual Servoing for Nanomanipulation and Nanocharacterization in Scanning Electron Microscope. *Micro and nanotechnologies/Microelectronics* **2013**.

(64) Park, J. Y.; Salmeron, M., Fundamental Aspects of Energy Dissipation in Friction. *Chem Rev* **2014,** *114* (1), 677-711.

(65) Ogletree, D. F.; Carpick, R. W.; Salmeron, M., Calibration of Frictional Forces in Atomic Force Microscopy. *Review of Scientific Instruments* **1996,** *67* (9), 3298-3306.

(66) Varenberg, M.; Etsion, I.; Halperin, G., An Improved Wedge Calibration Method for Lateral Force in Atomic Force Microscopy. *Review of Scientific Instruments* **2003,** *74* (7), 3362-3367.

(67) Khare, H. S.; Burris, D. L., The Extended Wedge Method: Atomic Force Microscope Friction Calibration for Improved Tolerance to Instrument Misalignments, Tip Offset, and Blunt Probes. *Rev Sci Instrum* **2013,** *84* (5), 055108.

(68) Asay, D. B.; Kim, S. H., Direct Force Balance Method for Atomic Force Microscopy Lateral Force Calibration. *Review of Scientific Instruments* **2006,** *77* (4).

(69) Asay, D. B.; Hsiao, E.; Kim, S. H., Corrected Direct Force Balance Method for Atomic Force Microscopy Lateral Force Calibration. *Rev Sci Instrum* **2009,** *80* (6), 066101.

(70) A. Schumacher, L. S., N. Kruse; Prins, R., Single-Layer MoS_2 on Mica: Studies by Means of Scanning Force Microscopy. *Surface Science Letters* **1993,** *289*, 595-598.

(71) Scandella, L.; Schumacher, A.; Kruse, N.; Prins, R., Tribology of Ultra-Thin MoS_2 Platelets on Mica: Studies by Scanning Force Microscopy. *Thin Solid Films* **1994,** *240*, 101-104.

(72) Kunz, E. J.; Risdon, T. J., Evaluation of Molybdenum Disulfide as an Additive for Railroad Wheel Mounting Compounds - Interim Report. *Lubrication Engineering* **1978,** *34* (8), 444-447.

(73) Bell, M. E.; Findlay, J. H., Molybdenite as a New Lubricant. *Phys. Rev.* **1941,** *59* (922).

(74) Novoselov, K. S.; Geim, A. K.; Morozov, S. V.; Jiang, D.; Zhang, H.; Dubonos, S. V.; Grigorieva, I. V.; Firsov, A. A., Electric Field Effect in Atomically Thin Carbon Films. *Sience* **2004,** *306*, 666-669.

(75) Li, H.; Contryman, A. W.; Qian, X.; Ardakani, S. M.; Gong, Y.; Wang, X.; Weisse, J. M.; Lee, C. H.; Zhao, J.; Ajayan, P. M.; Li, J.; Manoharan, H. C.; Zheng, X., Optoelectronic Crystal of Artificial Atoms in Strain-Textured Molybdenum Disulphide. *Nat Commun* **2015,** *6*, 7381.

(76) Conley, H. J.; Wang, B.; Ziegler, J. I.; Haglund, R. F., Jr.; Pantelides, S. T.; Bolotin, K. I., Bandgap Engineering of Strained Monolayer and Bilayer MoS_2. *Nano Lett* **2013,** *13* (8), 3626-30.

(77) Zhang, X.; Qiao, X. F.; Shi, W.; Wu, J. B.; Jiang, D. S.; Tan, P. H., Phonon and Raman Scattering of Two-Dimensional Transition Metal Dichalcogenides from Monolayer, Multilayer to Bulk Material. *Chem Soc Rev* **2015,** *44* (9), 2757-85.

(78) Lee, J.-U.; Kim, K.; Cheong, H., Resonant Raman and Photoluminescence Spectra of Suspended Molybdenum Disulfide. *2D Materials* **2017,** *2* (4).

(79) Li, H.; Zhang, Q.; Yap, C. C. R.; Tay, B. K.; Edwin, T. H. T.; Olivier, A.; Baillargeat, D., From Bulk to Monolayer MoS_2: Evolution of Raman Scattering. *Advanced Functional Materials* **2012,** *22* (7), 1385-1390.

(80) He, K.; Poole, C.; Mak, K. F.; Shan, J., Experimental Demonstration of Continuous Electronic Structure Tuning Via Strain in Atomically Thin MoS_2. *Nano Lett* **2013,** *13* (6), 2931-6.

(81) Castellanos-Gomez, A.; Roldan, R.; Cappelluti, E.; Buscema, M.; Guinea, F.; van der Zant, H. S.; Steele, G. A., Local Strain Engineering in Atomically Thin MoS_2. *Nano Lett* **2013,** *13* (11), 5361-6.

(82) Scheuschner, N.; Ochedowski, O.; Kaulitz, A.-M.; Gillen, R.; Schleberger, M.; Maultzsch, J., Photoluminescence of Freestanding Single- and Few-Layer MoS_2. *Physical Review B* **2014,** *89* (12).

(83) Sun, Y.; Wang, D.; Shuai, Z., Indirect-to-Direct Band Gap Crossover in Few-Layer Transition Metal Dichalcogenides: A Theoretical Prediction. *The Journal of Physical Chemistry C* **2016,** *120* (38), 21866-21870.

(84) Kam, K. K.; Parkinson, B. A., Detailed Photocurrent Spectroscopy of the Semiconducting Group Vi Transition Metal Dichaicogenldes. *J. Phys. Chem.* **1982,** *86*, 463-467.

(85) Zhao, W.; Ribeiro, R. M.; Toh, M.; Carvalho, A.; Kloc, C.; Castro Neto, A. H.; Eda, G., Origin of Indirect Optical Transitions in Few-Layer MoS_2, W S_2, and WSe_2. *Nano Lett* **2013,** *13* (11), 5627-34.

(86) Mak, K. F.; Lee, C.; Hone, J.; Shan, J.; Heinz, T. F., Atomically Thin MoS_2: A New Direct-Gap Semiconductor. *Phys Rev Lett* **2010,** *105* (13), 136805.

(87) Lembke, D.; Kis, A., Breakdown of High-Performance Monolayer MoS_2 Transistors. *ACS Nano* **2012,** *6* (11), 10070-10075.

(88) Cho, D. H.; Wang, L.; Kim, J. S.; Lee, G. H.; Kim, E. S.; Lee, S.; Lee, S. Y.; Hone, J.; Lee, C., Effect of Surface Morphology on Friction of Graphene on Various Substrates. *Nanoscale* **2013,** *5* (7), 3063-9.

(89) Spear, J. C.; Custer, J. P.; Batteas, J. D., The Influence of Nanoscale Roughness and Substrate Chemistry on the Frictional Properties of Single and Few Layer Graphene. *Nanoscale* **2015,** *7* (22), 10021-9.

(90) Ewers, B. W.; Batteas, J. D., Molecular Dynamics Simulations of Alkylsilane Monolayers on Silica Nanoasperities: Impact of Surface Curvature on Monolayer Structure and Pathways for Energy Dissipation in Tribological Contacts. *The Journal of Physical Chemistry C* **2012,** *116* (48), 25165-25177.

(91) Lee, S.; Heeb, R.; Venkataraman, N. V.; Spencer, N. D., Macroscopic Tribological Testing of Alkanethiol Self-Assembled Monolayers (SAMs): Pin-on-Disk Tribometry with Elastomeric Sliding Contacts. *Tribology Letters* **2007,** *28* (3), 229-239.

(92) Hu, Y.-z.; Zhang, T.; Ma, T.-b.; Wang, H., Molecular Dynamics Simulations on Atomic Friction between Self-Assembled Monolayers: Commensurate and Incommensurate Sliding. *Computational Materials Science* **2006,** *38* (1), 98-104.

(93) Tao Zhang, H. W. a. Y. H., Atomic Stick-Slip Friction between Commensurate Self-Assembled Monolayers. *Tribology Letters* **2003,** *14* (2), 69-76.

(94) Choi, J.; Ishida, T.; Kato, T.; Fujisawa, S., Self-Assembled Monolayer on Diamond-Like Carbon Surface: Formation and Friction Measurements. *Tribology International* **2003,** *36* (4-6), 285-290.

(95) K., C. P.; Singh, E.; Viana, B. C.; Gao, J.; Luo, J.; Lin, Z.; Elias, A. L.; Shi, Y.; Wang, Z.; Terrones, M.; Koratkar, N., Wetting of Mono and Few-Layered WS_2 and MoS_2 Films Supported on Si/SiO_2 Substrates. *ACSNANO* **2015,** *9* (3), 3023-3031.

(96) Zhao, X.; Perry, S. S., The Role of Water in Modifying Friction within MoS_2 Sliding Interfaces. *Applied Materials & Interfaces* **2010,** *2*, 1444-1448.

(97) Elinski, M. B.; Menard, B. D.; Liu, Z.; Batteas, J. D., Adhesion and Friction at Graphene/Self-Assembled Monolayer Interfaces Investigated by Atomic Force Microscopy. *The Journal of Physical Chemistry C* **2017,** *121* (10), 5635-5641.

(98) Huang, Y.; Sutter, E.; Shi, N. N.; Zheng, J.; Yang, T.; Englund, D.; Gao, H. J.; Sutter, P., Reliable Exfoliation of Large-Area High-Quality Flakes of Graphene and Other Two Dimensional Materials. *ACSNANO* **2015,** *9* (11), 10612-10620.

(99) Sader, J. E., Frequency Response of Cantilever Beams Immersed in Viscous Fluids with Applications to the Atomic Force Microscope. *Journal of Applied Physics* **1998,** *84* (1), 64-76.

(100) Sader, J. E.; Chon, J. W. M.; Mulvaney, P., Calibration of Rectangular Atomic Force Microscope Cantilevers. *Review of Scientific Instruments* **1999,** *70* (10), 3967-3969.

(101) Wang, Q. H.; Kalantar-Zadeh, K.; Kis, A.; Coleman, J. N.; Strano, M. S., Electronics and Optoelectronics of Two-Dimensional Transition Metal Dichalcogenides. *Nat Nanotechnol* **2012,** *7* (11), 699-712.

(102) Lee, C.; Yan, H.; Brus, L. E.; Heinz, T. F.; Hone, J.; Ryu, S., Anomalous Lattice Vibrations of Single- and Few-Layer MoS_2. *ACANANO* **2010,** *4* (5), 2695-2700.

(103) Li, X.-L.; Han, W.-P.; Wu, J.-B.; Qiao, X.-F.; Zhang, J.; Tan, P.-H., Layer-Number Dependent Optical Properties of 2d Materials and Their Application for Thickness Determination. *Advanced Functional Materials* **2017**, 1604468.

(104) Rice, C.; Young, R. J.; Zan, R.; Bangert, U.; Wolverson, D.; Georgiou, T.; Jalil, R.; Novoselov, K. S., Raman-Scattering Measurements and First-Principles Calculations of Strain-Induced Phonon Shifts in Monolayer MoS_2. *Physical Review B* **2013,** *87* (8).

(105) S. Bertolazzi, J. B., and A. Kis, Stretching and Breaking of Ultrathin MoS_2. *ACSNANO* **2011,** *5* (12), 9703-9709.

(106) Lee, C.; Wei, X.; Kysar, J. W.; Hone, J., Measurement of the Elastic Properties and Intrinsic Strength of Monolayer Graphene. *Sience* **2008,** *321*, 385-388.

(107) Lee, J. U.; Yoon, D.; Cheong, H., Estimation of Young's Modulus of Graphene by Raman Spectroscopy. *Nano Lett* **2012,** *12* (9), 4444-8.

(108) Grierson, D. S.; Flater, E. E.; Carpick, R. W., Accounting for the Jkr–Dmt Transition in Adhesion and Friction Measurements with Atomic Force Microscopy. *Journal of Adhesion Science and Technology* **2005,** *19* (3-5), 291-311.

(109) Persson, B. N. J., Contact Mechanics for Randomly Rough Surfaces. *Surface Science Reports* **2006,** *61* (4), 201-227.

(110) Castellanos-Gomez, A.; Poot, M.; Steele, G. A.; van der Zant, H. S.; Agrait, N.; Rubio-Bollinger, G., Elastic Properties of Freely Suspended MoS_2 Nanosheets. *Adv Mater* **2012,** *24* (6), 772-5.

(111) Fujisawa, S.; Kishi, E.; Sugawara, Y.; Morita, S., Fluctuation in Two-Dimensional Stick-Slip Phenomenon Observed with Two-Dimensional Frictional Force Microscope. *Jpn. J. Appl. Phys.* **1994,** *33*, 3752-3755.

(112) Lu, Z.; Liu, Q.; Xu, Z.; Zeng, H., Probing Anisotropic Surface Properties of Molybdenite by Direct Force Measurements. *Langmuir* **2015,** *31* (42), 11409-18.

(113) Wei, Z.; Wang, C.; Wang, Z.; Liu, D.; Bai, C., Topography Investigation of Water Layer and Self-Assembled Monolayer with Ots-Modified Afm Tips. *Surface and Interface Analysis* **2001,** *32* (1), 275-277.

(114) Bilgin, I.; Liu, F.; Vargas, A.; Winchester, A.; Man, M. K. L.; Upmanyu, M.; Dani, K. M.; Gupta, G.; Talapatra, S.; Mohite, A. D.; Kar, S., Chemical Vapor Deposition Synthesized Atomically Thin Molybdenum Disulfide with Optoelectronic-Grade Crystalline Quality. *ACSNano* **2015,** *9* (9), 8822-8832.

(115) Makarova, M.; Okawa, Y.; Aono, M., Selective Adsorption of Thiol Molecules at Sulfur Vacancies on MoS_2(0001), Followed by Vacancy Repair Via S–C Dissociation. *The Journal of Physical Chemistry C* **2012,** *116* (42), 22411-22416.

(116) Sim, D. M.; Kim, M.; Yim, S.; Choi, M.-J.; Choi, J.; Yoo, S.; Jung, Y. S., Controlled Doping of Vacancy-Containing Few-Layer MoS_2 Via Highly Stable Thiol-Based Molecular Chemisorption. *ACSNano* **2015,** *9* (12), 12115-12123.

(117) Chen, X.; Berner, N. C.; Backes, C.; Duesberg, G. S.; McDonald, A. R., Functionalization of Two-Dimensional Mos2 : On the Reaction between MoS_2 and Organic Thiols. *Angew. Chem. Int. Ed. Engl.* **2016,** *55* (19), 5803-8.

(118) Velusamy, D. B.; Kim, R. H.; Cha, S.; Huh, J.; Khazaeinezhad, R.; Kassani, S. H.; Song, G.; Cho, S. M.; Cho, S. H.; Hwang, I.; Lee, J.; Oh, K.; Choi, H.; Park, C., Flexible Transition Metal Dichalcogenide Nanosheets for Band-Selective Photodetection. *Nat Commun* **2015,** *6*, 8063.

(119) Sharma, R. K.; Sharma, S., Silica Nanosphere-Supported Palladium(Ii) Furfural Complex as a Highly Efficient and Recyclable Catalyst for Oxidative Amination of Aldehydes. *Dalton Trans* **2014,** *43* (3), 1292-304.

(120) Zhang, D.; Hegab, H. E.; Lvov, Y.; Dale Snow, L.; Palmer, J., Immobilization of Cellulase on a Silica Gel Substrate Modified Using a 3-Aptes Self-Assembled Monolayer. *Springerplus* **2016,** *5*, 48.

(121) Vansant, E. F.; Voort, P. v. d.; Vrancken, K. C., Characterization and Chemical Modification of the Silica Surface. Elsevier: Amsterdam ;, 1995. ebrary

(122) Yegin, C.; Lu, W.; Kheireddin, B.; Zhang, M.; Li, P.; Min, Y.; Sue, H.-J.; Sari, M. M.; Akbulut, M., The Effect of Nanoparticle Functionalization on Lubrication Performance of Nanofluids Dispersing Silica Nanoparticles in an Ionic Liquid. *JournalofTribology* **2017,** *139* (041802), 1-8.

(123) Wu, J.; Ling, L.; Xie, J.; Ma, G.; Wang, B., Surface Modification of Nanosilica with 3-Mercaptopropyl Trimethoxysilane: Experimental and Theoretical Study on the Surface Interaction. *Chem. Phys. Lett.* **2014,** *591*, 227-232.

(124) Qiao, B.; Wang, T. J.; Gao, H.; Jin, Y., High Density Silanization of Nano-Silica Particles Using Aminopropyltriethoxysilane (Aptes). *Appl. Surf. Sci.* **2015,** *351*, 646-654.

(125) Zhuravlev, L. T.; Potapov, V. V., Density of Silanol Groups on the Surface of Silica Precipitated from a Hydrothermal Solution. *Russian Journal of Physical Chemistry* **2006,** *80* (7), 1119-1128.

(126) Zhu, M.; Lerum, M. Z.; Chen, W., How to Prepare Reproducible, Homogeneous, and Hydrolytically Stable Aminosilane-Derived Layers on Silica. *Langmuir* **2012,** *28* (1), 416-23.

(127) Hu, M.; Noda, S.; Okubo, T.; Yamaguchi, Y.; Komiyama, H., Structure and Morphology of Self-Assembled 3-Mercaptopropyltrimethoxysilane Layers on Silicon Oxide. *Appl. Surf. Sci.* **2001,** *181*, 307-316.

(128) Addou, R.; Colombo, L.; Wallace, R. M., Surface Defects on Natural MoS_2. *ACS Appl Mater Interfaces* **2015,** *7* (22), 11921-9.

(129) Grierson, D. S.; Flater, E. E.; Carpick, R. W., Accounting for the JKR–DMT Transition in Adhesion and Friction Measurements with Atomic Force Microscopy. *J. Adhesion Sci. Technol.* **2005,** *19* (3-5), 291-311.

(130) Ren, J.-C.; Zhang, R.-Q.; Ding, Z.; Van Hove, M. A., Symmetry-Dependent Band Gap Opening in Graphene Induced by g-C_3N_4 Substrates. *RSC Adv.* **2014,** *4* (110), 64577-64582.

(131) Avouris, P., Graphene: Electronic and Photonic Properties and Devices. *Nano Lett* **2010,** *10* (11), 4285-94.

(132) Zhan, D.; Yan, J.; Lai, L.; Ni, Z.; Liu, L.; Shen, Z., Engineering the Electronic Structure of Graphene. *Adv Mater* **2012,** *24* (30), 4055-69.

(133) Tao, L.; Wang, D.; Jiang, S.; Liu, Y.; Xie, Q.; Tian, H.; Deng, N.; Wang, X.; Yang, Y.; Ren, T.-L., Fabrication Techniques and Applications of Flexible Graphene-Based Electronic Devices. *Journal of Semiconductors* **2016,** *37* (4).

(134) Sang, M.; Shin, J.; Kim, K.; Yu, K. J., Electronic and Thermal Properties of Graphene and Recent Advances in Graphene Based Electronics Applications. *Nanomaterials (Basel)* **2019,** *9* (3).

(135) Radisavljevic, B.; Radenovic, A.; Brivio, J.; Giacometti, V.; Kis, A., Single-Layer Mos2 Transistors. *Nat Nanotechnol* **2011,** *6* (3), 147-50.

(136) Kumar, A.; Ahluwalia, P. K., A First Principle Comparative Study of Electronic and Optical Properties of 1h – Mos2 and 2h – Mos2. *Materials Chemistry and Physics* **2012,** *135* (2-3), 755-761.

(137) Park, M.; Park, Y. J.; Chen, X.; Park, Y. K.; Kim, M. S.; Ahn, J. H., Mos2 - Based Tactile Sensor for Electronic Skin Applications. *Adv Mater* **2016,** *28* (13), 2556-62.

(138) Yang, Q.; Xiao, C.; Chen, B.; Ma, L.; Xu, L., Hydrothermal Synthesis of Mos2 Nanoflowers and Their Capacitive Property. *Micro & Nano Letters* **2019,** *14* (5), 493-495.

(139) Bell, M. E.; Findlay, J. H., Molybdenite as a New Lubricant. *Physical Review* **1940,** *59* (11), 922.

(140) Kunz, E. J.; Risdon, T. J., Evaluation of Molybdenum Disulfide (MoS_2) as an Additive for Railroad Wheel Mounting Compounds. *Lubrication Engineering* **1978,** *34* (8), 444-447.

(141) Jones, J. R.; Hoover, G. W., Abrasiveness of MoS_2 in Bonded Solid Lubricants. *A S L E Transactions* **2008,** *14* (1), 55-61.

(142) Shen, M.-x.; Cai, Z.-b.; Peng, J.-f.; Peng, X.-d.; Zhu, M.-h., Antiwear Properties of Bonded Mos2 Solid Lubricant Coating under Dual-Rotary Fretting Conditions. *Tribology Transactions* **2016,** *60* (2), 217-225.

(143) Sgroi, M. F.; Asti, M.; Gili, F.; Deorsola, F. A.; Bensaid, S.; Fino, D.; Kraft, G.; Garcia, I.; Dassenoy, F., Engine Bench and Road Testing of an Engine Oil Containing MoS_2 Particles as Nano-Additive for Friction Reduction. *Tribology International* **2017,** *105*, 317-325.

(144) Ren, S.; Shang, K.; Cui, M.; Wang, L.; Pu, J.; Yi, P., Structural Design of MoS_2-Based Coatings toward High Humidity and Wide Temperature. *Journal of Materials Science* **2019,** *54* (18), 11889-11902.

(145) Wang, Y.; Du, Y.; Deng, J.; Wang, Z., Friction Reduction of Water Based Lubricant with Highly Dispersed Functional MoS_2 Nanosheets. *Colloids and Surfaces A: Physicochemical and Engineering Aspects* **2019,** *562*, 321-328.

(146) Wang, H.; Yu, L.; Lee, Y. H.; Shi, Y.; Hsu, A.; Chin, M. L.; Li, L. J.; Dubey, M.; Kong, J.; Palacios, T., Integrated Circuits Based on Bilayer MoS_2 Transistors. *Nano Lett* **2012,** *12* (9), 4674-80.

(147) Xue, F.; Chen, L.; Wang, L.; Pang, Y.; Chen, J.; Zhang, C.; Wang, Z. L., MoS_2 tribotronic Transistor for Smart Tactile Switch. *Advanced Functional Materials* **2016,** *26* (13), 2104-2109.

(148) Javaid, M.; Drumm, D. W.; Russo, S. P.; Greentree, A. D., Surface-Gate-Defined Single-Electron Transistor in a MoS_2 Bilayer. *Nanotechnology* **2017,** *28* (12), 125203.

(149) Sim, D. M.; Kim, M.; Yim, S.; Choi, M.-J.; Choi, J.; Yoo, S.; Jung, Y. S., Controlled Doping of Vacancy-Containing Few-Layer MoS_2 Via Highly Stable Thiol-Based Molecular Chemisorption. *ACS Nano* **2015,** *9* (12), 12115-12123.

(150) Xue, X.; Zhang, J.; Saana, I. A.; Sun, J.; Xu, Q.; Mu, S., Rational Inert-Basal-Plane Activating Design of Ultrathin 1t Phase Mos2 with a Moo3 Heterostructure for Enhancing Hydrogen Evolution Performances. *Nanoscale* **2018,** *10* (35), 16531-16538.

(151) Wang, S.; Zhang, D.; Li, B.; Zhang, C.; Du, Z.; Yin, H.; Bi, X.; Yang, S., Ultrastable in-Plane 1T-2H MoS_2 Heterostructures for Enhanced Hydrogen Evolution Reaction. *Advanced Energy Materials* **2018,** *8* (25).

(152) Pradhan, G.; Sharma, A. K., Temperature Controlled 1T/2H Phase Ratio Modulation in Mono- and a Few Layered MoS_2 Films. *Applied Surface Science* **2019,** *479*, 1236-1245.

(153) Xia, Z.; Tao, Y.; Pan, Z.; Shen, X., Enhanced Photocatalytic Performance and Stability of 1t MoS_2 Transformed from 2h MoS_2 Via Li Intercalation. *Results in Physics* **2019,** *12*, 2218-2224.

(154) Dong Min Sim, M. K., Soonmin Yim, Min-Jae Choi, Jaesuk Choi, Seunghyup Yoo, and Yeon Sik Jung., Controlled Doping of Vacancy-Containing Few-Layer MoS_2 Via Highly Stable Thiol-Based Molecular Chemisorption. *ACS Nano* **2015,** *9* (12), 12115-12123.

(155) Donarelli, M.; Bisti, F.; Perrozzi, F.; Ottaviano, L., Tunable Sulfur Desorption in Exfoliated MoS_2 by Means of Thermal Annealing in Ultra-High Vacuum. *Chemical Physics Letters* **2013,** *588*, 198-202.

(156) Sim, D. M.; Kim, M.; Yim, S.; Choi, M.-J.; Choi, J.; Yoo, S.; Jung, Y. S., Controlled Doping of Vacancy-Containing Few-Layer MoS_2 Via Highly Stable Thiol-Based Molecular Chemisorption. *ACSNano* **2015,** *9* (12), 12115-12123.

(157) Ma, Q.; Odenthal, P. M.; Mann, J.; Le, D.; Wang, C. S.; Zhu, Y.; Chen, T.; Sun, D.; Yamaguchi, K.; Tran, T.; Wurch, M.; McKinley, J. L.; Wyrick, J.; Magnone, K.; Heinz, T. F.; Rahman, T. S.; Kawakami, R.; Bartels, L., Controlled Argon Beam-Induced Desulfurization of Monolayer Molybdenum Disulfide. *J Phys Condens Matter* **2013,** *25* (25), 252201.

(158) Chen, Y.; Huang, S.; Ji, X.; Adepalli, K.; Yin, K.; Ling, X.; Wang, X.; Xue, J.; Dresselhaus, M.; Kong, J.; Yildiz, B., Tuning Electronic Structure of Single Layer MoS_2 through Defect and Interface Engineering. *ACS Nano* **2018,** *12* (3), 2569-2579.

(159) Matsuura, K.; Ohashi, T.; Muneta, I.; Ishihara, S.; Kakushima, K.; Tsutsui, K.; Ogura, A.; Wakabayashi, H., Low-Carrier-Density Sputtered MoS_2 Film by Vapor-Phase Sulfurization. *Journal of Electronic Materials* **2018,** *47* (7), 3497-3501.

(160) Chu, X. S.; Yousaf, A.; Li, D. O.; Tang, A. A.; Debnath, A.; Ma, D.; Green, A. A.; Santos, E. J. G.; Wang, Q. H., Direct Covalent Chemical Functionalization of Unmodified Two-Dimensional Molybdenum Disulfide. *Chemistry of Materials* **2018,** *30* (6), 2112-2128.

(161) Sader, J. E.; Sanelli, J. A.; Adamson, B. D.; Monty, J. P.; Wei, X.; Crawford, S. A.; Friend, J. R.; Marusic, I.; Mulvaney, P.; Bieske, E. J., Spring Constant Calibration of Atomic Force Microscope Cantilevers of Arbitrary Shape. *Rev Sci Instrum* **2012,** *83* (10), 103705.

(162) Zhu, C. R.; Wang, G.; Liu, B. L.; Marie, X.; Qiao, X. F.; Zhang, X.; Wu, X. X.; Fan, H.; Tan, P. H.; Amand, T.; Urbaszek, B., Strain Tuning of Optical Emission Energy and Polarization in Monolayer and Bilayer MoS_2. *Physical Review B* **2013,** *88* (12).

(163) Lee, J. U.; Woo, S.; Park, J.; Park, H. C.; Son, Y. W.; Cheong, H., Strain-Shear Coupling in Bilayer Mos2. *Nat Commun* **2017,** *8* (1), 1370.

(164) Krane, N.; Lotze, C.; Franke, K. J., Moiré Structure of MoS_2 on Au(111): Local Structural and Electronic Properties. *Surface Science* **2018,** *678*, 136-142.

(165) Tumino, F.; Casari, C. S.; Passoni, M.; Russo, V.; Li Bassi, A., Pulsed Laser Deposition of Single-Layer MoS_2 on Au(111): From Nanosized Crystals to Large-Area Films. *Nanoscale Adv* **2019,** *1* (2), 643-655.

(166) Shen, T.-C.; Wang, C.; Abein, G. C.; Tucker, J. R.; Lyding, J. W.; Avouris, P.; Walkup, R. E., Atomic-Scale Desorption through Electronic and Vibrational Excitation Mechanisms. *Science* **1995,** *268*, 1590-1592.

(167) Naguib, M.; Come, J.; Dyatkin, B.; Presser, V.; Taberna, P.-L.; Simon, P.; Barsoum, M. W.; Gogotsi, Y., Mxene: A Promising Transition Metal Carbide Anode for Lithium-Ion Batteries. *Electrochemistry Communications* **2012,** *16* (1), 61-64.

(168) Ling, Z.; Ren, C. E.; Zhao, M.-Q.; Yang, J.; Giammarco, J. M.; Qiu, J.; Barsoum, M. W.; Gogotsi, Y., Flexible and Conductive Mxene Films and Nanocomposites with High Capacitance. *Proceedings of the National Academy of Sciences* **2014,** *111* (47), 16676-16681.

(169) Wang, X.; Kajiyama, S.; Iinuma, H.; Hosono, E.; Oro, S.; Moriguchi, I.; Okubo, M.; Yamada, A., Pseudocapacitance of Mxene Nanosheets for High-Power Sodium-Ion Hybrid Capacitors. *Nature Communications* **2015,** *6* (1), 6544.

(170) Lei, J.-C.; Zhang, X.; Zhou, Z., Recent Advances in Mxene: Preparation, Properties, and Applications. *Frontiers of Physics* **2015,** *10* (3), 276-286.